UNIVERSITY OF CALIFORNIA

Santa Barbara

Mechanistic Distinctions of Peripheral Neuropathies Induced via Microtubule-targeting Agents

A dissertation submitted in partial satisfaction of the

Requirements for the degree Doctor of Philosophy

in Biomolecular Science and Engineering

by

Brett Michael Cook

Committee in charge:

Professor Stu Feinstein, Co-Chair

Professor Leslie Wilson, Co-Chair

Professor Zach Ma

Professor Craig Montell

Professor Carol Vandenberg

September 2017

The dissertation of Brett Michael Cook is approved.

_____

Dr. Dzwokai (Zach) Ma

_____

Dr. Craig Montell

_____

Dr. Carol Vandenberg

_____

Dr. Stuart F. Feinstein, Committee Co-Chair

_____

Dr. Leslie Wilson, Committee Co-Chair

September 2017

Mechanistic Distinctions of Peripheral Neuropathies Induced

via Microtubule-targeting Agents

ACKNOWLEDGEMENTS

This work is the product of the collective efforts of many people who deserve recognition. First, I would like to thank my advisors Stu Feinstein and Les Wilson for providing excellent mentorship and giving me the opportunity to mature as a scientist in their labs. You both have stretched my thinking and I am deeply grateful for your continued guidance and support. Mary Ann Jordan and Bruce Littlefield were both instrumental in providing valuable ideas and interpretations in our many discussions of this work. Bruce and Eisai are responsible for providing continued support of our research and this work would exist without them. I am very appreciative of my committee members Zach Ma, Carol Vandenberg, and Craig Montell for keeping me on track and lending their perspectives along the way: your support has made this work indefinitely stronger. It is difficult to find words to express my gratitude for my many colleagues that have helped shape this thesis. They include, but are not limited to, Sarah Benbow, Nikki LaPointe, Olga Azarenko, Jen Smith, Julianna Erickson, Jack Reifert, Greg Smiyun, and Herb Miller. I was very fortunate to have had the pleasure of working with the incredibly gifted undergraduates Duncan Proctor and Rachel Bromberg. You both obviously have bright futures and your contributions shine clearly in this work. I need to especially thank all of the Neuroscience Research Institute and Biomolecular Science and Engineering Program staff who orchestrated all the behind the scenes operations. They are Max McCumber, Theresa Peña, Azeb Demisse, Kathleen McIntosh at the NRI and Stella Hahn and Lauren Baker of BMSE. The Neuroscience Research Institute's Microscopy Facility was essential in our ability to perform this work. I am very grateful for the facility directors Mary Raven and Ben Lopez for contributing their time to teach me the nuances of microscopy and image analysis. Our

collaborators deserve special recognition for their contributions to this work and include Krystyna Wozniak and Barbara Slusher at John Hopkins University. I owe so much to my parents Ron and Theresa Cook and family Natalie and Brandon Cook for their encouragement and support of my endeavors. Lastly, without the unconditional support from my incredible wife Ana I would never have survived the challenges of graduate school. It is impossible to imagine accomplishing this without you.

VITA OF BRETT MICHAEL COOK

June 2017

Education

2017 **Doctoral Candidate (Ph.D): Biomolecular Science and Engineering (BMSE),**
Emphasis in Molecular Biology
University of California, Santa Barbara
Advisers: Leslie Wilson and Stuart Feinstein

2017 **Graduate Certificate, Technology Management Program (TMP)**
University of California, Santa Barbara, CA

2008 **Bachelor of Science (B.S.): Molecular, Cellular, and Developmental Biology (MCDB), Minor: Chemistry**
University of Washington, Seattle, WA

Professional Experience

2015 – 2016 **UCSB Neuroscience Research Institute**
Microscopy Facility Co-director

2011 – 2017 **Graduate Student Researcher**, Biomolecular Science and Engineering,
University of California, Santa Barbara, CA

2008 – 2011 **Research Associate**
Biosearch Technologies Incorporated, Novato, CA

Publications

Cook BM, Benbow SJ, Wozniak KM, Slusher BS, Littlefield BA, Wilson L, Jordan MA, Feinstein SC. (2017) Rapid recovery from morphological and biochemical effects of chemotherapy-induced peripheral neuropathy in mouse sciatic nerve. *Manuscript in preparation*

Cook BM, Proctor D, Bromberg R, LaPointe NE, Feinstein SC, Wilson L. (2017) Digital Quantification of Neurite Outgrowth and Retraction by Phase Contrast Microscopy: a tau Perspective. *Submitted to Methods in Tau Biology*

Wozniak KM, Vornov JJ, Wu Y1, Liu Y, Carozzi VA, Rodriguez-Menendez V, Pozzi E, Ballarini E, Alberti P4, **Cook BM**, Littlefield BA, Nomoto K, Condon K, Eckley S, Desjardins C, Wilson L, Jordan MA, Feinstein SC, Polfdefkis M, Cavaletti G, Slusher BS (2017) Peripheral neuropathy induced by microtubule-targeted chemotherapies: insights into acute injury and long-term recovery. *Submitted to Cancer Research*

Benbow SJ, **Cook BM**, Reifert J, Wozniak KM, Slusher BS, Littlefield BA, Wilson L, Jordan MA, Feinstein SC (2016) Effects of paclitaxel and eribulin in mouse sciatic nerve: A microtubule-based rationale for the differential induction of chemotherapy-induced peripheral neuropathy. *Neurotoxicity Research*, 29(2):299-313

Rowe AA, Chuh KN, Lubin AA, Miller EA, **Cook BM,** Hollis DH, Plaxco KW (2011) Electrochemical biosensors employing an internal electrode attachment site and achieving reversible, high gain detection of specific nucleic acid sequences. *Analytical Chemistry*, 9462–9466

Weigle DS, Buben A, Burke CC, Carroll ND, **Cook BM**, Davis BS, Dubowitz G, et al. (2007) Adaptation to altitude as a vehicle for experiential learning of physiology by university undergraduates. *Advances in Physiology Education*, 31(3), 270-8

Abstract and Poster Presentations

Cook BM, Proctor D, Bromberg, R, Wozniak KM, Slusher BS, Wu Y, Littlefield BA, Jordan MA, Wilson L, Feinstein SC (2016) Rapid recovery from several morphological and biochemical effects of chemotherapy-induced neuropathy following paclitaxel and eribulin in mouse sciatic nerves. *Annual Meeting of the Society for Neuroscience, San Diego, CA*

Benbow SJ, **Cook BM**, Wozniak KM, Slusher BS, Littlefield BA, Wilson L, Feinstein SC and Jordan MA (2015) Eribulin and paclitaxel differentially affect mouse sciatic nerve biochemistry: implications for mechanisms underlying chemotherapy-induced peripheral neuropathy. *Annual Meeting of the Society for Neuroscience, Chicago, IL*

Benbow SJ, **Cook BM**, Wozniak KM, Slusher BS, Littlefield BA, Wilson L, Feinstein SC and Jordan MA (2015) Eribulin and paclitaxel uniquely affect axon biochemistry in mouse sciatic nerves. *Chemotherapy-Induced Peripheral Neuropathy Symposium, Santa Barbara, CA*

Cook BM, Benbow SJ, Wozniak KM, Slusher BS, Littlefield BA, Wilson L, Feinstein SC and Jordan MA (2015) Microtubule-targeting agents induce differential myelinated axon degeneration in a mouse model of peripheral neuropathy. *Chemotherapy-Induced Peripheral Neuropathy Symposium, Santa Barbara, CA*

Benbow SJ, **Cook BM**, Wozniak KM, Slusher BS, Littlefield BA, Wilson L, Feinstein SC and Jordan MA (2014) Effects of eribulin and paclitaxel treatment on microtubules of mouse sciatic nerves. *Annual Meeting of the American Association for Cancer Research San Diego, CA*

Cook BM, Benbow SJ, Slusher BS, Littlefield BA, Wilson L, Feinstein SC, Jordan MA (2014) Microtubule-targeted agent-induced degeneration of myelinated axons in a mouse model of peripheral neuropathy. *Annual Meeting of the American Association for Cancer Research, San Diego, CA*

Lyttle MH, **Cook BM** & Cook RM (2014) Thermolabile N-(*tert*-Butoxy Carbonyl) Protection for Deoxy-Nucleosides. *XXI International Round Table on Nucleosides, Nucleotides, and Nucleic Acid, 2014 Aug 24-28, Poznan, Poland*

Awards

2016 Best fifth-year Friday Noon Seminar in Biological Sciences
2015 Block Grant Fellowship Recipient
2015 Third Best Poster Award at MCDB Symposium and Retreat
2014 Doreen J. Putra Cancer Research Foundation Conference Fellowship

Invited Talks

Pharmacology and Biotechnology Colloquia Seminars, *Chemotherapy induced peripheral neuropathy: Mechanistic clues from microtubules*, UCSB, 6 May 2015

Chemotherapy-Induced Peripheral Neuropathy Symposium, *Comparative Study of microtubule targeted agents' effects on mouse sciatic nerves*, UCSB, 28 Feb 2015

Patents

Compounds Compositions and Methods Including Thermally Labile Moieties, Filed 15 April 2015, Patent WO2015/167620A1

Teaching Experience

2014 - 2017 Developmental Neurobiology

2012 - 2014 Biochemistry

2011 Pharmacology

Additional Experience and Interests

Proficiencies: Imaris Microscopy Analysis software, MetaMorph, Chromeleon and Empower Chromatography Data Systems, MassLynx Mass Spectroscopy, Pymol Molecular Visualization, UCSF Chimera, VMD Molecular Dynamics

ABSTRACT

Mechanistic Distinctions of Peripheral Neuropathies Induced

via Microtubule-targeting Agents

by

Brett Michael Cook

The overall goal of the experimental work undertaken in this thesis is to better understand the cellular and molecular mechanisms responsible for the onset, progression, and recovery from peripheral neuropathy, a painful and dose-limiting side effect of microtubule targeting agent (MTA) chemotherapies. The frequency of severe peripheral neuropathy varies among the different MTAs, and since the microtubule binding interactions and mechanisms of action also vary, we hypothesized that these distinct mechanisms may underlie the variability in pathophysiology of chemotherapy induced peripheral neuropathy (CIPN).

This work began with a correlative investigation of the morphological and biochemical effects that occur in peripheral nerves upon *in-vivo* treatment with MTAs in a maximum tolerated dose mouse model. We analyzed sciatic nerves from mice treated with the chemotherapy drugs paclitaxel (frequent severe neuropathy) or eribulin (infrequent severe neuropathy) and found that morphologically, paclitaxel increased the frequency of observed signs of axon degeneration more significantly than did eribulin. Alternatively, eribulin but not paclitaxel induced occasional myelin "halo" structures. Biochemically,

paclitaxel, and eribulin both induced α-tubulin expression (~1.9- and ~2.5-fold, respectively) and α-tubulin acetylation, a marker for microtubule stability, (~5- and ~11.7-fold, respectively). Eribulin but not paclitaxel-induced microtuble end-binding protein 1 (EB1) expression ~2.2-fold while paclitaxel but not eribulin mildly suppressed end-binding protein 3 (EB3) expression. Both EB proteins are associated with microtubule growth. Eribulin's combination of relatively mild deleterious morphological effects coupled with more potent biochemical changes promoting microtubule stability and growth in mice correlate with lower frequencies of severe neuropathy in humans. We hypothesized that these eribulin-induced effects created a relatively stable microtubule network that compensated, in part, for the toxic anti-cancer effects of the drug, leading to fewer reported incidences of peripheral neuropathy than for paclitaxel.

We then extended these comparative studies to acquire a more detailed understanding of the resolution from these initial effects over the course of 6 months after the completion of either paclitaxel, eribulin, or ixabepilone dosing. In paclitaxel-treated mice, axon area density was significantly decreased through 3 months of recovery. In contrast, axon area density in eribulin-treated mice recovered fully from initial deficits by the 2 week time point, with ixabepilone showing no change at any time point. Evidence of myelin abnormalities, likely secondary to axonopathy, was prominent at 2 weeks and 3 months and was consistently most frequent in paclitaxel-treated animals. Also, only paclitaxel-treated mice displayed a significant and persistent increase in the number of non-neuronal nuclei at the 2 week, 3 month and 6 month recovery time points, although ixabepilone-treated mice showed a similar trend at 2 weeks. These additional nuclei were positive for known Schwann cell markers S100B and GFAP, indicating that they are likely Schwann cells, the resident glia of the sciatic nerve. Biochemically, we found that two weeks into the recovery phase, α-tubulin

acetylation in eribulin-treated mice returned to control levels while it was greatly reduced but still significantly higher than vehicle treated mice in paclitaxel-treated mice. In contrast, axonal levels of both α-tubulin and end-binding protein 1 (EB1) rapidly returned to control values at 14 day from initially induced levels at the end of the MTD treatment in both paclitaxel and eribulin treated mice. In summary, we found that (i) morphologically, sciatic nerve axons recovered more rapidly from eribulin and ixabepilone-induced morphological and biochemical effects than did paclitaxel-treated mice, and (ii) biochemically, drug-induced increases in protein expression levels following paclitaxel and eribulin treatment are relatively transient. Taken together, our data in mice indicate a milder onset and faster recovery with eribulin and ixabepilone treatment than for paclitaxel.

Finally, we made progress developing an in-vitro cell culture model for studying the cellular and molecular mechanisms that regulate neuron's response to microtubule inhibition. We found that all MTAs reduced neurite area of neuronal cells at concentrations that coincided with a possible shift in microtubule mass and a change in cytosolic α-tubulin acetylation. When we compared the IC_{50} concentrations for neurite area and inhibition of cancer cell proliferation, we found that eribulin was far less potent to neurons than it was to cancer cells, indicating that neurons are more tolerant of eribulin's action as compared to ixabpilone, paclitaxel, and vincristine.

TABLE OF CONTENTS

Chapter 1: General Introduction

Microtubules are essential for vital cell processes

The microtubule cytoskeleton is so crucial to the cell that without it, eukaryotic life could not continue. The very process of ensuring transfer of genetic material between dividing cells requires an intact and properly functioning microtubule cytoskeleton. Among their many duties in cells, microtubules are involved in diverse and dynamic functions such as maintaining cell shape, vesicle trafficking, cellular transport, and mitosis.

The highly dynamic behavior of microtubules allows the cell to rapidly respond to both intracellular and extracellular signaling. Such signals influence cell shape, motility, and cell division. In addition to providing physical structure and support for the cytoplasm, microtubules provide a vast network of conduits on which to transport cargoes from the protein-producing endoplasmic reticulum to the periphery of the cell. These cargoes include vesicles containing membrane-bound channels and receptors, transcription factors or nucleic acid coding sequences, and organelles such as mitochondria. If one desired to induce great inconvenience to a cell, interfering with its microtubules would be a fantastic strategy.

Microtubule structure and dynamic instability

Each microtubule is composed of repeating heterodimer subunits of closely homologous α and β-tubulin monomers. These heterodimers bind in a head to tail fashion to form linear protofilaments. Each protofilament is polarized, with the β-tubulin end facing outward (the plus end) and the α-tubulin end facing inward (minus end). Once assembled, the microtubule resembles a hollow cylinder with a diameter of ~24nm and containing an average of 13 protofilaments (Akmanova and Steinmetz 2008).

Each microtubule is able to grow and shorten as needed depending on spatiotemporal requirements of the cell. There are two important dynamic activities of microtubules: treadmilling and dynamic instability. The first behavior involves net growth at one microtubule end and balanced net shortening at the opposite end, creating a retrograde flow of subunits from the plus end to the minus end. The rate of treadmilling is determined by differences in the critical subunit concentrations at the opposite microtubule end (Margolis and Wilson 1978, Rodionov and Borisy 1997, Panda et al. 1999). The second dynamic behavior of microtubules, called dynamic instability, is characterized by four main activites: growing, shortening, transitioning from the growth or paused state to shortening, or transitioning from shortening to growth or pausing. To accomplish these complex polymerization dynamics, αβ-tubulin cycles between two distinct states: GTP- and GDP-bound, with an intermediate conformation of GDP+Pi existing between these two states. A long-standing model for how αβ-tubulin associated with GTP make it more microtubule compatible stated that GTP induces a more straight conformation of the heterodimer that lowers the energy of polymerization (Mandelkow et al. 1991, Melki et al. 1989, Alushin 2014). A generally accepted model states that the bent unpolymerized αβ-tubulin monomer is straightened upon binding GTP. Thus, the growing plus end of a microtubule is protected from depolymerization by a GTP cap of αβ-tubulin bound to GTP. Following incorporation into the lattice, each dimer then hydrolyzes its bound GTP to GDP. The GDP-bound conformation becomes strained, but remains polymerized due to stabilizing interactions within the surrounding heterodimer lattice. If the pace of GTP hydrolysis exceeds that of subunit addition, a depolymerizing event called a catastrophe occurs causing the microtubule end to rapidly lose subunits in a peeling fashion. Following this rapid depolymerization, new subunits can again be added to re-initiate the process the assembly, a process known as

a rescue. This switching between alternating phases of growth and disassembly allows individual microtubules to sample cellular regions and retract in cases where they do not encounter a stabilizing environment or their protein targets, such as kinetochores during mitosis.

Regulation of microtubule dynamics

The coordinated regulation of microtubule function and assembly, a process thought to be closely regulated and reflecting integration of various extracellular signals, requires very tight regulation of MT dynamics. Considering the importance of microtubules to normal cell functions, it is not surprising that cells have evolved robust strategies for properly regulating their microtubules using multiple molecular mechanisms, including altered tubulin isotype expression patterns, post-translational modifications and the action of a number of microtubule associated proteins (MAPs). Alone or in combination these mechanisms can provide highly tunable regulatory power (Bhattacharya et al. 2011; Janke and Bulinski 2011; Lu and Luduena 1993; Savage et al. 1989; Song and Brady 2015). The highly dynamic nature of microtubules can be modified to suit the different requirements of different cellular compartments, for example, in the cell body versus the distal axon of a neuron.

Dynamic instability is also tied to cellular metabolism via intracellular levels of GTP, as well as by the concentration of available tubulin subunits. The amount of total tubulin protein in the cells is regulated through a negative auto-feedback loop, where non-polymerized tubulin protein subunits bind and specifically inactivate tubulin mRNA. This occurs when the concentration of tubulin subunits is elevated. On the other and, when tubulin protein subunit levels decrease, the feedback loop is not active and tubulin translation proceeds to restore the desired balance (Gay et al. 1987; Pachter et al. 1987).

The binding of microtubule associated proteins (MAPs) can directly influence MT dynamics as well as serve as scaffolds for the binding of additional proteins. For example, microtubule end binding proteins EB1 (end binding protein 1) and EB3 (end binding protein 3) bind selectively to the growing plus ends of microtubules, facilitating MT polymerization, directional cues, and cross-links to actin filaments (Akhmanova and Steinmetz 2015; Maurer et al. 2012). EB1 has been implicated in promoting microtubule growth and axonal transport while EB3 can serve as a linker between dynamic microtubules and the actin cytoskeleton (Geraldo et al. 2008; Gu et al. 2006; Jaworski et al. 2009).

The post-translational modifications of tubulin are so diverse that they rival histone modifications in the nucleus, leading some to call it a tubulin code (Janke 2014). While the functions of many tubulin modifications are unknown, some modifications have been shown to regulate the dynamicity and stability of the microtubule lattice (Janke and Bulinski 2011). The C-terminal tail of tubulin is the most well-known site of modification. This unstructured polypeptide chain is exposed on the outer face of the microtubule and is subject to many potential modifications including glycosylation, glutamylation, detyrosination, and polyamylation (Janke and Kneussel 2010). These modifications can in turn influence the ability of proteins to interact with the microtubule, such as motor proteins (Reed et al. 2006).

While the majority of regulatory sites are located at the outer face of the microtubule cylinder or at tubulin's C-terminal tail, another regulatory site is found in the lumen. Acetylation of α-tubulin's lysine40, via the tubulin acetyltransferase (αTAT) is correlated with long-lived and stable microtubules (Palazzo et al. 2003, Hubbert et al., 2002; Matsuyama et al. 2002). The ability to acetylate and deacetylate microtubules provides a tunable mechanism for regulating dynamic instability. Interestingly, the presence of αTAT, and not the sole presence of the acetyl group, seems to be necessary for the additional

stability of microtubules assembled in-vitro (Haggarty et al. 2003). The current model states that the small αTAT enzyme diffuses into the lumen through the terminal pore and slowly catalyzes the addition of acetyl groups to α-tubulin at lysine-40 (Soppina et al. 2012, Syzk et al. 2016). Remaining bound to the lumen, αTAT stabilizes the lattice from the lumen. The reverse reaction of deacetylation is performed primarily by a histone-deacetylase HDAC6, with functional redundancy provided by other HDAC family members (Dompierre et al. 2007).

One hypothesis for the structural effects of tubulin acetylation suggests that an inter-protofilament salt bridge is responsible for regulating the interactions between protofilaments and thus may regulate protofilament number (Cueva et al. 2012). Interestingly, electron micrographs do not indicate any gross structural changes to the microtubule itself compared to non-acetylated microtubules. It remains to be confirmed whether acetylation endows stability or rather accumulates on low-turnover tubulin subunits that have been stabilized in other ways. Nonetheless, tubulin acetylation has cellular consequences. For example, multiple lines of evidence indicate that acetylation improves the affinity and processivity of kinesin-based molecular transport (Konishi and Setou, 2009; Reed et al., 2006).

Mechanism of Action of Microtubule Targeting Agents I: Anti-cancer efficacy, Binding Sites and Effects on Microtubules

The anti-cancer activity of microtubule targeting drugs is widely believed to derive from their ability to alter normal regulatory mechanisms controlling microtubule dynamics. Rapidly dividing cells such as cancer cells are especially dependent on the MT network and are therefore more sensitive to drug induced changes in MT dynamics (Jordan and Wilson 2004). It is generally accepted that microtubule targeting agents (MTAs) combat tumor growth by altering the growing and shortening dynamics of microtubules that are essential for cells to undergo chromosome segregation and mitosis (Giannakakou et al. 2002; Jordan and Wilson 2004). Cells rely heavily on properly functioning MTs during mitosis to form spindles that organize and allocate genetic material to their progeny by binding to kinetochores. Disruption of these essential functions lead to deleterious effects and cell death through apoptosis (Argyriou et al. 2012; Fehrenbacher 2015; Field et al. 2014; Jordan and Wilson 2004; Poruchynsky et al. 2015).

While all MTAs target microtubules, various MTAs differ greatly in their mechanisms of microtubule binding and their effects upon microtubule dynamics. There are two main classes of microtubule targeting drugs that are grouped according to their effects on microtubules: 1) compounds that shift the equilibrium toward polymerized microtubules and 2) compounds that shift the equilibrium toward soluble tubulin subunits. Both mechanisms of action result in apoptosis and are effective in reducing the growth of various types of cancers. Paclitaxel, a first-line agent of the taxane class, binds along the inner surface of the entire microtubule length to a binding site in the β-subunit, but not to soluble tubulin, to promote stabilization and net microtubule polymerization that is driven in large part by suppression of shortening events (Jordan 1993 et al., Derry et al. 1995, Parness and

Horwitz 1981; Nogales et al., 1995). Similarly, ixabepilone (an epothilone) stabilizes the microtubule lattice and thus results in an excess of microtubule polymer leading to an inability of the cell to complete mitosis. In contrast, eribulin (a halichondrin) binds only at the plus (+) ends of microtubules and to free tubulin subunits, promotes microtubule dynamic instability and net microtubule depolymerization (Jordan et al., 2005; Smith et al., 2010; Bai et al.,2011). Another molecule in the class of destabilizing drugs, vincristine (a vinca alkaloid) binds to tubulin and microtubules and promotes depolymerization and destruction of mitotic spindles. Importantly, the most important effects of these agents (anti-mitotic) are based on their ability to suppress spindle-microtubule dynamics and not by changing microtubule polymer mass. Drugs that increase or decrease microtubule polymerization at high concentrations suppress dynamics at 10-100 fold lower concentrations. Thus it simplifies the story to consider MTAs as either polymerizing or depolymerizing however it seems to be their chemotherapeutic effects on dynamics that mitotically blocks cells and initiates apoptosis (Jordan and Wilson 2004).

Nociception and susceptibility of peripheral nerves

The peripheral nervous system has evolved to detect and transmit environmental stimuli to the central nervous system. As such, many of the neurons in the peripheral nervous system (PNS) have taken on extremely elongated morphologies. Indeed, many of the nerve cells of the PNS are among the longest cells in the human body. For the axons of sensory neurons innervating the hands and feet, cells send processes from their cell bodies just outside the spinal cord to the periphery. Their axons are contained in tightly packed bundles that eventually terminate at muscle tissue, in encapuslated endings (such as Meisner's or Pacinian corpuscles), or in free, unencapsulated endings. Each bundle is organized and

protected by Schwann cells, which may or may not myelinate the axons contained within the bundle. There are two major classes of neurons: the fast, large myelinated Aδ fibers which are responsible for perception of intense mechanical and thermal stimuli, and the slow, smaller unmyelinated C fibers which transmit thermal, mechanical, and chemical information (Woolf 2007). Thin, unmyelinated axons are organized into Remak bundles protected by a single Schwann cell. The cell bodies, or soma, of the long sensory axons of the sciatic nerve are organized in the dorsal root ganglia (DRG), positioned just outside of the spinal cord in the dorsal horn. The speed of electrochemical transmission is directly proportional to the diameter and degree of myelination. Fast myelinated Aδ fibers transmit action potentials at 5-30 m/s and respond to intense mechanical and thermal stimuli while the smaller unmyelinated C fibers respond at 2 m/s and respond to thermal, mechanical, and chemical stimuli (referred to as "polymodal").

Although the axonal and somal compartments are of the same cells, the long axons and cell bodies are highly specialized and distinct from one another in their structure and function. For example, axonal microtubules are more stable/less dynamic than cell body microtubules (Janke 2014; Song and Brady 2015). Therefore, it is reasonable to hypothesize that somal and axonal microtubules may respond differently to stress and stimuli (e.g., chemotherapeutic assault).

The neural process of encoding and processing noxious stimuli, termed nociception, is transmitted through specialized sensory nerve fibers called nociceptors. Noxious stimuli are damaging or potentially damaging stimuli including extremes of temperature, mechanical stimulation, and allogens that provoke an avoidance response. A nociceptor is thus a peripherally localized neuron preferentially sensitive to a noxious stimulus. Peripheral nociceptive axons arise from DRGs and terminate in free endings in peripheral tissues that

contain a diverse repertoire of receptors. These excitatory neurons release glutamate as their primary neurotransmitter and are generally electrically silent. They transmit an all or none action potentials when stimulated by noxious stimuli to produce a pain response that responds to the frequency of action potentials.

Schwann cells are resident microglia of the peripheral nervous system

Schwann cells are intimately involved with peripheral axons. They provide the myelin insulation required for signal propagation, trophic support, and even take on immune function in response to nerve injury. Schwann cells are required for peripheral nerve regeneration and together with macrophages, are responsible for the clearance of molecular debris following injury (Lutz and Barres 2014). Upon nerve injury, Schwann cells undergo transformations that include de-differentiation, proliferation, and subsequent re-differentiation to establish a pro-regenerative environment for axons (Rosenberg et al 2012).

Specialized function of microtubules in neurons

After development, neurons no longer undergo cell division. Their long processes are specialized to transmit electrical impulses from the periphery of an organism into the central processing centers such as the spinal cord and brain. Some cells must be extremely long to cover the great distances required between input locations and the CNS. In some peripheral nerve fibers, the distance from the nucleus to distal end of the axon can be longer than 1m! This is an enormous distance over which to maintain homeostasis, as the soma of each cell is the protein-producing center and needs to package and translocate newly synthesized proteins to the distal tips. Each nerve ending and synapse is rich with a variety of channels and receptors that detect many different stimuli from the environment (Julius and Basbaum

2001). The different requirements of microtubules in different neuronal compartments dictates that they need to behave differently. Indeed, the post-translational modifications of microtubules in axons differ from those in cytoplasmic microtubules (Janke and Kneussel 2010). In neurons, the axon must be maintained as a semi-permanent structure, and microtubules are one of the primary components of the axonal cytoskeleton. Axonal MTs must establish and maintain a stable microtubule lattice to provide intact structure and transport capabilities to and from the soma.

Transport of cargo along microtubule networks

The polarity of microtubules allows directional movement of motor proteins in a retrograde direction towards the soma or anterograde direction toward the distal synapse. Different motor proteins exhibit a preference for directional travel along microtubule networks: dynein transports retrograde cargo while the kinesin family of proteins directs anterograde cargo (Morfini et al. 2011)

Neurons require vast amounts of energy to repolarize their membranes after depolarization. This energy requirement means that mitochondria must constantly be supplied from the nucleus to the distal ends of the axon to maintain proper resting membrane potentials. Among the many cargoes that rely on microtubules for transport, mitochondria are one of the most abundantly transported organelles along the microtubule cytoskeleton in neurons (Millecamps and Julien 2013). These ATP-producing machines are targeted for release from microtubules at nodes of Ranvier where channels are clustered (Pareyson et al. 2015, Saxton and Hollenbeck 2012).

In addition, many proteins synthesized in the ER are loaded onto microtubules in vesicles and shipped to distal processes. These proteins include synaptic proteins, channels,

cytoskeletal subunits, and microtubule associated proteins. Interestingly, a small amount of mRNA bound to ZBP (zip-code-binding) proteins is also loaded onto kinesins for anterograde trafficking, which supports the hypothesis of local protein translation in distal axons (Yoo et al. 2013, Merianda et al. 2013).

Retrograde trafficking along microtubules is primarily driven by minus-end directed dynein motors. The various retrograde cargoes include survival factors (NGF/TrkA), lysosomes (containing proteins to be degraded), damaged mitochondria, and injury response signals (Morfini 2011). When the injury response is activated in the distal axon, retrograde signaling results in altered gene expression in the nucleus (Watkins et al. 2013). One example is the JNK-interacting proteins that are found at the JNK-interacting family of linkage proteins (JIPs) that interface cargo with motor protein domains. When JNK is activated via phosphorylation, it in turn activates the transcription factor c-Jun via phosphorylation to induce an injury response. Genes activated by this transcription factor include both degenerative and pro-regenerative proteins, which prepare the neuron for both programmed axon degeneration and subsequent regrowth (Tedeschi and Bradke 2013).

Chemotherapy Induced Peripheral Neuropathy

Microtubule-targeting chemotherapy drugs have been among the most successful treatments in slowing the progression of many different types of cancers over recent decades. However, their ability to control rapidly proliferating cancer cells continues to be marred by the induction of severe dose-limiting side effects. MTAs are generally delivered to patients systemically, exposing both tumor and non-tumor tissues to the chemical assault, which can lead to serious side effects including chemotherapy-induced peripheral neuropathy (CIPN) (Argyriou et al. 2012; Argyriou et al. 2014; Carlson and Ocean 2011; Grisold et al. 2012).

For example, the untargeted systemic injection of these potent anti-neoplastics exposes the microtubule-rich axons of the peripheral nervous system to their effects.

CIPN impedes favorable clinical outcomes and represents a major obstacle to chemotherapy due to the frequency of dose reductions and elective treatment cessations. This debilitating sensory neurotoxicity of the limb extremities often results in attenuation of dosage, up to complete cessation of chemotherapy, such that very aggressive cancers cannot be adequately controlled (Argryiou et al. 2012). Traditional pain management strategies such as analgesics, anti-inflammatories, and opioids have had negligible success in reducing chronic neuropathic pain. Part of the challenge in developing effective treatments for managing neuropathy during chemotherapy is that the underlying cellular mechanisms of chemotherapy-induced peripheral neuropathy are currently undefined.

A number of clinically based scales are available for grading of the severity of CIPN, which are based upon the extent of disruption of daily living activities. Although none has achieved universal acceptance, the National Cancer Institute's Common Terminology Criteria for Adverse Events (NCI-CTCAE) is one of the most commonly used scales. It ranges from grade 1, representing asymptomatic effects, to grade 4 representing severe disruption in activities of daily living and life-threatening consequences requiring immediate intervention (Carlson and Ocean 2011, Argyriou et al. 2014; Fehrenbacher 2015). Currently there is no efficacious therapy for peripheral neuropathy besides dosage reduction, leading to poorer patient outcomes (Jaggi and Singh 2012). Traditional pain management strategies including analgesics and anesthetics have been largely unsuccessful (Argyriou et al. 2012). A clinician's ability to treat aggressive cancers is dependent on the management of this dose-limiting condition, and improved chemotherapy will result from more effective control of neuropathy.

For patients receiving microtubule targeting agents, approximately 30–40% will experience severe CIPN symptoms that are largely sensory in nature. The described pain includes hypersensitivity to pressure and hot or cold temperatures, tingling, burning sensations, numbness, and/or a loss of deep tendon reflexes. Symptoms can occur shortly after the first dose of some MTAs, and are closely correlated dosage: either single or cumulative (Argyriou et al. 2008). These symptoms often begin in the distal extremities (i.e., fingertips and toes) and progress proximally up the arms and legs, suggesting that the longest nerves are most vulnerable (Argyriou et al. 2012; Carlson and Ocean 2011; Fehrenbacher 2015; Grisold et al. 2012; Windebank and Grisold 2008).

Most clinical investigations on the incidence and severity of neuropathy during treatment are compounded by the reality that patients often receive different doses on different schedules. In clinical practice patients are also often treated with combinations of drugs that are individually known to cause CIPN and then receive sequential treatments for recurring cancers with additional CIPN-inducing drugs. For example, paclitaxel is indicated as a first line therapy for many types of cancers. If a patient becomes resistant to paclitaxel then usually an epothilone regimen, such as ixabepilone (a second line defense) is begun. If the patient's cancer continues to elude epothilone treatment, a third line defense is needed such as eribulin. Thus the difficulty in comparing the incidence of neuropathy for ixabepilone and paclitaxel is that patients will likely already have pre-existing neuropathy from prior paclitaxel treatment when they receive additional or combinatorial therapies.

Incidence, Progression, and Reversibility of Clinical CIPN Symptoms

The onset, rate of progression, severity and reversibility of CIPN symptoms vary greatly among different MTA treatments (Argyriou et al. 2012; Carlson and Ocean 2011;

Windebank and Grisold 2008). The incidence and severity of MTA-induced neuropathy depend on many factors such as the agent used, cumulative dose, dose intensity, treatment schedule, duration of infusion, pervious chemotherapy regimens, and agents used in combination (Lee and Swain 2006). The following section summarizes the distinct characteristics for each of four commonly used microtubule-targeting agents. The diversity of these agents in their rates of onset, progression, and recovery allows correlative relationships of their cellular and molecular effects to be identified so that the underlying molecular mechanisms can be better understood.

Paclitaxel

Paclitaxel neuropathy is primarily sensory in nature and includes painful numbness, decreased vibration sensitivity, and loss of deep tendon reflex (Lipton et al. 1989, Stubblefield et al. 2009). The incidence of severe neuropathy (grades ¾) ranges from 2-32% at doses from 100-300 mg/m^2 over a 3 hour infusion period (Gradishar et al. 2005, Jones et al. 2005, Seidman 1995). Patients treated with paclitaxel tend to exhibit a higher frequency of severe CIPN than do patients treated with eribulin (Carlson and Ocean 2011, Windebank and Ocean 2011, Argyriou et al. 2012; Gradishar et al. 2011). Generally, symptoms of taxane-induced CIPN improve or resolve within the first 3–6 months after the discontinuation of treatment (Grisold et al. 2012). While 50% of patients treated with paclitaxel recovered within 9 months, symptoms persisted in 41% of patients at 3 years, suggesting that neurotoxicity can persist long-term (Pace et al. 2007). After a median follow up of 23.5 months, 40.9% of patients showed persistent PIPN (de la Morena Barrio et al. 2015).

Ixabepilone

Ixabepilone is indicated for the treatment of breast cancer after taxane failure and is primarily sensory with painful numbness and burning in the extremities similar to paclitaxel. The incidence of severe neuropathy ranges from 12-20% at doses of 40-120 mg/m^2 (Roche et al. 2007, Steinberg et al. 2008, Thomas et al. 2007). In a study comparing neuropathy induced by eribulin and ixabepilone, the median time to onset for ixabepilone was 2.7 months from the start of treatment (Vahdat et al. 2013). The median and maximum times to resolution of ixabepilone neuropathy were 1.2 and 2.3 months, respectively (Perez et al. 2007, Vahdat et al. 2013). Interestingly, the reversibility of neuropathy after dosage intervention appears to be more rapid with ixabepilone than with taxanes (Swain and Arezzo 2008).

Vincristine

Out of all the agents described here, vincristine induces the highest levels of severe neuropathy and is associated with a severe mixed sensory/motor polyneuropathy. Grades ¾ neuropathy present at the relatively low dose of 2 mg/m^2 (Sarris et al.2000). Vinorelbine, another vinca alkaloid, requires higher doses of 25-30 mg/m^2 to induce severe neuropathy in about 6% of patients and presents symptoms within the first 3 months (Vogel et al. 1999). While symptoms are usually reversible within 2 months after dosing, a long-term follow up of vincristine-treated patients revealed that 32% had mild but persistent sensory symptoms 34 months after the end of treatment (Postma et al. 1993).

Eribulin

Eribulin is a more recently approved third line therapy for metastatic breast cancer therapy for patients who had previously received at least two prior chemotherapy regimens, including an anthracycline and a taxane. Eribulin has a more favorable safety profile and is normally provided at low doses similar to vincristine at 1.4 mg/m^2, over a much faster infusion time of 3-5 minutes due to its improved solubility (Vahdat et al. 2013). Eribulin is associated with the lowest incidence of neuropathy of the agents described here, from 3-8% experiencing severe neuropathy (Puhalla and Brufsky 2008, Cortes et al. 2011). Compared to paclitaxel, the median time to clinical onset of eribulin-induced neuropathy is more delayed at 8.3 months from the start of treatment. However, symptoms resolve more quickly at a median time to total resolution of 1.8 months and lasting up to 11 months from the last dose only in rare cases (Vahdat et al. 2013). Thus eribulin produces more mild, later onset, and more quickly resolving neuropathy in patients compared to paclitaxel, ixabepilone, and vincristine.

Effects of MTAs on peripheral nerve morphology and function

The free endings of nociceptors contain many specialized receptors such as the transient receptor potential (TRP) family of ion channels (Woolf and Ma 2007). Spinal administration of antisense oligonucleotides to the TRP family member TRPV4 abolished taxol-induced mechanical hyperalgesia in a rat model of peripheral neuropathy (Alessandri-Haber et al. 2004). A current debate in the field is whether preferential degeneration of either Aδ or C fibers play a role in CIPN. There is building evidence that taxol-induced sensory disturbance is characterized by preferential impairment of myelinated Aδ fiber function (Dougherty et al. 2004, Flatters et al. 2006). Spontaneous discharge by both fibers has been reported in response to paclitaxel and vincristine (Xiao and Bennet 2008). Skin

biopsies of human patients treated with either vincristine or paclitaxel showed deficiencies in mechanoreceptors and intraepidermal nerve fiber densities in the reported painful tissues (Boyette-Davis et al. 2011). In a recent study comparing the effects of paclitaxel, ixabepilone, and eribulin on peripheral mouse tail nerves, our collaborators found a significant decrease in nerve conduction velocity (NCV) and nerve conduction amplitude (NCA) following paclitaxel and ixabepilone treatment at their maximum tolerated doses for two weeks. Severe degenerative pathologic changes in morphology such as cytoplasmic inclusions, clear vacuolations, and swelling phenomenon have also been observed (Tanner et al. 1998). Eribulin, which causes less neuropathy in humans, did not induce significant NCV or NCA deficits and caused milder morphological changes in the sciatic nerve, indicating that peripheral neuropathy in mice correlates with electrical and morphological evidence of axon degeneration (Wozniak et al. 2011). The effects observed by these drugs in both skin biopsies and peripheral nerve electrophysiology point to axonal loss as an underlying mechanism for chemotherapy induced peripheral neuropathy. Understanding the molecular events leading to these electrophysiological and patholigcal effects is the central motivation for the work described in this thesis.

Models of CIPN

Animal models have proven useful to investigate how chemotherapies differ in their patterns of producing neuropathy, axonopathy and myelinopathy (Han et al. 2013). The maximum tolerated dose model is a commonly used animal model that involves establishing a maximum tolerated dose for each agent that is characterized by the loss of 20% of the animal's body weight. The MTD was defined as the highest dose level at which no more than 10% deaths occurred and/or at which no mice displayed more than 20% individual

weight loss and/or overt clinical signs of distress and/or inability to eat and drink, thus requiring euthanasia. Mice treated at their MTD's display reproducible dose-dependent reductions in caudal and digital nerve conduction velocities and amplitudes (Wozniak et al. 2011)

Relative Uptake and retention of each drug

MTAs penetrate peripheral nervous tissue at vastly different rates. Recent pharmacokinetic studies demonstrated that the tissue penetration index of the sciatic nerve for eribulin is 30 times that of paclitaxel (0.6 vs 0.02) (Wozniak et al. 2016). In contrast to their rapid clearance from plasma, both drugs were retained in sciatic nerve and DRG tissue. While plasma concentrations were undetectable at 24 hours following the last dose of 2-week MTD schedule, concentrations of paclitaxel and eribulin were maintained in sciatic nerve and DRG tissues for up to 26 days after the completion of dosing. Paclitaxel exposure reached maximal levels in the DRG after the first dose, while in the sciatic nerve there was accumulation with multiple doses. In contrast, eribulin exposure showed increasing accumulation in both DRG and sciatic nerve with multiple administrations (Wozniak et al. 2016).

Clinical considerations

The demonstration that eribulin induces less frequent severe CIPN than the widely used paclitaxel raises the question of its relative anti-cancer efficacy relative to paclitaxel. A lower incidence of severe peripheral neuropathy would be most meaningful if it were coupled with equal or greater anti-cancer efficacy. Unfortunately, to date there have been no

clinical studies directly comparing the anti-cancer efficacies of eribulin and paclitaxel in the clinical setting. That said, eribulin was FDA approved in 2010 as a third line therapy for patients with metastatic breast cancer who had previously received at least two prior chemotherapy regimens, including an anthracycline and a taxane. At the time of the pivotal Phase III EMBRACE trial which led to the FDA approval, there was no standard of care for third line metastatic breast cancer, so EMBRACE was designed, in conjunction with the FDA, as a two-arm study of eribulin monotherapy versus "treatment of physician's choice" (TPC), essentially capturing the individual judgments of hundreds of oncologists' decisions as to the best personalized treatment of their specific patients (Cortes et al. 2012). EMBRACE stipulated that enrolled patients must have progressed within 6 months or less of the latest chemotherapy (Cortes et al. 2012). As such, the statistically significant 24 % increase in median overall survival between the two groups (13.1 months vs. 10.6 months for eribulin versus TPC, respectively) indicates that many patients exhibited prolonged survival on the eribulin arm despite the fact that they had previously progressed on taxane-containing therapies. In addition, the preclinical work of Towle et al. (2001), demonstrated that eribulin is more effective at considerably lower doses than paclitaxel (at empirically determined MTD levels) in four different human tumor xenograft growth models in mice: potency differentials for eribulin versus paclitaxel based on complete tumor suppression ranged from 20- to 100-fold for different human tumors. Additionally, in these in vivo studies, eribulin consistently showed a wider therapeutic window compared to paclitaxel. Finally, eribulin showed an average 4.1-fold increased potency compared to paclitaxel on a molar basis in a library of eight human cancer cell lines, with ratios in the individual lines ranging from 2.0-fold to 27.8-fold. Thus, although no direct head-to-head comparisons of eribulin versus paclitaxel have been conducted, existing clinical evidence from the

EMBRACE Phase III clinical trial pointing to eribulin activity after progression on taxanes, coupled with consistent preclinical evidence of greater potency both in cancer cell lines and human tumor xenograft models, raise the possibility that eribulin is either an equipotent or more potent anti-cancer agent relative to paclitaxel. In this context, the apparently lower neuropathic effects of eribulin relative to paclitaxel in both the clinic and laboratory settings can be viewed as not simply a consequence of lower overall potency, but rather a bona fide reduction in one of the most significant and troubling side effects of treatment with these two agents.

Thesis Data

The identification of molecular players involved in the onset and progression of CIPN will allow for new strategies to block or prevent neurodegeneration in peripheral neuropathy and other neurological diseases. Since the timing of cancer treatment is known, a neuroprotective companion therapy for prevention of neuropathy would have great potential to minimize this toxic side effect. However, our knowledge of the underlying physiological mechanisms responsible for the induction of peripheral neuropathy by MT-targeting drugs remains surprisingly limited.

The overall goal of the experimental work undertaken in this thesis is to elucidate the cellular and molecular mechanisms of chemotherapy induced peripheral neuropathy. This project began with correlative work in an MTD mouse model to investigate the onset and recovery from morphological and biochemical effects that occur in peripheral nerves upon treatment with MTAs. We found that paclitaxel induced markedly more deleterious effects upon sciatic nerve morphology, such as nerve fiber loss and signs of axon degeneration (for example, solid circular regions of myelin signal lacking a phosphoneurofilament signal),

relative to the effects of eribulin (Benbow 2016). Additionally, eribulin had more potent positive effects upon microtubule biochemistry, creating an environment consistent with increased microtubule stabilization and growth. These findings led us to hypothesize that long-term treatment with eribulin generates a more functional microtubule cytoskeleton than does similar treatment with paclitaxel, accounting at least in part for the reduced levels of severe CIPN observed with eribulin-treated versus paclitaxel-treated patients.

To expand this work, we then examined the recovery from these initial effects over the course of six months. We found that (i) morphologically, sciatic nerve axons recover more rapidly in eribulin treated animals than in paclitaxel treated animals and (ii) biochemically, drug-induced increases in protein expression levels following paclitaxel and eribulin treatment are relatively transient. Interestingly, the effects of ixabepilone were mild compared to paclitaxel and eribulin despite its propensity for neuropathy in patients. Taken together, our data in mice indicate a milder onset and faster recovery with eribulin and ixabepilone treatment than for paclitaxel.

Finally, we developed an in-vitro cell culture model for studying the cellular and molecular mechanisms that regulate the cell's response to microtubule inhibition. We found that all agents reduced neurite area of neuronal cells at concentrations that coincided with a possible shift in microtubule mass and cytosolic α-tubulin acetylation. When the drug concentration that induced a 50% reduction in neurite area was compared to the concentrations that inhibit cancer cell proliferation, eribulin was different in that it was far less potent to neurons than it was in inhibiting cancer cell growth, indicating that neurons are more tolerant of eribulin's action as compared to ixabpilone, paclitaxel, and vincristine.

Chapter 1 Figures:

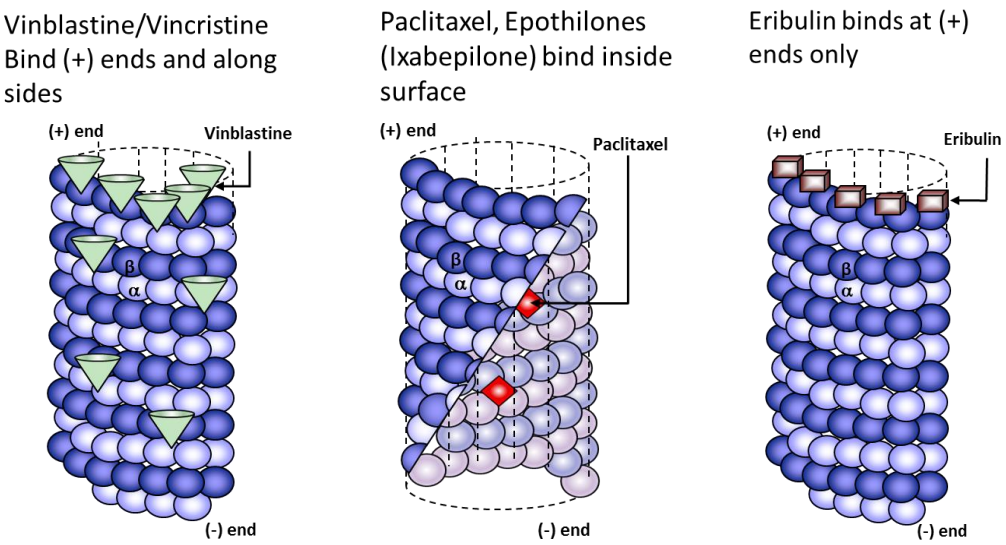

Figure 1. Binding characteristics of common microtubule targeting agents of the vinca family (left), taxane and epothilone families (middle), and halichondrins (right). Adapted from Jordan and Wilson 2004.

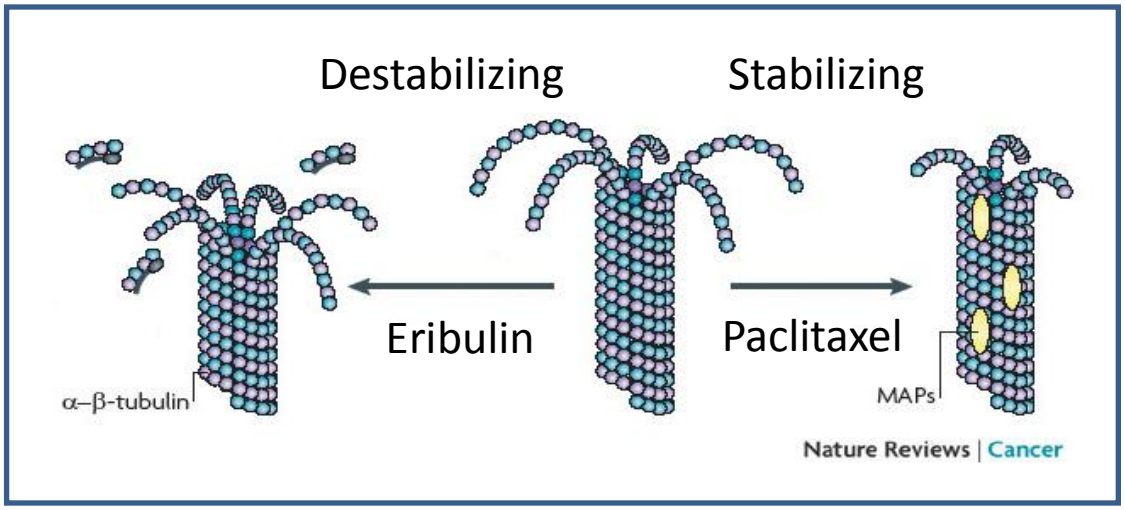

Figure 2. Examples of the mechanism of action of microtubule targeting agents. The mechanism of action of eriblin (destabilizes microtubules) and paclitaxel (stabilizes microtubules) are shown. Adapted from Kavallaris 2010.

Table 1. Incidence of Severe Neuropathy and Relevant Dosages of MTAs

Drug	Incidence of Grade 3/4 Neuropathy (% of patients)	Patient dose per cycle (mg/m^2)	Maximum tolerated dose in mice (mg/kg)§
Eribulin	7.8*	1.4	1.25
Vincristine	31*	2	0.85
Paclitaxel	2-32*	100-300	30
Ixabepilone	12-24**	40-120	3

* Carlson and Ocean. Clin Breast Cancer. 2011; 11, 2: 73-81

** Gradishar, Curr Onc Rep. 2011; 13: 11-16

§ Q2D3 dosing schedule, defined by 20% reduction in body weight

ND = not determined

Chapter II. Effects of Paclitaxel and Eribulin in Mouse Sciatic Nerve: A Microtubule Based Rationale for the Differential Induction of Chemotherapy-Induced Peripheral Neuropathy

Summary

Microtubule targeting agents (MTAs) often lead to treatment limiting and life threatening side effects, including chemotherapy-induced peripheral neuropathy (CIPN). The frequency of severe CIPN varies among different MTAs. Since the microtubule binding interactions and mechanisms of action also vary among MTAs, we hypothesized that these distinct mechanisms may underlie the variability in frequency of severe CIPN. Using a two-week, maximum tolerated dose model, we morphologically and biochemically analyzed sciatic nerves from mice treated with either paclitaxel or eribulin. These drugs differ in their manner of microtubule binding and mechanisms of action and reports indicate paclitaxel also induces a higher frequency of severe CIPN than does eribulin. Morphologically, paclitaxel increased the frequency of observed signs of axon degeneration more significantly than did eribulin. Alternatively, eribulin but not paclitaxel induced occasional myelin "halo" structures. Biochemically, paclitaxel, and eribulin both induced α-tubulin expression (~1.9- and ~2.5-fold, respectively) and tubulin acetylation, a marker for microtubule stability, (~5- and ~11.7-fold, respectively). Eribulin but not paclitaxel-induced EB1 expression ~2.2-fold while paclitaxel but not eribulin mildly suppressed EB3 expression. Both EB proteins are associated with microtubule growth. Eribulin's combination of relatively mild deleterious morphological effects coupled with more potent biochemical changes promoting microtubule stability and growth in mice correlate with lower frequencies of severe CIPN in humans. We suggest that these eribulin-induced effects create a relatively stable microtubule

network that compensates, in part, for the toxic anti-cancer effects of the drug, leading to fewer reported incidences of CIPN than for paclitaxel.

Introduction

The anti-tumor activity of MTAs stems from their ability to alter normal regulatory mechanisms controlling microtubule dynamics and microtubule-based transport, which can in turn lead to tumor cell death (Argyriou et al. 2012; Field et al. 2014; Jordan and Wilson 2004; Poruchynsky et al. 2015). Unfortunately, MTAs also expose non-target tissues to chemical assault that can cause significant adverse side effects. As the peripheral nervous system is highly susceptible to deleterious MTA-induced effects, chemotherapy-induced peripheral neuropathy (CIPN) is among the most frequent and serious side effects of MTA treatment. CIPN can cause symptoms ranging from numbness and tingling to hypersensitivity and severe neuropathic pain. These symptoms generally begin at the distal extremities, such as the fingertips and toes, and progress proximally toward the trunk, suggesting that the longest axons are the most vulnerable (Argyriou et al. 2012; Carlson and Ocean 2011; Windebank and Grisold 2008). These symptoms can become treatment limiting, and in some cases, even life threatening. The only strategies to address CIPN are to either reduce drug dosage or cease treatment altogether, both of which undermine attempts to control a patient's cancer. Since MTAs are a major component of available clinical anti-cancer strategies, CIPN can be a major obstacle to successful clinical anti-cancer efforts.

The severity, clinical presentation and reversibility of neuropathic symptoms can vary greatly between different MTA treatments (Argyriou et al. 2012; Argyriou et al. 2011; Carlson and Ocean 2011; Windebank and Grisold 2008). For example, paclitaxel treated patients generally exhibit a higher frequency of severe neuropathy than do eribulin treated

patients (Carlson and Ocean 2011; Gradishar 2011). Consistent with these observations, paclitaxel treatment of mice causes significant axon loss, morphological changes in myelin and reduction of nerve conduction velocity whereas eribulin treatment generated significantly milder morphological changes with no impairment of conduction velocity (Boehmerle et al. 2014; Wozniak et al. 2011). Importantly, different MTAs also differ greatly in their mechanisms of microtubule binding and their effects upon microtubule dynamics. For example, the taxanes (e.g. paclitaxel) bind the inner surface along the entire length of microtubules, tend to stabilize microtubules and to promote net microtubule polymerization. These activities are driven, in large part, by suppression of microtubule shortening events (Derry et al. 1995). In contrast, eribulin (a halichondrin) binds only at the plus (+) ends of microtubules, promotes microtubule dynamic instability and promotes net microtubule depolymerization. These activities are driven, in large part, by binding to soluble tubulin and shifting the balance between soluble tubulin and microtubules, thus resulting in net loss of microtubule polymer (Jordan et al. 2005; Smith et al. 2010). Over the past two decades, it has become increasingly clear that the regulation of microtubule growing and shortening events is key to understanding microtubule action and the resulting cellular consequences, thereby providing a potential molecular link between MTA action and clinical observations. Taken together, these observations lead us to hypothesize that different patterns of CIPN induced by different MTAs are the result of their different underlying mechanisms of action.

In addition to their important roles in dividing cells (i.e., cell division and transport), microtubules are also essential for many functions in post-mitotic mature neurons, including the maintenance of highly elongated neuronal morphologies and axonal transport, the rapid movement of cargo between neuronal cell bodies and distal axonal regions (Carlson and

Ocean 2011). One often stated hypothesis for MTA-induced CIPN posits that the drugs interfere with normal microtubule-dependent axonal transport, which in turn initiates downstream biochemical and morphological neurodegeneration (Morfini et al. 2009). Consistent with this model, paclitaxel treatment can slow the rate of kinesin-driven anterograde transport more than eribulin treatment (Lapointe et al. 2013), in parallel with the relative neuropathic potencies of these two drugs.

Cells possess numerous mechanisms to regulate microtubule dynamics. For example, α–tubulin subunits in relatively stable microtubules are often acetylated at lysine-40. While tubulin acetylation has historically been viewed as a marker but not a cause of microtubule stability, recent work suggests a more active role. For example, increasing α–tubulin acetylation can rescue dysfunctional axonal transport and locomotor deficits in Drosophila (Godena et al. 2014) and can promote recruitment of dynein and kinesin-1 to microtubules in vitro and in mammalian cells (Dompierre et al. 2007). Additionally, microtubule dynamics can be influenced by a number of different microtubule-associated proteins (MAPs), including the end binding proteins EB1 and EB3. EB1 has been implicated in promoting microtubule growth and axonal transport while EB3 can serve as a link between dynamic microtubules and the actin cytoskeleton (Geraldo et al. 2008; Gu et al. 2006; Jaworski et al. 2009). We have previously proposed that proper function and viability of cells, including post-mitotic neurons, requires that cells actively maintain and regulate their microtubule dynamics within a window of tolerable activity levels (Bunker et al. 2004) – both overly dynamic and overly stable microtubules can lead to neuronal cell death.

Here, we sought to compare cellular and molecular changes within mouse sciatic nerves following treatment with two different MTAs possessing different mechanisms of action and different probabilities of inducing severe CIPN. The goal was to correlate cellular

and molecular effects with the frequency of inducing severe CIPN. Specifically, we compared mice treated at their maximum tolerated dose (MTD) of either paclitaxel or eribulin with vehicle treated control mice. We found that paclitaxel induced markedly more deleterious effects upon sciatic nerve morphology, such as nerve fiber loss and signs of axon degeneration (for example, solid circular regions of myelin signal lacking a phosphoneurofilament signal), relative to the effects of eribulin. Additionally, eribulin had more potent positive effects upon microtubule biochemistry, creating an environment consistent with increased microtubule stabilization and growth. Taken together, we propose that eribulin treatment generates a more stable and functional microtubule network than that produced by paclitaxel treatment. This perspective provides a molecular rationale for the observation that eribulin induces less frequent CIPN than does paclitaxel in human patients.

Materials and Methods

Antibodies

The following primary antibodies were used in immunohistochemical analyses: anti-α-tubulin (Millipore, 04-1117, 1:100 dilution (Zhang et al. 2011)), anti-acetylated tubulin (Cell Signal, 5335, 1:800 dilution, (Creppe et al. 2009)), anti-EB1 (Millipore, AB6057, 1:500 dilution, (Vitre et al. 2008)), anti-EB3 (Santa Cruz, SC-101475, 1:200 dilution, (Levy et al. 1994)), anti-myelin basic protein (Millipore, AB9348, 1:100 dilution, (Heller et al. 2014), anti-phosphoneurofilament (Covance, SMI-31R, 1:2000 dilution, (Choi et al. 2008)). FITC, Cy3 and Cy5 conjugated secondary antibodies were purchased from Jackson ImmunoResearch and used at 1:200 dilution.

Drugs

Eribulin mesylate (synthesized at Eisai Research Institute and stored at -80^{o} C in the dark) was dissolved in 100% anhydrous DMSO (Sigma-Aldrich) to produce a 10 mg/ml stock solution, which was aliquoted and stored at -80^{o} C until the day of administration. Each administration day, the stock solution was thawed and diluted with saline to a final concentration of 0.25 mg/mL in 2.5% DMSO/97.5% saline yielding dosing solutions in a 10 mL/kg volume. Paclitaxel, (LC Laboratories, Woburn, MA; stored at -20 ^{o} C in the dark) was dissolved in ethanol (100%) at 10% of final volume. An equal volume of cremophor (10% of final volume) was then added and the mixture re-vortexed for about 10 min. Immediately prior to injection, ice cold saline was added to final volume (as 80% of final), and the solution was maintained on ice during dosing. Dosing solutions were made fresh daily and dosed in a volume of 10 mL/kg.

Animal Studies

Female BALB/c mice (approximately 7–8 weeks old at onset of dosing) were obtained from Harlan Laboratories Inc. (Indianapolis, IN) and maintained with free access to water and a standardized synthetic diet (Harlan Teklab). Animal housing and procedure room temperature and humidity were maintained at 20 ± 2^{o} C and 55 ± 10%, respectively. Artificial lighting provided a 12 h light/12 h dark cycle (light 7 a.m.–7 p.m.). All experimental protocols were approved by the Institutional Animal Care and Use Committee of Sobran Inc (Baltimore, MD) and adhered to all of the applicable institutional and governmental guidelines for the humane treatment of laboratory animals. Mice were randomly assigned into vehicle, eribulin or paclitaxel treatment group (n= 5)

Drugs were administered 3 times a week (Monday, Wednesday, Friday) for 2 weeks into the caudal vein at a dose that was earlier determined to be MTD (Wozniak et al. 2011), specifically 30 mg/kg and 1.25 mg/kg for paclitaxel and eribulin, respectively. Twenty-four hours after administration of the sixth and final dose, mice were deeply anesthetized with 10% chloral hydrate and euthanized by transcardial perfusion with PBS followed by 4% paraformaldehyde in 0.1 mM phosphate buffer, pH 7.4, for 10–15 min. Subsequently whole mid-thigh sections of sciatic nerve were dissected and placed in perfusion fixative at 4^{o}C.

Sectioning

Fixed nerves were embedded in 10% agarose and cross-sectioned using a Leica VT1000S vibratome. 100μm slices were taken in the distal to proximal direction in 1X PBS at room temperature, then transferred to a 4% paraformaldehyde/PBS solution for storage at 4^{o} C until staining. Approximately 0.75 cm of Sciatic nerve tissue was sectioned.

Antibody Staining

Sections were stained from both proximal and distal ends from a total approximate length of 0.75 cm of nerve. Individual sections were stained with antibodies recognizing α-tubulin, acetylated tubulin , EB1 or EB3. All sections were also stained with anti-phosphoneurofilament and anti-myelin basic protein as internal controls and in order to identify regions of interest (for example, neuronal cells). Sections were incubated in PBT blocking agent (1X PBS (1.37M NaCl, 27mM KCl, 100mM Na_2HPO_4, 18mM KH_2PO_4), 0.1% TritonX-100, 1% BSA, 1% donkey serum) overnight. Sections were then incubated free floating with primary antibodies for seven days, rocking at 4°C. The long duration of incubation was used to promote better antibody penetration. Primary antibody dilution

solutions were removed and sections washed four times with PBT on a shaker at room temperature (8 minutes/wash). Sections were next incubated with secondary antibodies for two days. Secondary antibody dilutions were removed and sections washed as described above. Sections were then mounted on glass slides using ProLong Gold mounting media with DAPI (Life Technologies P36935). Slides were sealed and stored at 4°C. Each slide contained one section from each of the four treatments (eribulin and its vehicle, paclitaxel and its vehicle, Figure S1A), all stained simultaneously with the same antibody solution.

Fluorescence microscopy

Images were collected using an Olympus Fluoview 1000 Spectral confocal system equipped with 405nm, 488nm, 559nm, and 635nm laser lines, and PMT detectors. Each slide containing one section from each of the four treatments and incubated in the same antibody solution was imaged with the same exposure settings, determined by identifying the brightest-fluorescing section on each slide. 20 μm sample depths of two sections from each nerve (one relatively proximal and one relatively distal) were imaged by sequential laser scanning and 0.5μm step size with an Olympus PLANAPOSC 60x (1.40 NA) high refractive index oil immersion objective. In practice, we imaged and assessed 120 μm of tissue from each end of the 0.75 cm nerve length. This corresponds to 20 μm sections for each α-tubulin, acetylated tubulin, EB1 and EB3, or 80 μm total from each end. Two additional sections were cut from each end for backup and/or testing of other antibodies. As noted above, all sections were also stained with anti-MBP and anti-phosphoneurofilament. Where applicable, the anti-MBP and anti-phosphoneurofilament signals in these additional sections were included in the statistical analyses.

Image and Statistical Analysis

Images from each slide were imported into Imaris Version 7.5.2 (Bitplane, Zurich, Switzerland) and rendered into three dimensional maximum intensity z-stack projections for analysis. To assess changes in gross morphological structure, nuclei, myelin and axons were identified using DAPI stain, anti-myelin basic protein and anti-phosphoneurofilament, respectively. Using the Imaris software surfaces tool, we identified nuclei, myelin sheaths and axons based on the fluorescent signal from their appropriate antibody or stain, manually thresholding signal to background noise. To maintain consistency in object identification in similarly treated samples, one set of threshold parameters was applied to those sections stained with the same antibody solutions and imaged with the same microscope settings. After identification, these objects were counted automatically. Signs of axon degeneration, defined as solid, circular regions of myelin lacking a phosphoneurofilament signal, were identified and counted manually and compared with the total number of myelin objects identified by the software. For axon density measurements, the image stack was flattened in Fiji using the maximum intensity setting and the number of axons per region of interest (defined by phosphoneurofilament signal) was quantified using Imaris.

In order to quantify fluorescence changes, fluorescence values were collected and normalized within each slide first, before comparisons were made between slides. Normalization of axonal Cy2 fluorescent signals (depicted in Supplementary Figure S1) was accomplished by first identifying the axonal region using the anti-phosphoneurofilament (PNF) signal to mask the axon regions specifically differentiating axons from surrounding Schwann cells or other cell types present. The raw values of Cy2 fluorescence were determined for each axonal region within the treatment field of view. The mean Cy2 signal per axon was calculated for each treatment to give the "treatment mean." These values were

normalized by dividing each treatment mean by the sum of all four treatment means per slide. This method was employed in order to retain the natural variability seen in vehicle treatments.

Student's T-tests with Bonferroni correction for multiple comparisons were used to identify significant differences in mean comparisons of the drug groups to their respective vehicles and between the two drug treatment groups, (*$p<0.0167$, **$p<0.003$, ***$p<0.003$). In some cases, the singular comparison of the drug to appropriate vehicle group by Student's T-test provided additional insight.

Results

Paclitaxel and eribulin differentially induce morphological changes

We began our analyses by quantifying the neurodegenerative effects of paclitaxel and eribulin on sciatic nerve axon density, defined by anti-phosphoneurofilament (PNF) signal, in cross-sections of nerves from drug treated mice and vehicle treated controls. Paclitaxel treatment resulted in a statistically significant 30% reduction in axon density (196.3 ± 18.52 axons per 10^4 μm^2 compared to 281.8 ± 22.2 axons per 10^4 μm^2 for its vehicle control; Figures 1A, 1B, 2A and 2B). In contrast, eribulin administration generated a 21% reduction in axon density (234.1 ± 18.52 axons per 10^4 μm^2 compared to 296.6 ± 18.43 per 10^4 μm^2 for its vehicle controls (mean ± SEM,; Figure 1A, 1B, 2C and 2D). While neither of these reductions are statistically significant when compared using a Bonferroni corrected Student's T-test, it appears that the densities reported here trend toward axonal loss after treatment with both eribulin and paclitaxel.

We next sought to examine the effects of paclitaxel and eribulin upon axon-myelin morphology by quantifying the extent of fiber disruption in cross-sections of sciatic nerves

harvested from drug-treated mice relative to vehicle treated, control animals. Paclitaxel treatment increased the percent of observed signs of axon degeneration relative to total myelin positive objects. "Signs of axon degeneration" are defined as structures with clear anti-myelin basic protein (MBP) signals but lacking any anti-PNF signal (Figure 1B-D and figure 2). Specifically, we observed 6.6% of myelin sheaths (anti-MBP stained objects) in paclitaxel treated nerves exhibiting signs of axon degeneration (vs. 0.21% for vehicle treated nerves; $p<0.0003$). In contrast, eribulin induced three fold fewer degenerative axons (2.2% vs. 0.32% for vehicle treated nerves; $p<0.0003$). Additionally the difference between paclitaxel and eribulin treated groups is also statistically significant ($p<0.003$). Similar degenerative events have been described in several instances of neuronal toxicity and injury, where the space normally occupied by the axon is lost and has been replaced by myelin (Muguruma et al. 2006; Schnaar et al. 2014; Wozniak et al. 2011). Additionally, in nerves from both paclitaxel and eribulin treated mice, we qualitatively observed an increase in myelin fragmentation (thinning and discontinuity of sheath) that often lacked an associated phosphoneurofilament stain (For example, see 2E-H). Given that these morphological changes were almost exclusively observed in tissue from drug treated mice, we conclude that these are treatment induced changes.

Finally, we occasionally observed an unusual morphology, specifically, a thinly myelinated axon fiber within a separated and larger diameter concentric myelin ring, which we have termed a "halo" or "double ring". (Figure 2D, 2H [see arrows]). This feature was more commonly observed in eribulin than paclitaxel treated nerves, and very infrequent in vehicle treatments.

We next hypothesized that there could be changes among the non-neuronal cell population within the nerve in response to neurodegenerative processes. As the cell nuclei

for sciatic nerve axons are located within the dorsal root ganglia far from the site of our sectioning, any nuclei present in our images must be non-neuronal. We quantified the population of nuclei present in the sections by staining with DAPI (Figure 3A, 3B). Paclitaxel treatment significantly increased the average number of non-neuronal nuclei present from 28.0 ± SEM 1.4 per 10^4 μm^2 in the vehicle control to 43.8 ± SEM 2.0 per 10^4 μm^2 in the paclitaxel treated nerves ($p<0.0003$). In contrast, there was no significant difference in the average number of nuclei present in eribulin treated nerves (29.48 ± SEM 1.4 per 10^4 μm^2) versus vehicle treated nerves (27.2± 1.3; per 10^4 μm^2).

In summary, paclitaxel more potently induced deleterious morphological effects, correlating with its greater probability of inducing severe CIPN relative to eribulin.

Paclitaxel and eribulin differentially affect tubulin composition

Axons of long peripheral neurons are highly sensitive to changes to the normal balances between microtubule stability, dynamic instability and changes in tubulin post-translational modifications (Almeida-Souza et al. 2011; Avila et al. 1994; Matsuyama and Jarvik 1989). Given that paclitaxel and eribulin each possess different mechanistic capabilities targeted at microtubules, we hypothesized that sciatic nerves from drug treated mice might exhibit drug specific effects upon their microtubule biochemistry. We stained nerves from drug-treated and vehicle-treated mice with antibodies specific to α-tubulin and acetylated tubulin. Axons from eribulin-treated sciatic nerves exhibited a marked, statistically significant 2.6 fold increase in α-tubulin signal, from 12.6± SEM 3.0 fluorescence units for controls to 32.5± SEM 3.7 fluorescence units for eribulin treatment ($p<0.0167$; Figure 4A, 4B). Axons from paclitaxel treated mice trended toward a smaller

increase in α-tubulin signal relative to vehicle treated mice (1.9 fold; 16.4 ± SEM 2.7 and 8.5 ± SEM 1.1, respectively ($p=0.0246$ ($p>0.167$), and $p<0.0167$ when paclitaxel and eribulin groups are compared, Figure 4A, 4B). While not statistically significant when the multiple comparison penalty is applied with a minimum significance threshold 0.0167, the p value is significant when a standard Student's T-test is applied to singularly test the difference between the means of paclitaxel and its vehicle. Increased tubulin levels have been observed as a result of paclitaxel treatment in multiple cell types (Banerjee 2002; Ranganathan et al. 1998), we therefore believe that this increase is worth consideration. These inductions are especially remarkable considering the high abundance of tubulin in neurons under normal conditions, especially in axons. To control for the artifactual possibility that these increased signals resulted from a constant signal being concentrated into a smaller area because of axon diameter constriction, we quantified the axon surface area and average axon diameters for paclitaxel-treated, eribulin-treated and vehicle-treated nerves. No changes in either parameter or G-ratio (outer diameter of the myelin sheath to the diameter of the axonal PNF signal, supplemental figure S2) were observed. Additionally, α-tubulin fluorescence intensity did not correlate positively with axon size (Figure S3)

We next assessed changes in tubulin acetylation, a post-translational marker of stable microtubules. Not surprisingly given its mechanism of action, paclitaxel notably increased axonal acetylated tubulin expression relative to vehicle controls by 4.6 fold (16.8 ± SEM 5.1 and 3.6 ±SEM 1.0, respectively; $p=0.0349$; Figure 4C, 4D). This data demonstrates a clear trend supported by the well-established notion that paclitaxel increases microtubule acetylation in treated cells (de Pennart et al. 1988; Piperno et al. 1987). However, given that eribulin can promote microtubule depolymerization in vitro and upon short term administration to cultured cells, it was surprising to observe that eribulin treatment

dramatically increased axonal acetylated tubulin expression relative to vehicle controls by 11.7 fold (51.8 ± SEM 3.01 and 4.4 ± SEM 0.24, respectively; $p<0.0003$; Figure 4C, 4D), demonstrating a remarkably greater increase in tubulin acetylation compared to paclitaxel ($p<0.0003$). Similarly to α-tubulin, this effect was not dependent upon axon size (Supplemental Figure S3).

These quantitative analyses allow us to calculate the effect of these two drugs upon the ratio of acetylated tubulin to total tubulin relative to their vehicle controls; this ratio should be a measure of drug induced microtubule stability (Table 1). Eribulin treatment increases the acetylated tubulin to total tubulin ratio by 4.5 fold relative to its vehicle control whereas paclitaxel treatment increases this ratio by only 2.4 fold relative to its vehicle control.

Eribulin but not paclitaxel treatment increases the abundance of EB1; neither drug affects EB3 levels

The microtubule End Binding proteins 1 and 3 (EB1 and EB3) are two highly conserved microtubule binding proteins that selectively track with the plus ends of growing microtubules (Akhmanova and Steinmetz 2008; Jiang and Akhmanova 2011; Jimenez-Mateos et al. 2005; Moughamian et al. 2013). As a result, increased quantities of EB1and/or EB3 are indicative of an increase in the number of growing microtubule ends. Treatment with eribulin induced a ~2.2 fold increase of immunofluorescence signal for EB1 ($p<0.0003$) relative to vehicle controls (26.8 ± SEM 0.9 versus 12.0 ± SEM 0.7, respectively; Figure 5A, 5B) and was significantly different compared to the tissue from paclitaxel treated mice ($p<0.0003$). This effect is apparent in axons with a wide range of diameters, as demonstrated in heat maps of tissue sections showing the relative intensity of EB1-

associated fluorescence (Figure S3). In contrast, paclitaxel did not cause a significant change in the quantity of axonal EB1compared to controls (12.2 ± SEM 1.4 and 10.7 ± SEM 0.57, respectively; Figure 5A). On the other hand, EB3 levels were slightly reduced with paclitaxel treatment compared to controls (12.4 ± SEM 0.9 and 15.6 ± SEM 0.5, respectively; $p<0.05$). In contrast, eribulin treatment did not statistically affect EB3 levels relative to controls (Figures 5C, 5D).

Using the same rationale as used above for acetylated and total tubulin, we calculated the ratio of EB1 and EB3 to total tubulin for each drug treatment relative to its control. These ratios should be indicators of drug-induced microtubule growing events (Table 1). The EB1 to tubulin ratio is higher following eribulin treatment than following paclitaxel treatment, suggesting greater microtubule growth in long-term eribulin treated nerves compared with long-term paclitaxel-treated nerves. The EB3 to tubulin ratio is the same following eribulin and paclitaxel treatment.

Discussion

In order to begin to identify and dissect molecular mechanisms underlying the initiation and progression of anti-cancer chemotherapy-induced peripheral neuropathy, we compared drug-induced changes in sciatic nerve tissue between mice treated with one of two microtubule targeting chemotherapeutic agents - paclitaxel, a drug commonly used in the clinic that causes relatively high frequencies of severe peripheral neuropathy and eribulin, a less commonly used drug that induces a lower frequency of severe neuropathic side effects. We sought to ask how these two different microtubule targeting drugs affect mouse sciatic nerve morphology and biochemistry. From our observations of both motor and sensory

neurons (both of which may be affected in severe neuropathy), we seek to pose testable hypotheses focusing upon the induction and progression of peripheral neuropathy.

Our most important results are:

1. Both paclitaxel and eribulin trended toward axon loss;
2. Systemic administration of paclitaxel, and to a lesser extent eribulin increased signs of axon degeneration
3. Systemic administration of paclitaxel, but not eribulin,
    a. increased the abundance of non-neuronal cells;
    b. slightly decreased the level of axonal EB3
4. Systemic administration of eribulin, and to a lesser extent paclitaxel
    a. induced total tubulin accumulation;
    b. induced tubulin acetylation, a marker for microtubule stability
5. Systemic administration of eribulin, but not paclitaxel
    a. increased the abundance of myelin halos/double rings
    b. increased the abundance of EB1, a marker for growing microtubules

These observations demonstrate that paclitaxel and eribulin each exert quantitatively and qualitatively distinct effects on axon degeneration, myelin morphology and microtubule composition in mouse sciatic nerve tissue. Further, the data indicate that paclitaxel treatment is much more potent than eribulin with respect to inducing signs of axon degeneration, while eribulin more effectively induces potentially positive biochemical effects (i.e., increased levels of tubulin, tubulin acetylation and EB1). Changes in axon density trended clearly toward axon loss within both drug treated groups, but were not statistically significant at our statistical thresholds. Three reasons that may account for the lack of statistical significance

in observed axon losses despite these trends are (i) that our sampling region within the mid-thigh region of the mouse sciatic nerve is a relatively great distance from the distal extremities where symptoms are most pronounced and nerve endings where high degrees of fiber loss has been observed in previous studies (Boyette-Davis et al. 2011), (ii) there may be a high degree of individual variability in the number of neurons that retract over that distance and (iii) mouse to mouse axon density may vary over a short distance of sciatic nerve and experimental logistics prevented tight control over the exact position of nerve. Given this, we believe that a stronger measure of axon degeneration is found within our assessment of positive signs of axon degeneration relative to axons present. This data demonstrates clear changes upon drug treatment and between paclitaxel and eribulin groups. Eribulin does induce more myelin halos compared to paclitaxel (and absent in vehicle controls), which may represent a relatively early stage of the neurodegenerative process. These observations are consistent with recent work by Vahdat et al., and colleagues who found that the onset of eribulin-induced neuropathy occurred later than that induced by the microtubule stabilizing drug ixabepilone, which normally displays a higher incidence of neuropathy than paclitaxel (Steinberg 2008; Vahdat et al. 2013).

Based on these observations, we propose that the greater clinical probability of severe peripheral neuropathy by paclitaxel relative to eribulin may be a function of its greater relative damage to the nervous system coupled with eribulin's ability to promote a more stable and growth oriented microtubule network than does paclitaxel. With respect to the latter, we note that the regulation of microtubule dynamics is a balancing act between microtubule shortening events, microtubule lengthening events and a population of stable non-changing microtubules. We propose that the long-term combined effects of increased total tubulin (providing more building blocks for microtubule assembly), tubulin acetylation

(indicating greater microtubule stability) and EB1 (suggesting more growing microtubule ends) more than compensate for eribulin's inherent ability to suppress microtubule growth events (see below for more discussion). The net effect is an extensive and functional microtubule network. Such a compensatory or neuroprotective mechanism could also be at play in electrophysiological experiments demonstrating that paclitaxel but not eribulin causes a loss of caudal nerve amplitude and reduced conduction velocity (Wozniak et al. 2011); indeed, eribulin administration actually increases caudal nerve amplitude and exhibits no reduction in conduction velocity in these studies. Wozniak et al. (2011) also observed signs of axon degeneration, similar to those described in this work, more frequently in tissue from paclitaxel treated mice as compared to eribulin treated mice, correlating with the functional deficits seen in paclitaxel, but not eribulin. Unfortunately, due to the higher level of drug required to achieve a maximum tolerated dose, we are unable perform functional assessments on the same mice receiving drugs. However, based upon previous data, we predict that paclitaxel would demonstrate greater functional deficits compared to eribulin, but lack the ability to make direct conclusions at this time.

Mechanistic considerations

Perhaps the most surprising observations presented here are that long-term eribulin treatment leads to a marked increase in the abundance of both total tubulin and acetylated tubulin. The simplest interpretation of these observations is that eribulin treatment results in an increase in the abundance of stable microtubules. This is surprising because eribulin is generally viewed as a microtubule depolymerizing agent. However, it is important to emphasize that the previously demonstrated microtubule depolymerizing activity of eribulin has been observed in short-term in vitro biochemical reactions or when added to

proliferating cultured cells for a few hours. In contrast, our investigations were performed following two weeks of systemic drug administration to mice and focused primarily on post-mitotic neurons. Mechanistically, one could imagine that microtubules in the sciatic nerve might exhibit net depolymerization upon initial exposure to eribulin. However, either depolymerization itself or some other aspect of eribulin action leads to subsequent regulatory mechanisms that induce tubulin levels, tubulin acetylation levels, EB1 levels and perhaps additional proteins. As one possibility, the binding of eribulin to free tubulin subunits may inactivate the normal tubulin auto-regulatory mechanism by which free tubulin subunits bind to tubulin mRNA and thereby promote tubulin mRNA degradation, which in turn leads to a reduction of tubulin protein synthesis (Gay et al. 1987; Pachter et al. 1987). By this mechanism, eribulin would inhibit tubulin mRNA turnover, leading to the accumulation of increased levels of tubulin mRNA and tubulin protein. Together, these stabilizing effects could compensate for the destabilizing effects of eribulin on the microtubule network, leading to a more robust and stable microtubule network that can function relatively effectively. These effects may be neuronal specific, thereby providing protection from the drug for neurons while not compromising the action of the drug on tumor cells.

Another possibility that must be considered is that perhaps eribulin does not effectively get into the nerve and this underlies its reduced frequency of severe CIPN. We think this is extremely unlikely. Indeed, recent work from some of our labs directly assessed the pharmacokinetics and peripheral nerve distribution of eribulin and paclitaxel following administration via the caudal vein. Both drugs rapidly penetrated the sciatic nerves and dorsal root ganglia, with maximal concentrations achieved within 15 minutes. With the passage of time, dose normalized area under the curve in the sciatic nerves was actually greater for eribulin than for paclitaxel (unpublished data, KW, BAL, BSS). These findings

indicate that limited peripheral nerve exposure is likely not the underlying mechanism for the differential propensity of eribulin and paclitaxel to produce neurotoxicity.

The increase in total tubulin in both eribulin and paclitaxel treated cells provides an enormous supply of additional microtubule building blocks. Given sufficient GTP and growth and/or stabilization regulatory cues, this would enable the neuronal cells to markedly augment their microtubule networks. The increased ratios of acetylated tubulin to total tubulin in drug versus vehicle axons suggest drug induced microtubule stability. The fact that this ratio is 1.9 fold greater in eribulin treated nerves than in paclitaxel treated nerves (4.5/2.4; Table 2) implies that the microtubule network in eribulin treated nerves is considerably more stable than in paclitaxel treated nerves. It is also interesting to consider recent work demonstrating that tubulin acetylation can also influence the interaction between MAPs and microtubules. For example, recent work suggests that tubulin acetylation may, in part, control the affinity between microtubules and kinesin (Almeida-Souza et al. 2011; Dompierre et al. 2007; Reed et al. 2006; Walter et al. 2012).

Increased levels of EB1 may also play an important role in eribulin's relatively benign induction of CIPN via a number of possible mechanisms. Similarly to acetylation, the EB1 to total tubulin ratio in drug treated versus control axons is higher for eribulin than for paclitaxel treatment. This higher ratio of EB1 to total tubulin suggests a greater proportion of growing microtubule plus ends in eribulin versus paclitaxel treatment. Additionally, evidence suggests that EB1 can promote de-novo microtubule nucleation (Vitre et al. 2008). Finally, EB1 is known to influence microtubule dynamics both directly and indirectly. Upon binding directly to microtubule plus ends EB1 recognizes GTP tubulin and an intermediate form as tubulin changes from GTP to GDP bound, preferentially binding the intermediate form and increasing the rate of tubulin maturation to stable, polymerized GDP-bound tubulin

(Kumar and Wittmann 2012; Maurer et al. 2012). This action directly influences microtubule dynamicity. EB1 can also influence microtubule dynamics indirectly via its recruitment of other proteins known to influence microtubule dynamics, including +TIPS such as the CLIP family members, CLASPs and APC as well as XMAP (Akhmanova and Steinmetz 2008).

Increased population of non-neuronal cells in paclitaxel-treated nerves

Our data demonstrate that paclitaxel but not eribulin treatment increases the number of non-neuronal nuclei (and hence cells) present in sciatic nerve tissue. Schwann cells likely account for the majority of nuclei found in tissue from vehicle and eribulin treated mice. However, the identity of the additional cells seen in paclitaxel treated nerves is less obvious. Increased Schwann cell division could account for the increased nuclear population, but invasion by immune cells responding to degenerative axons may also contribute to the effect. Invasion of the sciatic nerve by immune cells and release of pro-inflammatory factors have been observed after nerve injury and neuropathic pain-inducing paclitaxel treatment (Janes et al. 2014; Peters et al. 2007a; Peters et al. 2007b; Rotshenker 2011).

Eribulin and Paclitaxel: Anti-Cancer Efficacy

The demonstration that eribulin induces less frequent severe CIPN than the widely used paclitaxel raises the question of its relative anti-cancer efficacy relative to paclitaxel. A lower incidence of severe peripheral neuropathy would be most meaningful if it were coupled with equal or greater anti-cancer efficacy. Unfortunately, to date there have been no completed clinical studies directly comparing the anticancer efficacies of eribulin and paclitaxel in the clinical setting. That said, eribulin was FDA approved in 2010 as a third line therapy for patients with metastatic breast cancer who had previously received at least

two prior chemotherapy regimens, including an anthracycline and a taxane. At the time of the pivotal Phase III EMBRACE trial which led to the FDA approval, there was no standard of care for third line metastatic breast cancer, so EMBRACE was designed, in conjunction with the FDA, as a two-arm study of eribulin monotherapy versus "treatment of physician's choice" (TPC), essentially capturing the individual judgements of hundreds of oncologists' decisions as to the best personalized treatment of those specific patients (Cortes et al., Lancet 2011). EMBRACE stipulated that enrolled patients must have progressed within 6 months or less of the latest chemotherapy (Cortes et al., Lancet 2011). As such, the statistically-significant 24% increase in median overall survival between the two groups (13.1 months versus 10.6 months for eribulin versus TPC, respectively) indicates that many patients enjoyed prolonged survival on the eribulin arm despite the fact that they had previously progressed on taxane-containing therapies. In addition, the preclinical work of Towle et al., (2001), demonstrated that eribulin is more effective at considerably lower doses than paclitaxel (at empirically determined MTD levels) in four different human tumor xenograft growth models in mice: potency differentials for eribulin versus paclitaxel based on complete tumor suppression ranged from 20- to 100-fold for different human tumors. Additionally, in these in vivo studies, eribulin consistently showed a wider therapeutic window compared to paclitaxel. Finally, eribulin showed an average 4.1-fold increased potency compared to paclitaxel on a molar basis in a library of 8 human cancer cell lines, with ratios in the individual lines ranging from 2.0-fold to 27.8-fold. We conclude that, although direct head-to-head comparisons of eribulin versus paclitaxel have yet to be reported in the clinical setting, existing clinical evidence from the EMBRACE Phase III clinical trial pointing to eribulin activity after progression on taxanes, coupled with consistent preclinical evidence of greater potency both in cancer cell lines and human tumor

xenograft models, make a compelling case that eribulin is either an equipotent or more potent anticancer agent relative to paclitaxel. In this context, the apparently lower neuropathic effects of eribulin relative to paclitaxel in both the clinic and laboratory settings can be viewed as not simply a consequence of lower overall potency, but rather a bona fide reduction in one of the most significant and troubling side effects of treatment with these two agents.

Summary

Work presented here leads us to hypothesize that long-term treatment with eribulin generates a more functional microtubule cytoskeleton than does similar treatment with paclitaxel, accounting at least in part for the reduced levels of severe CIPN observed with eribulin-treated versus paclitaxel-treated patients. With this foundation, future investigations will include testing this hypothesis mechanistically, both in animal and cell culture models.

Figures

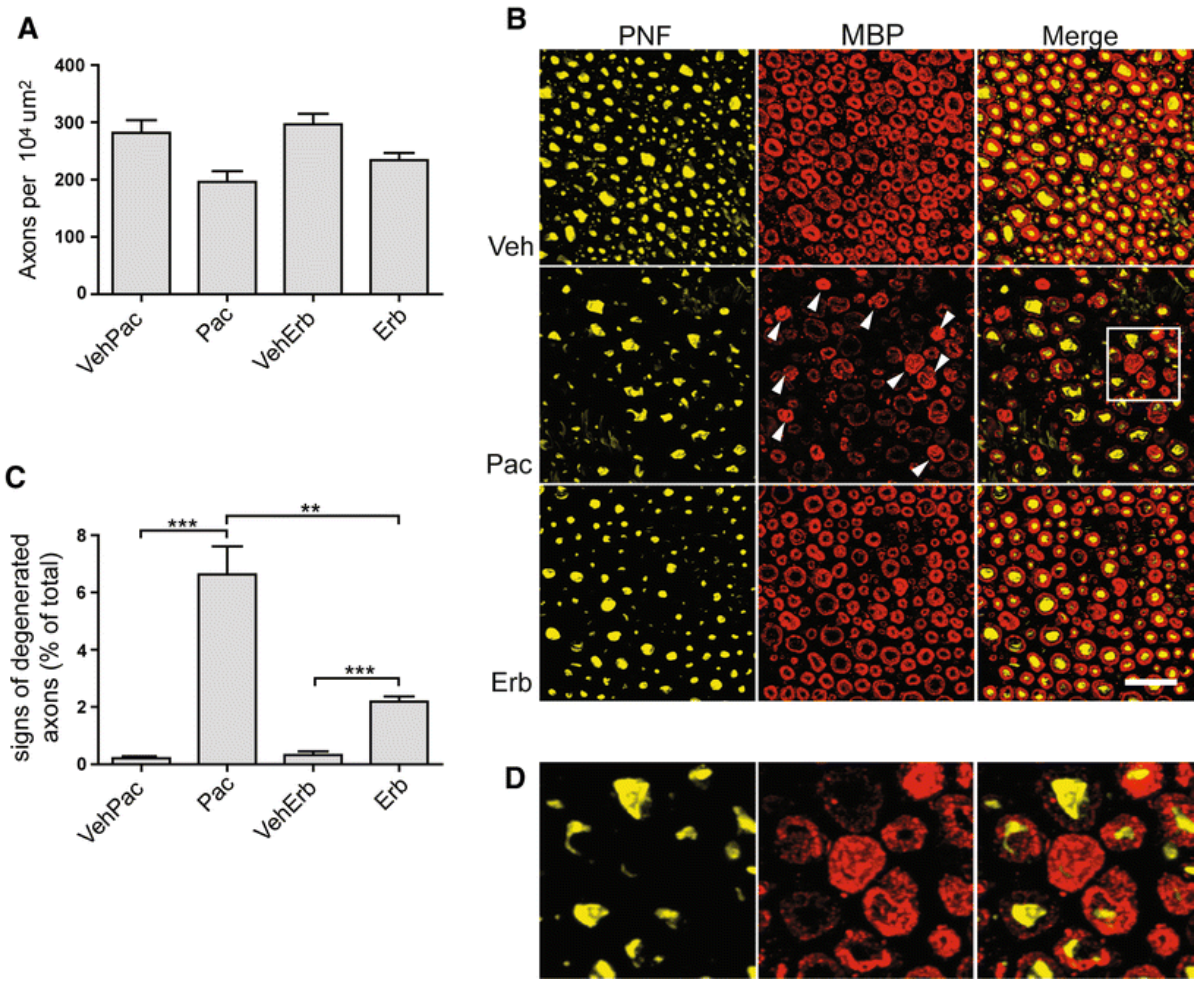

Figure 1. Paclitaxel and Eribulin Differentially Affect Sciatic Nerve Morphology

A. Quantification of axon density per 10^4 μm^2. (n = 5p>0.0167) **B.** Representative confocal images of paclitaxel and eribulin treated sciatic nerves; phosphoneurofilament (yellow), myelin basic protein (red). White arrow heads indicate observed signs of axon degeneration. **C**. Quantification of observable signs of axon degeneration per total number of anti-myelin basic protein (MBP) stained objects, **p<0.003, ***p<0.0003). **D**. Enlarged region of paclitaxel image to show axon degenerative events from boxed area indicated on panel C. Scale bar 20µm.

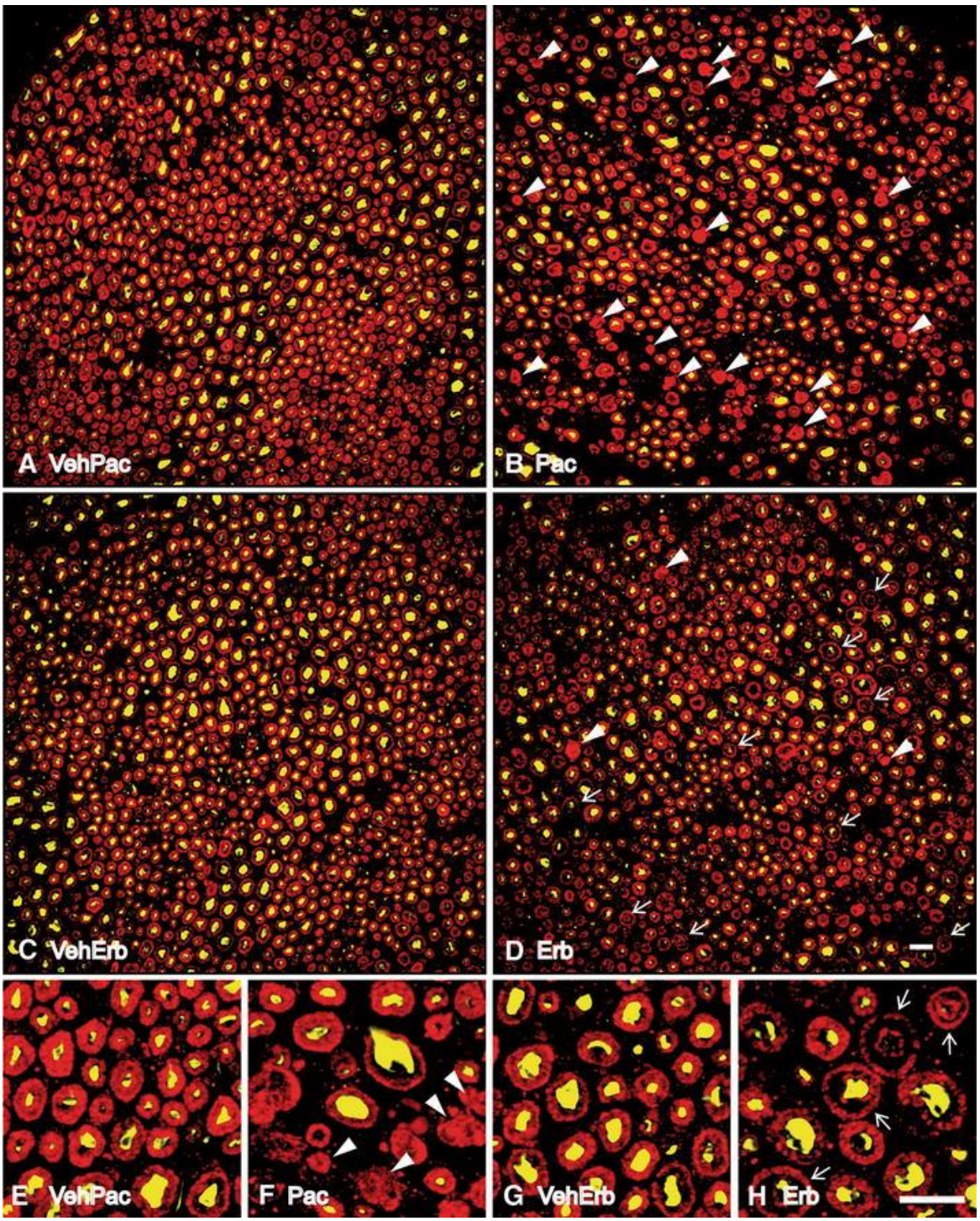

Figure 2. Paclitaxel and Eribulin differentially disrupt normal myelin morphology and differentially lead to degradation of myelin sheaths. A, B. Phosphoneurofilament (PNF; yellow) and myelin basic protein (MBP; red) expression in sciatic nerve tissue from mice treated with the vehicle for paclitaxel and paclitaxel. Tissue from mice treated with paclitaxel shows frequent signs of axon degeneration (white arrowheads) and

increased fragmentation. **C, D.** PNF and MBP expression in vehicle for eribulin and eribulin treated nerves. Tissue from mice treated with eribulin reveals fewer signs of axon degeneration but occasional instances of thinly myelinated axon fibers and separation of myelin layers ("halos"; white arrows) accompanied by myelin fragmentation. **E**, **F.** Enlarged views of vehicle paclitaxel and paclitaxel treatments, respectively. **G, H.** Enlarged regions of vehicle eribulin and eribulin respectively. Scale bars 10μm.

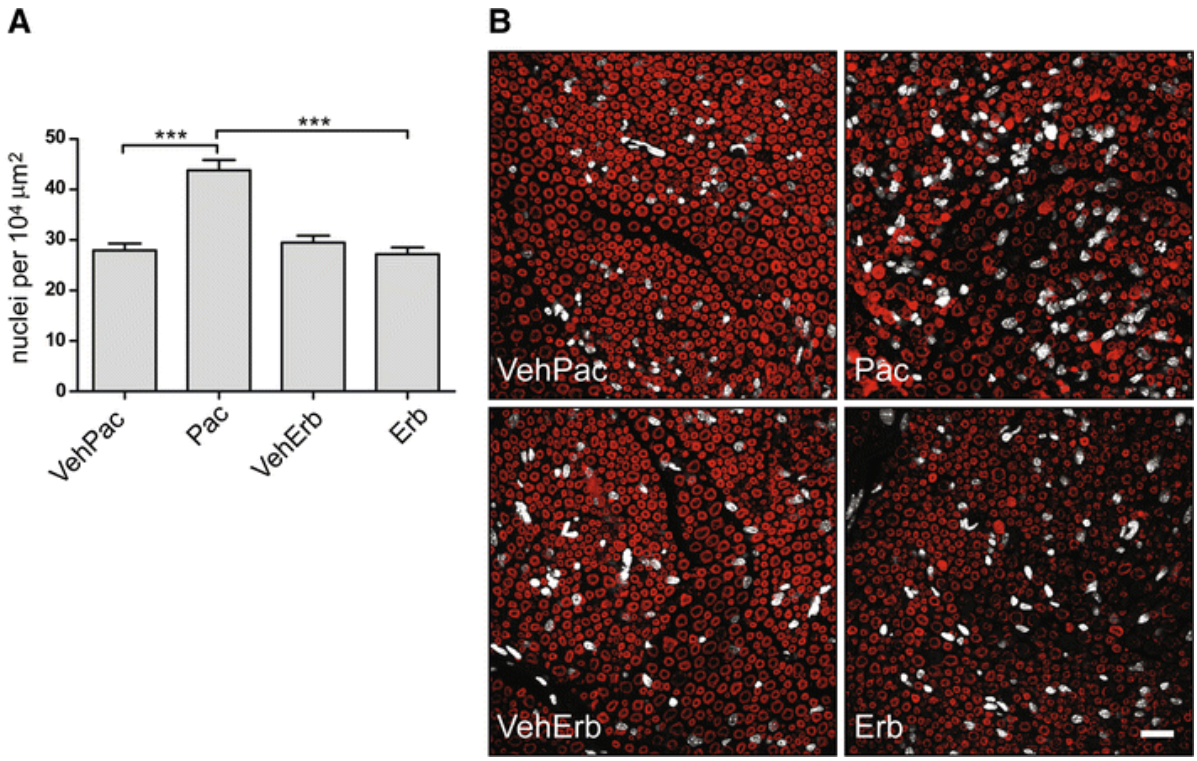

Figure 3. Paclitaxel but not Eribulin treatment leads to increased numbers of non-neuronal nuclei. A. Quantification of non-neuronal nuclei present in drug and control nerves (n=5, ***p< 0.0003) **B.** Representative images showing DAPI stained nuclei (white) and myelin basic protein (red) for reference; scale bar 20µm.

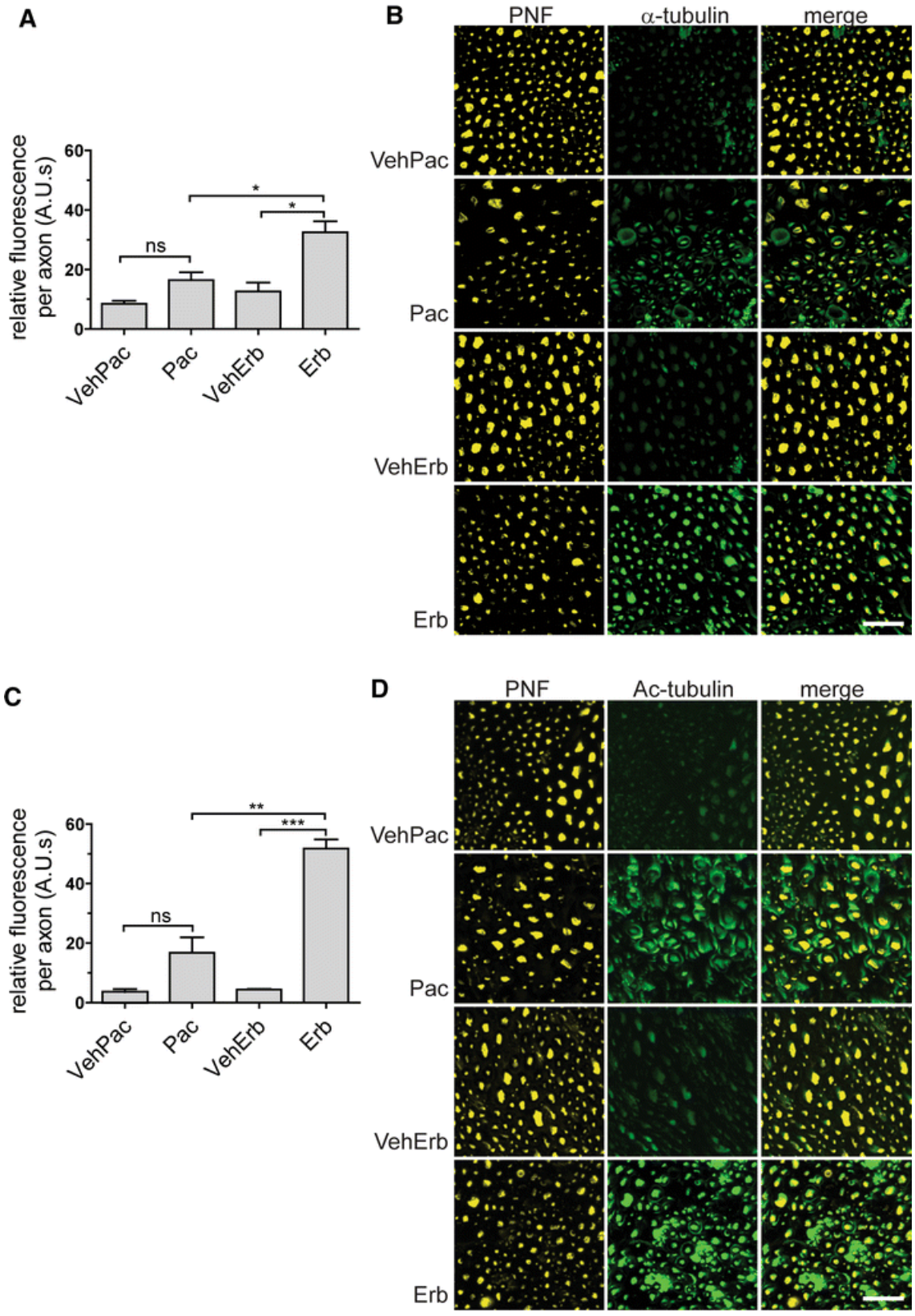
A
relative fluorescence per axon (A.U.s)
60
40
20
0
ns
*
*
VehPac
Pac
VehErb
Erb
B
PNF
α-tubulin
merge
VehPac
Pac
VehErb
Erb
C
relative fluorescence per axon (A.U.s)
60
40
20
0
ns
**
***
VehPac
Pac
VehErb
Erb
D
PNF
Ac-tubulin
merge
VehPac
Pac
VehErb
Erb

Figure 4. Eribulin induces greater α-tubulin abundance and tubulin acetylation than Paclitaxel. A. Quantification of tubulin levels in drug and vehicle treated nerves. Eribulin increased axonal levels of tubulin ~2.6 fold relative to control (n=5, *p<0.0167) while paclitaxel increased axonal tubulin ~1.9 fold (n=5,p=0.0246 (p>0.0167))(Paclitaxel compared to eribulin, *p<0.0167). **B.** Representative images immunostained for α-tubulin (green) and quantified within the axon region defined by PNF signal (yellow). Acquisition settings were adjusted to the brightest fluorescing tissue section. Therefore, because of the pronounced difference in relative fluorescence, the less intensely fluorescing sections appear quite dim. Please see materials and methods for more detail **C.** Quantification of acetylated tubulin levels in drug and control nerves. Paclitaxel treatment increased axonal acetylated tubulin ~4.6 fold relative to control (n=5, p= 0.0349 (p>0.0167)) while eribulin increased axonal acetylated tubulin ~11.7 fold compared to its control (n=5, ***p<0.0003, paclitaxel compared to eribulin: **p<0.003). **D.** Representative images of sciatic nerve tissue, acetylated tubulin (green) was quantitated within the axon region defined by PNF. Scale bars 20μm.

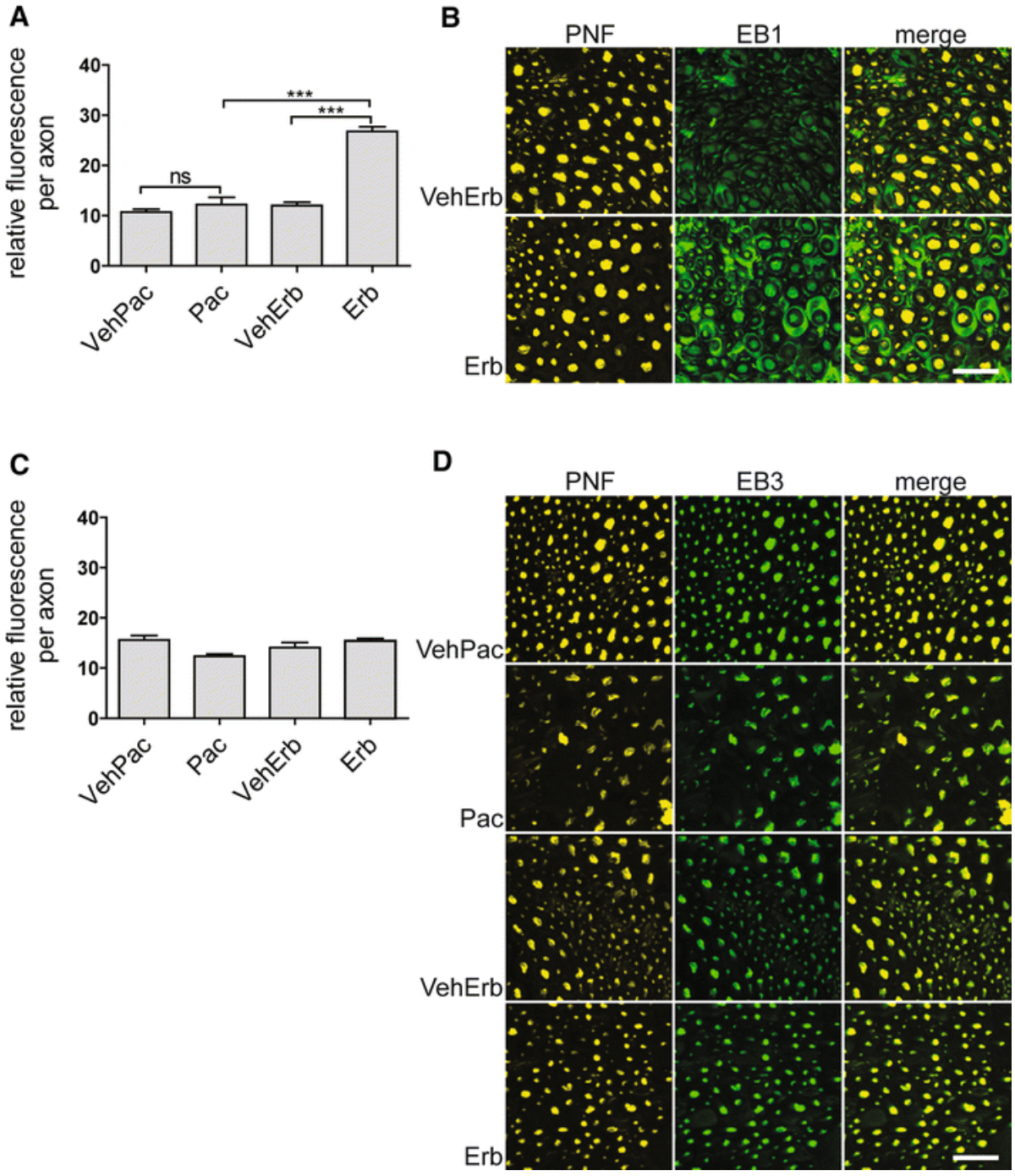

Figure 5. Eribulin but not Paclitaxel induces EB1 abundance in axons and Schwann cells; Paclitaxel but not Eribulin reduces EB3 abundance in axons and Schwann cells. A. Quantification of EB1 levels in drug and control nerves. Axonal EB1 in eribulin treated nerves increased ~2.2 fold as compared to controls (n=5, ***p<0.0003). No change is observed following paclitaxel treatment as compared to its vehicle. **B.** Representative nerve section images; axons are identified by phosphoneurofilament (PNF, yellow), EB1

(green). Qualitatively, an increase in EB1 abundance was observed in surrounding Schwann cells. **C.** EB3 levels did not significantly change with either paclitaxel or eribulin treatment. **D.** Representative nerve section images; axons are identified by anti-phosphoneurofilament (PNF, yellow, left panel), EB3 (green, middle panel), merge seen in right panel. Scale bars 20μm.

Table 1. Fold change in abundance following drug treatment (drug/vehicle)

	Erb	Pac
α-tubulin	2.6	1.9
Ac-α-tubulin	11.7	4.6
EB1	2.2	1.1

Table 2. Ratios of fold change in abundance following drug treatment

	Erb	Pac
Ac-α-tubulin	4.5	2.4
EB1	0.85	0.58

Supplementary Figures

a

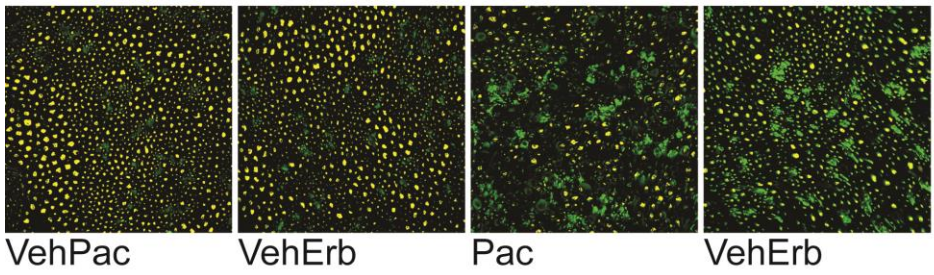

VehPac = Vehicle for Paclitaxel, VehErb = Vehicle for Eribulin, Pac = Paclitaxel, Erb = Eribulin

b

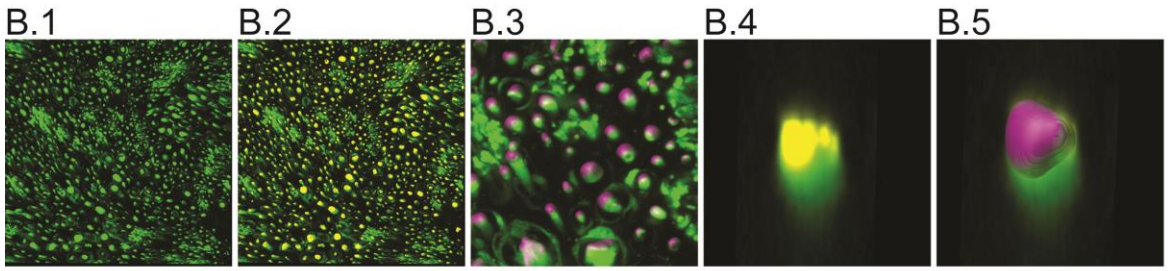

c

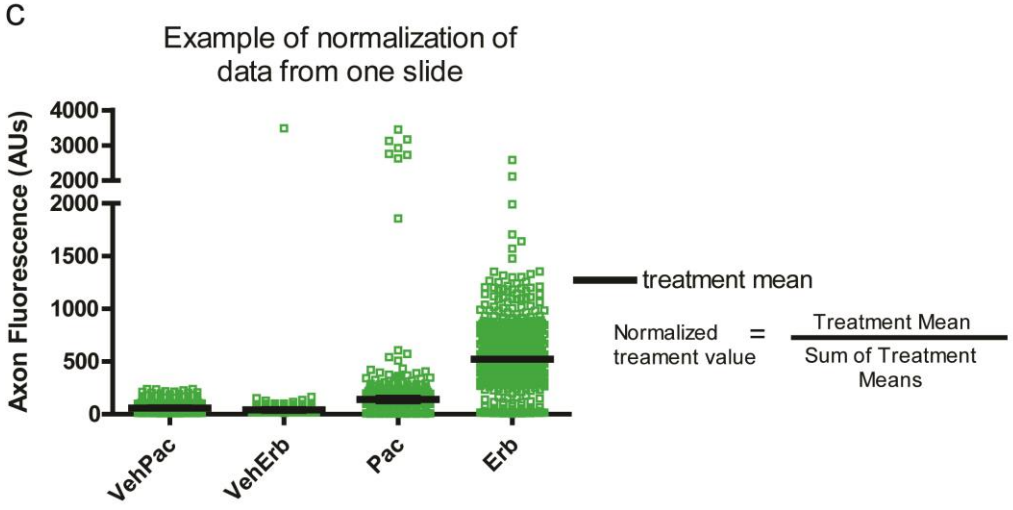

Fig. S1. Quantification and Normalization of Cy2 fluorescent signal. Sections were incubated in appropriate primary and secondary antibody solutions. Control and drug treated sections that had been incubated with the same antibody solution were mounted on a slide as in (**a**) for imaging. Images were imported into the Imaris software package to visualize 3D reconstructed stacks and complete further analysis. **b.** In order to quantify the axonal specific cy2 (eg. α-tubulin in this case, green) fluorescence in the 3D reconstructed image stacks (B.1) we used merged images of α-tubulin (green) and phosphoneurofilament (PNF, an axon marker, yellow) as in B.2 and B.4 (single axon view). Axon regions were defined by PNF signal, manually threshholded to separate signal from noise. The Imaris surface tool determines the volume occupied by the thresholded PNF signal and outlines a boundary that defines the axon volume (B3 and B5 (single axon view), purple). With boundaries established for axonal regions, we the amount of cy2 (e.g. α-tubulin) fluorescence within the axon boundary is queried. The Cy2 fluorescence value identified per axon is represented by the green boxes (**c**). All axons per treatment were averaged to give the treatment mean. The treatment means were then normalized by dividing each treatment mean by the sum of treatment means observed on the slide. Each normalized value was multiplied by 100, to allow comparison of relative fluorescence units between sections processed separately. This was repeated twice per nerve for each of 5 nerves per treatment to obtain a nerve value. The mean of the 5 nerve values is represented in the graphs in main figures

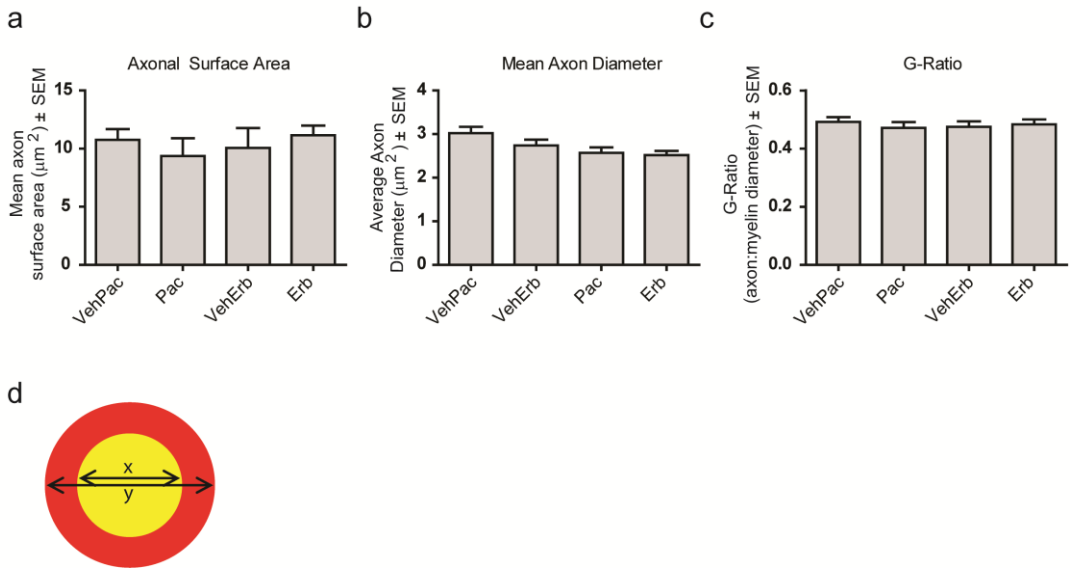

Fig. S2 Axon properties as determined by Imaris software. a. axon surface area identified by 2D rendering of z-stack using Imaris software, **b.** mean axonal diameter and **c.** g-ratio. None of these three parameters are significantly different in axons from drug-treated mice as compared to their vehicle treated controls. **d.** diagram defining G-ratio as the axon diameter (*x*) divided by the myelin outer diameter (*y*)

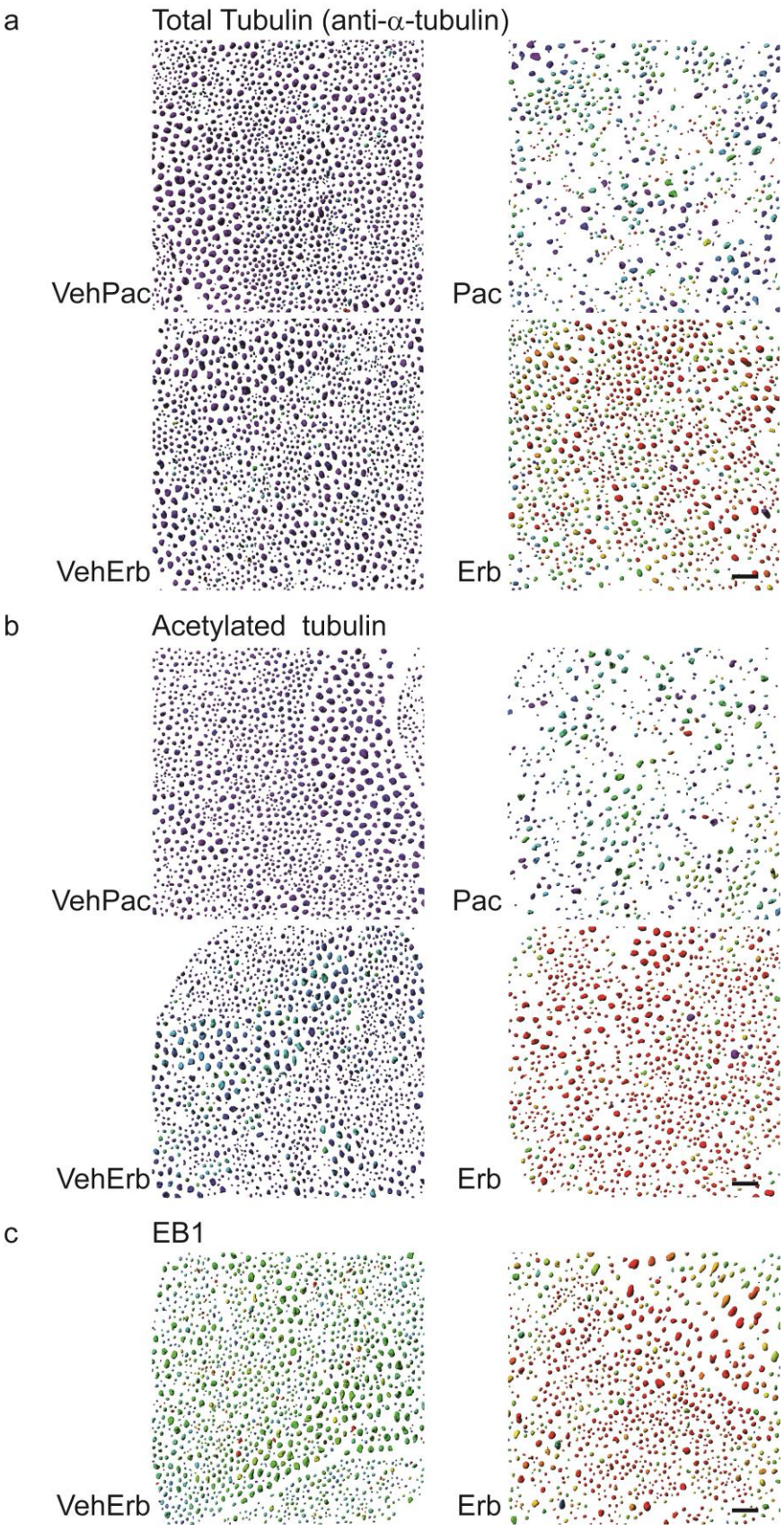
a
Total Tubulin (anti-α-tubulin)
VehPac
Pac
VehErb
Erb
b
Acetylated tubulin
VehPac
Pac
VehErb
Erb
c
EB1
VehErb
Erb

Fig. S3 Heatmaps illustrating α-tubulin, acetylated tubulin, or EB1 signal intensity within the axon region defined by anti-phosphoneurofilament (PNF) signal. Each object represents a single axon and the color represents the intensity of the indicated antibody signal within that axon. Cool colors represent relatively low intensities and warm colors represent relatively high intensities. The relative size of the axon does not appear to correlate with the relative intensity of tubulin signals or EB1 signal, thus we infer intensity is not size-dependent. Scale bars 20μm.

Table S1. Antibodies used for immunofluorescence labeling.

Primary Antibodies	Company	Catalog number	Dilution used
Chicken Anti-Myelin Basic Protein	Millipore	AB9348	1:100
Mouse Anti- Phosphoneurofilament (SMI 31)	Covance	SMI-31R	1:2000
Rabbit Anti-EB1	Millipore	AB6057	1:500
Rat Anti-EB3	Santa Cruz	SC-101475	1:200
Rabbit Anti-A Tubulin	Millipore	04-1117	1:500
Rabbit Anti-Acetylated-α-Tubulin	Cell Signaling	5335	1:800
Rat Anti-Tyrosinated Tubulin	Abcam	AB6160	1:1000
Rabbit Anti-detyrosinated Tubulin	Millipore	AB3201	1:500
Secondary Antibodies			
Goat Anti-Rabbit IgG DyLight 488	Jackson ImmunoResearch	111-485-003	1:200
Goat Anti-Rat IgG DyLight 488	Jackson ImmunoResearch	112-485-003	1:200
Goat Anti-Mouse IgG DyLight 649	Jackson ImmunoResearch	115-495-003	1:200
Goat Anti-Chicken IgY DyLight 488	Jackson ImmunoResearch	103-165-155	1:200

Chapter III. Rapid recovery from several morphological and biochemical effects of chemotherapy-induced neuropathy following paclitaxel and eribulin in mouse sciatic nerves

Summary

Improvements in cancer treatment with microtubule-targeting agents (MTAs) have led to a growing population of cancer survivors. As the focus shifts to quality of life during and after chemotherapy, the reversibility of chemotherapy-induced peripheral neuropathy (CIPN), a disabling and potentially permanent side effect of MTAs is becoming increasingly important. The time to onset, frequency, and recovery from CIPN varies between the common MTAs paclitaxel and eribulin and is manifested through unknown mechanisms. Previously, we found that after 2 weeks of maximum tolerated doses (MTD) in mice, paclitaxel treatment resulted in a 30% reduction in sciatic nerve axons per unit area while eribulin generated a 21% reduction compared to controls (Benbow et al. 2016). Paclitaxel also increased the frequency of myelin abnormalities more significantly than did eribulin (6.6% and 2.2% of total axons, respectively), as well as led to an increase in the number of non-neuronal nuclei in sciatic nerves. Biochemically, paclitaxel and eribulin both induced α-tubulin expression (1.9- and 2.5-fold, respectively) and tubulin acetylation (5- and 11.7-fold, respectively). Eribulin but not paclitaxel induced EB1 expression 2.2 fold. Here**,** we extended these comparative studies to acquire a more detailed understanding of the recovery from drug treatment. Mice were dosed with maximum tolerated doses of eribulin (1.2 mg/kg), paclitaxel (30 mg/kg), or their respective vehicles; each drug was administered intravenously 3 times per week for 2 weeks and mice were followed for up to 6 months after the completion of dosing. In paclitaxel-treated mice, axon area density was significantly

decreased through 3 months of recovery. In contrast, axon area density in eribulin-treated mice recovered fully from initial deficits by the 2 week time point, with ixabepilone showing no change at any time point. Evidence of myelin abnormalities, likely secondary to axonopathy, was prominent at 2 weeks and 3 months and was consistently most frequent in paclitaxel-treated animals. Also, only paclitaxel-treated mice displayed a significant and persistent increase in the number of non-neuronal nuclei at the 2 week, 3 month and 6 month recovery time points, although ixabepilone-treated mice showed a similar trend at 2 weeks. These additional nuclei were positive for known Schwann cell markers S100B and GFAP, indicating that they are likely Schwann cells, the resident glia of the sciatic nerve. Biochemically, we found that two weeks into the recovery phase, α-tubulin acetylation in eribulin-treated mice returned to control levels while it was greatly reduced but still significantly higher than vehicle treated mice in paclitaxel-treated mice. In contrast, axonal levels of both α-tubulin and end-binding protein 1 (EB1) rapidly returned to control values at 14 day from initially induced levels at the end of the MTD treatment in both paclitaxel and eribulin treated mice. Overall, mice treated with eribulin and ixabepilone recovered more rapidly from drug-induced morphological and biochemical effects than did paclitaxel-treated mice. In summary, we found that (i) morphologically, sciatic nerve axons recover more rapidly in eribulin and ixabepilone treated animals than in paclitaxel treated animals and (ii) biochemically, drug-induced increases in protein expression levels following paclitaxel and eribulin treatment are relatively transient. Taken together, our data in mice indicate a milder onset and faster recovery with eribulin and ixabepilone treatment than for paclitaxel.

Introduction

Chemotherapy-induced peripheral neuropathy (CIPN) is a major dose-limiting and potentially permanent side effect of cancer treatment with microtubule-targeting agents (MTAs). The anti-tumor activity of MTAs is widely accepted as deriving from their ability to alter the normal regulatory mechanisms controlling microtubule dynamics and microtubule-based transport that are required for cell survival (Argyriou et al. 2012; Field et al. 2014; Jordan and Wilson 2004; Poruchynsky et al. 2015). While effective in reducing tumor growth, the systemic administration of MTAs also exposes non-target tissues, such as the peripheral axons that transmit sensory and motor input to their mechanistic actions. Such chemotherapeutic assault on peripheral nerves can result in pain, numbness, and burning sensations originating in the distal extremities and progressing proximally toward the trunk as dosing increases and drug accumulates over time (Dougherty et al. 2004, Boyette-Davis et al. 2013).

CIPN can significantly impact quality of life, both during and after administration of MTAs (Cavaletti et al. 2010, Cavaletti et al. 2014, Shimozuma et al. 2009, Dumontet and Jordan 2010, Grisold et al. 2012). In fact, CIPN is the most often cited reason for patient-elected dose reduction during treatment and occasionally necessitates complete cessation of chemotherapy (Agryriou et al. 2012, Agryriou et al. 2008, Bhatnagar et al. 2014, Miltenburg and Boogerd 2014). Early discontinuation of chemotherapy is associated with increased mortality (Hershman et al. 2011). Given the key roles played by MTAs in current anti-cancer therapies, it follows that a more detailed understanding of mechanisms controlling the onset and reversibility from CIPN would be extremely valuable, hopefully leading to improved strategies to manage CIPN.

There is significant variability in the time to onset, duration, and reversibility of CIPN among the different classes of commonly prescribed MTAs. Paclitaxel, of the taxane class, is among the most effective antineoplastic agents and is commonly used as a first-line treatment for ovarian, breast, and lung cancers (Rowinsky et al. 1993, Choy et al. 1994). However, the high incidence of severe neuropathy in about 30% of paclitaxel-treated patients is a significant drawback that can limit its use. Paclitaxel-induced peripheral neuropathy has a median time to clinical onset of 1.1 months, although symptoms can arise shortly after the first dose (Forsyth et al. 1997). Often, symptoms improve or resolve within the first 3-6 months after discontinuation of treatment, and for the subset of people who achieve a full recovery, the median time to total resolution is 9-10 months (Grisold et al. 2012, Pace et al. 2007, Forsyth et al. 1997). However, 41-80% of patients experience delayed recovery of CIPN symptoms two years after the last dose after paclitaxel while some patients never fully recover (de la Morea Barrio et al. 2015, Hershman et al. 2011). Taken together, paclitaxel treatment frequently produces rapid onset and long lasting peripheral neuropathy.

Following the development of paclitaxel resistance, patients may receive ixabepilone, an epothilone D analog that induces microtubule stabilization similar to paclitaxel. Treatment with ixabepilone is associated with an incidence of severe sensory peripheral neuropathy of 6-21% (Roche et al. 2007, Steinberg et al. 2008, Thomas et al. 2007, Dreicer et al. 2007). Compared to paclitaxel, the median time to onset is longer for ixabepilone at 2.7 months from the start of treatment but complete resolution is more rapid at 2.3 months from the last dose (Perez et al. 2007, Vahdat et al. 2013).

Paclitaxel and ixabepilone both induce a higher incidence of neuropathy in patients than eribulin (Argyriou et al. 2012, Puhalla et al. 2008, Cortes et al. 2011, Vahdat et al.

2013). Eribulin, a halichondrin, is a more recently approved third-line therapy for breast cancer with a more favorable safety profile: 7.7% of patients report cases of severe neuropathy while undergoing chemotherapy (Cortes et al. 2012). Compared with paclitaxel and ixabepilone, the median time to clinical onset of eribulin-induced neuropathy is more delayed (8.3 months from the start of treatment) and symptoms resolve more quickly (median time to total resolution of 1.8 months)(Vahdat et al. 2013, Kaufman et al .2014). Thus compared with paclitaxel and ixabepilone, clinical data indicates that eribulin produces a peripheral neuropathy that is later onset, less severe, and more quickly resolving.

Cells possess intricate mechanisms to regulate their microtubule networks. First, the concentration of soluble α/β-tubulin dimers regulates polymerization of the dimer subunits into microtubules. Once assembled, post-translational modifications can alter microtubule stability and modify microtubule dynamics. For example, long-lived and stable microtubules are known to be decorated with acetyl groups on α-tubulin's lumenal lysine-40. Additionally, microtubule-associated proteins bind and regulate microtubule dynamics. End-binding protein 1 (EB1) is a plus-end binding protein and marker of microtubule stability that is necessary for scaffolding other proteins at the plus tip (Geraldo et al. 2008; Gu et al. 2006; Jaworski et al. 2009). We have proposed previously that cells must maintain the dynamics of their microtubule cytoskeleton within a functional range and that conditions (such as induced by MTAs) can lead to neuronal cell dysfunction and eventual neurodegeneration (Bunker et al. 2004, Feinstein and Wilson 2005).

While the taxane, epothilone, and halichondrin classes of MTAs each target microtubules, they each exert different binding and kinetic effects on microtubules (Derry et al. 1995). Paclitaxel binds along the length of the inner microtubule surface and prevents disassembly, thereby promoting microtubule assembly and stability (Horwitz et al. 1994).

The antitumor effect of paclitaxel is predominantly believed to occur via its ability to arrest cells in metaphase by preventing chromosome-kinetochore attachment (Jordan et al. 1993, Waters et al. 1998, Kapoor et al. 2013). Similar to taxanes, epothilones exert their effect by binding to a site close to or at the taxane binding site and stabilizing microtubules (Bollag et al. 1995, Giannakakou et al. 2000, Nogales et al. 1995, Ojima et al. 1999). In contrast, eribulin binds to both soluble tubulin subunits as well as microtubules and results in net depolymerization of microtubules. Unlike paclitaxel's dispersed binding along the microtuble lumen, the halichondrin eribulin is known to bind only at the growing plus end of microtubules where additional subunits are added to the extending polymer (Smith et al. 2010).

Recently, we investigated the effects of paclitaxel and eribulin on the morphology and biochemistry of peripheral sciatic nerve axons 24 hours after the last dose of a 2 week maximum tolerated dose treatment. We observed key differences in the propensity of each agent to induce deleterious morphology as well as differences in altered protein biochemistry. We proposed that the positive biochemical effects of eribulin (more α-tubulin, acetylated-α-tubulin, and EB1) in peripheral axons compensated in part for its deleterious morphological effects. In the present study, we have built upon our previous work by determining the extent to which these morphological and biochemical changes persist after 6 months of recovery following the same two-week maximum tolerated dose animal model. We compared the recovery rates of eribulin-, paclitaxel-, and ixabepilone-induced deficits in axon density, signs of axon degeneration, abundance of Schwann cell nuclei, and abundance of α-tubulin, acetylated α-tubulin, and EB1. We found that (i) morphologically, sciatic nerve axons recover more rapidly in eribulin- and ixabepilone-treated animals than in paclitaxel-treated animals and (ii) surprisingly, drug-induced increases in protein expression following

paclitaxel and eribulin treatment were relatively transient. Interestingly, the morphological effects of ixabepilone were mild compared with paclitaxel and eribulin despite its propensity to induce neuropathy in patients. Taken together, our data in mice indicate a milder onset and faster recovery with eribulin and ixabepilone treatment than with paclitaxel.

Materials and Methods

Antibodies

The following primary antibodies were used in immunohistochemical analyses: anti-α-tubulin (Millipore, 04-1117, 1:100 dilution (Zhang et al. 2011)), anti-acetylated tubulin (Cell Signal, 5335, 1:800 dilution, (Creppe et al. 2009)), anti-EB1 (Millipore, AB6057, 1:500 dilution, (Vitre et al. 2008), anti-myelin basic protein (Millipore, AB9348, 1:100 dilution, (Heller et al. 2014), anti-phosphoneurofilament (Covance, SMI-31R, 1:2000 dilution, (Choi et al. 2008), anti-S100B (Abcam, ab11178 1:500 dilution), and anti-GFAP (Abcam, ab7260 1:200). FITC, Cy3 and Cy5 conjugated secondary antibodies were purchased from Jackson Research and used at 1:200 dilutions.

Drugs

Eribulin mesylate (synthesized at Eisai Research Institute and stored at -80°C degrees in the dark) was dissolved in 100% anhydrous DMSO (Sigma-Aldrich, St. Louis, MO) to produce a 10 mg/mL stock solution, which was separated into aliquots and stored at -80°C until day of administration. Each administration day the stock solution was thawed and diluted with saline to a final concentration of 0.125mg/mL in 2.5% DMSO/97.5% saline and administered in a 10 mL/kg volume. Paclitaxel (LC Laboratories, Woburn, MA) was stored at -20°C in the dark was dissolved in 100% ethanol at 10% final volume. An equal volume

of cremophor (10% of final volume) was then added and the mixture re-vortexed for about 10 minutes. Immediately prior to injection, ice-cold saline was added to final volume (as 80% of final) and the solution was maintained on ice during dosing. Dosing solutions of 3mg/mL were made fresh daily and administered in a 10 mL/kg volume. Ixabepilone was purchased as part of an IXEMPRA kit (Bristol-Myers Squibb) for clinical administration. The ixabepilone solution was prepared according to instructions provided in the package insert. The kit consists of 2 vials, 1 containing 47 mg ixabepilone powder and the other containing 23.5 mL diluent, which were stored in the refrigerator at 4°C. The total volume of the diluent was added to the total amount of powder; therefore, after reconstitution, the concentration of ixabepilone in the solution was 2 mg/mL. The diluent supplied consists of a sterile nonpyrogenic solution of 52.8% (w/v) purified polyoxyethylated castor oil and 39.8% (w/v) dehydrated alcohol. The formulated ixabepilone stock solution (2 mg/mL) was immediately aliquoted and stored at -80C until use. On each experimental day, the stock solution was diluted by adding 50% ethanol/50% cremophor with subsequent vortexing to yield a solution that was 5 times the required dosing concentration. Finally, 4X volumes of PBS were added, while vortexing, to achieve a final dosing concentration of 10 mL/kg.

Animal Studies

Female BALB/c mice (approximately 7–8 weeks old at onset of dosing) were obtained from Harlan Laboratories Inc. (Indianapolis, IN) and maintained with free access to water and a standardized synthetic diet (Harlan Teklab). Animal housing and procedure room temperature and humidity were maintained at 20 ± 2^{o}C and 55 ± 10°C, respectively. Artificial lighting provided a 12 h light/12 h dark cycle (light 7 a.m.–7 p.m.). All experimental protocols were approved by the Institutional Animal Care and Use Committee

of Sobran Inc (Baltimore, MD) and adhered to all of the applicable institutional and governmental guidelines for the humane treatment of laboratory animals.

Mice were randomly assigned into vehicle, eribulin, ixabepilone, or paclitaxel treatment group (n= 3). Drugs were administered 3 times per week (Monday, Wednesday, Friday) for 2 weeks into the caudal vein at a dose that was perviously determined to be the MTD (Wozniak et al. 2011), specifically 30 mg/kg, 1.25 mg/kg, and 2 mg/kg for paclitaxel, eribulin, and ixabepilone respectively. Following two weeks, three months or six months of recovery after the last dose, mice were deeply anesthetized with 10% chloral hydrate and euthanized by transcardial perfusion with PBS followed by 4% paraformaldehyde in 0.1 mM phosphate buffer, pH 7.4, for 10–15 min. Subsequently whole mid-thigh sections of sciatic nerve were dissected and placed in perfusion fixative at 4^{o}C.

Tissue Preparation

Fixed whole sciatic nerves were processed as described previously (Benbow et al. 2016). Briefly, sciatic nerves were embedded in 10% agarose (w/v) dissolved in 1X PBS containing 0.01% sodium azide and cross-sectioned in 100μm steps from distal to proximal end using a Leica VT1000S vibratome. Sections were stored in 1X PBS (1.37M NaCl, 27mM KCl, 100mM Na_2HPO_4, 18mM KH_2PO_4) containing 0.01% sodium azide at 4^{o} C until immunostaining.

Antibody Staining

Sciatic nerve sections were grouped so that one section from each treatment condition was incubated with a given antibody solution. Individual sections were stained with antibodies recognizing α-tubulin, acetylated tubulin, EB1, or S100B (a Schwann cell-specific marker).

All sections were also stained with anti-phosphoneurofilament and anti-myelin basic protein as internal controls and in order to identify regions of interest (for example, neuronal cells). Free-floating sections were incubated in PBT blocking agent (1X PBS, 0.1% TritonX-100, 1% BSA, 1% donkey serum) overnight at 4°C. Sections were then incubated with primary antibodies for 7 days at 4°C with agitation to promote antibody penetration. Primary antibody dilution solutions were removed and sections washed 3 times with PBT at room temperature (8 minutes/wash). Sections were next incubated with secondary antibodies for 2 days at 4°C with agitation and protected from light. Secondary antibody dilutions were removed and sections washed as described above. Sections were then mounted on glass slides using ProLong Gold mounting media with DAPI (Life Technologies P36935) so that each slide contained one section from each of the five treatments (paclitaxel, ixabepilone, eribulin, and their respective vehicles, Figure S1) that were all stained simultaneously with the same antibody solution. Slides were sealed with nail polish and stored at 4°C in the dark until imaging.

Fluorescence microscopy

Images were collected using an Olympus Fluoview 1000 Spectral confocal system equipped with 405nm, 488nm, 559nm, and 635nm laser lines. Each slide containing one section from each of the 4 treatments and incubated in the same antibody solution was imaged with the same exposure settings, determined by identifying the brightest-fluorescing section on each slide. 20 μm sample depths from each nerve were imaged by sequential laser scanning using a 0.5μm step size with an Olympus PLANAPOSC 60x (1.40 NA) high refractive index oil immersion objective.

Image Analysis

Images from each slide were imported into Imaris Version 7.5.2 (Bitplane, Zurich, Switzerland) and rendered into three dimensional maximum intensity z-stack projections for analysis. To assess changes in gross morphological structure the nuclei, myelin and axons were identified using the DAPI, anti-myelin basic protein and anti-phosphoneurofilament channels, respectively. Using the Imaris software surfaces tool, we identified nuclei, myelin sheaths and axons based on the fluorescent signal from their appropriate antibody or stain, manually thresholding signal-to-background ratio. To maintain consistency in object identification in similarly treated samples, one set of threshold parameters was applied to all sections stained with the same antibody solutions and imaged with the same microscope settings. Signs of axon degeneration, defined as solid, circular regions of myelin lacking a phosphoneurofilament signal, were identified and counted manually and expressed as a percentage of total phosphoneurofilament-positive objects present within the nerve bundle. For axon area density (defined as the number of objects per μm^2 in a 2 dimensional image) and nuclei measurements, the 41-image 3D stack was flattened to a 2D image in Fiji using the maximum intensity setting. The number of axons per region of interest (defined by phosphoneurofilament signal) or nuclei (defined by DAPI) was quantified using Imaris. The region of interest was manually defined by manually drawing around the edge of each nerve bundle with the cursor, referred to as "masking." The masked area of this region was recorded and only axons or nuclei within this area were included for analysis and calculation of frequency of myelin abnormalities. The number of axons or nuclei was normalized to a $10^4 um^2$ masked area.

In order to quantify fluorescence intensity changes, fluorescence values were collected and normalized within each slide first, before comparisons were made between slides.

Normalization of axonal Cy2 fluorescence signals (depicted in Supplementary Figure S1) was accomplished by first identifying the axonal region using the anti-phosphoneurofilament (PNF) signal to mask the axon regions specifically differentiating axons from surrounding Schwann cells or other cell types present. The raw values of Cy2 fluorescence were determined for each axonal region within the field of view. The mean Cy2 signal per axon was calculated for each treatment to give the "treatment mean." These values were normalized by dividing each treatment mean by the sum of all four treatment means per slide. This method was employed in order to retain the natural variability seen in vehicle treatments. This was the same methodology used previously (Benbow et al. 2016). The fold change values were calculated by first taking an average of the percent fluorescent per axon values for each treatment at each timepoint (n = 3-5), then dividing the drug average value by its respective vehicle average value.

Statistical Analysis

Sciatic nerve tissue from three mice for each treatment was analyzed. For axon area density, myelin abnormalities, and nuclei analyses a Student's T-test was used to compare values for each treatment and its vehicle control at each recovery time point. For fluorescence intensity comparisons, a one-way ANOVA with post-hoc Tukey's tests was employed to test the statistical significance between the means of treatment groups separately for each time point. In all cases the statistical significance values were set at: *$p<0.05$, **$p<0.01$, ***$p<0.001$.

Results

Paclitaxel-treated animals exhibit a persistent reduction in axon area density over the entire 6 month recovery period, unlike ixabepilone- or eribulin-treated animals

To investigate the recovery from MTA-induced CIPN, we compared sciatic nerve tissue from mice allowed to recover for two weeks, three months, or six months after induction of neuropathy via an initial 2 week maximum tolerated dosing schedule (dosing on days 1, 3, 5, 8, 10, 12) with either paclitaxel (30 mg/kg), ixabepilone (2 mg/kg), eribulin (1.25 mg/kg), or their respective vehicles. We first sought to determine the extent to which the deficits in axon area density we previously observed at the onset of neuropathy persist over the recovery period. In our previous work, we determined that two weeks of paclitaxel treatment induced a 30% loss of axon area density while eribulin treatment induced a milder 21% reduction (Benbow et al. 2016). Subsequent work revealed a similar 20% reduction induced by treatment with ixabepilone. To address the question of the relative recovery potential for each drug, we first quantified axon area density over a 6 month period of recovery for mice treated with either paclitaxel, ixabepilone, eribulin, or their corresponding vehicles in our usual 2-week MTD regimen, defining axons as regions positive for anti-phosphoneurofilament (PNF) signal in sciatic nerve cross sections (Figure 1A). Our analysis was performed on sciatic nerve tissue from the mid-thigh region, where the nerve is composed of about 6% motor, 71% sensory, and 23% unmyelinated sympathetic axons (% total number of axons present) (Schmalbruch 1986). After two weeks of recovery, paclitaxel-treated sciatic nerves exhibited a persistent reduction in axon area density of 188 ± 12 axons per 10^4 μm^2 compared to 250 ± 19 axons per 10^4 μm^2 for control (mean ± SEM, $p<0.05$; Figure 1B). After 3 months of recovery, paclitaxel-treated sciatic nerves exhibited additional axonal loss to 174 ± 13 axons per 10^4 μm^2 compared to 213 ± 17 for its vehicle control. After 6 months of recovery, animals began recovering from paclitaxel-induced axonal loss, but had not completely recovered to numbers similar to control (223 ± 15 for paclitaxel vs. 256 ± 21 axons per 10^4 μm^2 for control). In contrast, while eribulin-treated

mice did exhibit a significant loss of axon density at the end of the 2-week MTD treatment, 2 weeks of subsequent recovery time resulted in 221 ± 11 axons per 10^4 μm^2 compared to 214 ± 11 axons per 10^4 μm^2 for control indicating a recovery from the initial effects present immediately after dosing. Subsequent time points continued to show similarity between the eribulin-treated and vehicle-treated axon area densities, demonstrating the stability of the recovery process. Finally, ixabepilone treatment did not induce any significant change in axon area density, either at the end of the 2-week MTD treatment or at any subsequent time point during the recovery period (221 ± 11 axons per 10^4 μm^2 compared to 275 ± 26 axons per 10^4 μm^2 for control at recovery day 1, $p = 0.09$).

The abundance of myelin abnormalities rapidly declines after cessation of MTA treatment in paclitaxe-l, ixabepilone-, and eribulin-treated animals

Myelin basic protein (MBP) is a major component of the insulating myelin sheath that peripheral glia provide to axons which is essential for proper preservation of nerve conduction velocity and amplitude across long distances in peripheral neurons. We examined the extent to which signs of axon degeneration and myelin abnormalities persisted over the recovery period using immunofluorescence microscopy with an anti-MBP antibody (Figure 2A). A sign of axon degeneration was defined as a fiber structure with a collapsed MBP signal and a severely reduced or absent PNF signal. Similar degenerative events have been described in several instances of neuronal toxicity and injury, where the space normally occupied by the axon is lost and has been replaced by myelin (Muguruma et al. 2006; Schnaar et al. 2014; Wozniak et al. 2011).

The frequency of myelin abnormalities in paclitaxel-, ixabepilone- and eribulin-treated animals declined rapidly from their maximum levels observed at the end of their 2-week

MTD treatments (6.6%, 0.8% and 2.2%, of total axons, respectively). Significant residual effects on myelin were still present after 2 weeks of recovery from paclitaxel and eribulin treatment (0.82% and 0.64% of total axons, respectively), but not for ixabepilone (Figure 2B). This is likely a consequence of the fact that paclitaxel induced by far the greatest abundance of myelin abnormalities. After three months of recovery the frequency of myelin abnormalities present in paclitaxel-, ixabepilone- or eribulin-treated nerves had recovered to values similar to control.

Paclitaxel- and ixabepilone- but not eribulin-treated animals exhibited increased Schwann cell numbers during the post-MTD treatment recovery period

The neuronal cell bodies for peripheral nerve axons that innervate the extremities reside in the dorsal root ganglia adjacent to the spinal column, far from the region of nerve imaged in this study. Therefore, all nuclei in our images are non-neuronal. We quantified the population of non-neuronal nuclei present in sciatic nerve cross sections by counting the number of DAPI objects identified by Imaris analyses (Figure 3A). Our previous work demonstrated that paclitaxel treatment but not eribulin treatment led to an increase in the number of DAPI-positive structures in sciatic nerves (Benbow et al 2016). After two weeks of recovery, paclitaxel-treated nerves maintained a significantly higher average number of non-neuronal nuclei of 41 ± 2.2 per 10^4 μm^2 compared to 26 ± 2.3 per 10^4 μm^2 in the control (Figure 3B, *$p<0.05$). Interestingly, this increase persisted in paclitaxel-treated nerves even after six months of recovery (40 ± 3.5 per 10^4 μm^2 compared to vehicle control 24 ± 4.3 per 10^4 μm^2). In contrast, exposure to ixabepilone results in a statistically significant increase after two weeks of recovery, then subsided to control levels at the 3 and 6 month time points.

Finally, there was no significant difference in the average number of nuclei present in eribulin-treated nerves at any time during the recovery period.

We next sought to identify the additional non-neuronal nuclei in paclitaxel-treated nerves. We hypothesized that due to the fiber disruption in paclitaxel-treated nerves the additional nuclei might be additional Schwann cells since these cells are known to dedifferentiate and proliferate in order to provide a suitable environment for regeneration following nerve injury (Scherer and Salzer 2001, Ceci et al. 2014). In support of this hypothesis, all additional non-neuronal nuclei in paclitaxel-treated nerves were positive for both Schwann cell markers S100B (Figure 4) and GFAP (data not shown) at all recovery time points.

MTD-induced levels of tubulin, acetylated tubulin and EB1 rapidly return to control levels following cessation of drug treatment

We previously determined the α-tubulin composition in paclitaxel- and eribulin-treated sciatic nerves at the onset of neuropathy and reported that both drugs increased the abundance of axonal α-tubulin 1.9- and 2.6-fold, respectively (Benbow et al. 2016). A parallel analysis of ixabepilone treatment revealed almost no change in α-tubulin level. Surprisingly, after two weeks of recovery the levels of α-tubulin quickly returned to control levels for both paclitaxel- and eribulin-treated mice and was maintained at that level throughout the recovery period (Figure 5A, B, C). Ixabepilone did not induce any changes in α-tubulin abundance at any time point during the recovery period.

Next we assessed changes in tubulin acetylation, a marker of long-lived and stable microtubules over the course of recovery. We previously determined the levels of axonal tubulin acetylation in paclitaxel- and eribulin-treated sciatic nerves at the onset of

neuropathy and reported that both drugs increased the tubulin acetylation, by 4.6- and 11.7-fold, respectively (Benbow 2016). Acetylated tubulin levels declined from maximum levels determined during onset, but remained significantly elevated 1.6-fold for paclitaxel (20.49 ± 1.11 vs. vehicle control 12.33 ± 0.40 relative fluorescence units per axon, Figure 6A, B, C) whereas with eribulin acetylated tubulin levels had completely returned to control levels from its initial ~11.7-fold increase following two weeks of recovery. Parallel analyses of ixabepilone-treated mice revealed no changes in the abundance of acetylated α-tubulin at any time point during the recovery period.

To assess the state of microtubule dynamicity during the recovery period, we next quantified the axonal levels of microtubule end binding protein 1 (EB1), a highly conserved microtubule associated protein that selectively tracks with the plus ends of growing microtubules (Akhmanova and Steinmetz 2008; Jiang and Akhmanova 2011; Jimenez-Mateos et al. 2005; Moughamian et al. 2013). We previously determined the levels of EB1 in paclitaxel- and eribulin-treated sciatic nerves at the onset of neuropathy and reported that only eribulin, and not paclitaxel, increased the abundance of axonal EB1 by ~2.2-fold compared to its vehicle control. EB1 levels in eribulin-treated nerves declined rapidly from maximum levels at the end of the MTD treatment, returning to control levels after only two weeks of recovery (Figure 7A, B, C). Again, and consistent with the other proteins analyzed, ixabepilone did not induce any changes in EB1 abundance at any time point during the recovery period.

Discussion

The mechanisms responsible for regulating the onset and resolution of CIPN remain poorly understood. Here, we sought to test the hypothesis that the differences among MTA

mechanism of action underlie their variation in clinical CIPN onset and recovery. Prior to this work, we characterized the initial effects upon sciatic nerve axons immediately following a two week maximum tolerated dose (MTD) treatment model of microtubule-targeting agent (MTA)-induced peripheral neuropathy (Benbow 2016). To expand this work, we report here a timeline of resolution from these initial effects during a six month recovery period.

We found that paclitaxel produced longer-lasting morphological changes in sciatic nerves (in axon area density, frequency of myelin abnormalities, and number of Schwann cell nuclei) as compared with eribulin and ixabepilone. Interestingly, with eribulin and paclitaxel, many of the substantial biochemical changes in microtubule biochemistry previously observed at the onset of neuropathy quickly resolved to control levels after two weeks of recovery. Acetylated α-tubulin remained elevated with paclitaxel after two weeks of recovery whereas eribulin had completely recovered from its ~12-fold increase at the onset of neuropathy. In addition, we identified a novel effect of paclitaxel to stimulate and sustain the number of Schwann cells. Therefore, it appears that persistence of drug-induced morphological effects after long-term MTA treatment characterizes recovery from CIPN while changes in protein abundance are relatively transient. Understanding these changes are initial steps toward identifying the mechanisms responsible for the onset and resolution of CIPN.

Paclitaxel induces severe and long-lasting changes to sciatic nerves

The morphological assessments of sciatic nerve injury demonstrate a uniquely severe effect of paclitaxel, with reduced axon area density, increased signs of myelin abnormalities, and increases in Schwann cell abundance observed most frequently after paclitaxel

treatment. Ixabepilone, which also has notable electrophysiological effects, also produced some signs of structural change, but the effects were in general milder than those caused by paclitaxel and recovery was more rapid. In general, eribulin caused few, if any, degenerative effects, other than early signs of myelin structure disruption.

Paclitaxel's induction of Schwann cells at all time points during the recovery phase is consistent with the notion that it generates the most cellular damage. Schwann cells are crucial for the proper function and maintenance of peripheral nerves. These cells are responsible for encapsulating axons with a myelin-rich sheath that preserves action potentials originating in distal sensory termini and are intimately involved in the regeneration process after nerve injury (Lehmann and Hoke 2010, Fu et al. 1997). Remarkably, paclitaxel-treated animals continue to exhibit increased levels of Schwann cells following 6 months of recovery whereas eribulin-treated animals showed no change and ixabepilone-treated animals had a brief increase at two weeks followed by recovery at 3 months. Paclitaxel may be unique in inducing Schwann cell proliferation due to its more significantly deleterious initial effects on axon area density and abundance of myelin abnormalities as compared with ixabepilone or eribulin.

Tubulin composition and biochemistry rapidly returns to control levels

Our previous work demonstrated that eribulin and (to a lesser extent) paclitaxel both induced levels of acetylated α-tubulin in sciatic nerve axons (Benbow et al. 2016). In the present study, axonal levels of acetylated α-tubulin rapidly returned to control levels for both drugs during the recovery period. Interestingly, EB1 is known to co-immunoprecipitate with the tubulin deacetylating enzyme HDAC6, indicating a possible regulatory link between microtubule acetylation and binding of end-binding proteins (Zilberman et al. 2009).

Further, eribulin's initial increase in α-tubulin acetylation in microtubule networks may rescue axonal transport deficits by increasing recruitment of kinesin-1 to microtubules (Reed et al. 2006, Bulinski et al. 2006). Taken together, the presence of beneficial biochemical changes during eribulin treatment may create an environment that more easily supports the regeneration of damaged nerve fibers when the drug is removed.

Our previous work demonstrated that eribulin but not paclitaxel treatment induced the level of EB1 expression in sciatic nerve axons. During the recovery period, axonal levels of EB1 rapidly return to the control level in the eribulin group. Recent studies in differentiated neuronal SK-N-SH cells revealed that the normal comet-tail distribution of EB1 on microtubule plus tips is perturbed after paclitaxel treatment, suggesting that disruption of microtubule dynamics is a key event in paclitaxel-induced neurotoxicity (Rovini et al. 2010).

Long-term retention of paclitaxel in sciatic nerve

In contrast to their rapid clearance from plasma, paclitaxel, ixabepilone, and eribulin enter and are retained in sciatic nerve tissue at vastly different rates (Wozniak et al. 2011). Recent pharmacokinetic studies demonstrated that the tissue penetration index (a measure of how likely the drug is to enter the tissue) of the sciatic nerve was 30 times higher for eribulin than that of paclitaxel, indicating that more eribulin enters the sciatic than paclitaxel (Wozniak et al. 2016). Despite the increased relative uptake of erublin, the observed functional impairment and degenerative pathologic changes in dorsal root ganglia and sciatic nerves are consistently more severe with paclitaxel (Wozniak et al. 2011). The relative retention also differed greatly between these two drugs. Mass spectroscopic analysis of peripheral nervous tissue 26 days after the first dose of a 2 week MTD schedule (recovery

day 12 of this work) revealed that only a small fraction of the maximum level of eribulin detected in the sciatic nerve remained (Wozniak et al. 2016). In contrast, a significant amount of paclitaxel was still detectable in sciatic nerves at 26 days. While the absolute amount pf paclitaxel falls over time, the residual drug is likely tightly bound to microtubules causing persistent disruption of function and delaying recovery. These data are consistent with a model in which the delayed recovery of paclitaxel-treated nerves may be due to accumulation of the drug in nerve tissue after repeated doses. In support of this model, a cumulative dose of paclitaxel is the critical metric for clinical neuropathy risk (Gornstein et al. 2014). Taken together, these data suggest that the incidence and recovery of neuropathy may not be correlated with the level of initial uptake, but may instead depend on the retention time of each drug in nervous tissue. We suggest that the sustained morphological changes observed in paclitaxel-treated animals are occurring as a result of long-term drug retention which at least in part regulates the resolution of neuropathy.

The first-line drug paclitaxel induces the most severe and longest lasting deleterious effects

The goal of the current work was to investigate the molecular mechanisms involved in regulating the onset and resolution of MTA-induced peripheral neuropathy. To accomplish this goal, we treated naïve mice (without pre-existing neuropathy) with maximum tolerated doses of paclitaxel, ixabepilone, and eribulin to compare their relative induction of morphological and biochemical changes. Clinical treatment with MTAs often involves sequential treatment with the drugs investigated here. For example, paclitaxel is commonly used as a first line cancer therapy until drug resistance develops, which then may require treatment with a second line drug such as ixabepilone. If a second line therapy fails, a third line therapy may be administered, such as eribulin. In this clinical setting, eribulin is

associated with a relatively low incidence of neuropathy as compared with paclitaxel and ixabepilone (Jain and Vahdat 2011, Swami et al. 2012, Vahdat et al 2009). Our data presented here provide a molecular rationale for the more rapid clinical onset and longer persistence of paclitaxel-induced neuropathy as compared with eribulin-induced neuropathy. However, it should be appreciated that patients who receive second and third line therapies most likely begin these additionally therapies with pre-existing neuropathy. Recent work demonstrated that eribulin administered to mice with pre-existing paclitaxel-induced peripheral neuropathy had limited additional deleterious effects whereas a second regimen of paclitaxel caused additional nerve conduction and amplitude effects (Wozniak 2013). Our preclinical findings raise the possibility that peripheral neuropathy during chemotherapy with microtubule targeting agents might be more efficiently managed by optimizing the sequential administration of drugs with respect to their severity and potential reversibility of neuropathy.

Figures

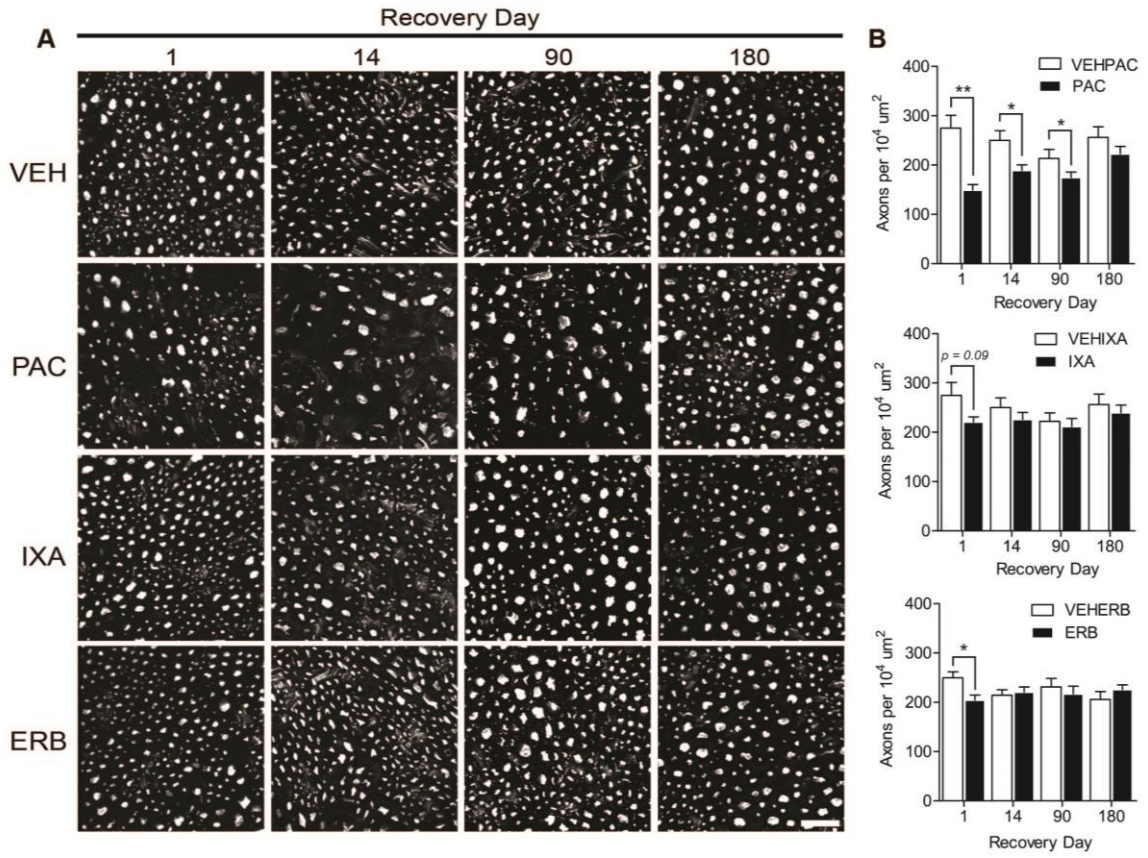

Figure 1. Persistent reductions in axon area density were most severe following paclitaxel treatment, with ixabepilone and eribulin showing mild effects. ***A***, Representative immunofluorescent images of sciatic nerve axons during recovery from paclitaxel, ixabepilone, eribulin or vehicle paclitaxel/ixabepilone treatment. As there was no statistical difference between the respective vehicles for paclitaxel/ixabepilone and vehicle eribulin at any time point, only the vehicle for paclitaxel/ixabepilone is shown in the representative images panel. Axons were identified by phosphoneurofilament (PNF) signal (white). The area of the nerve bundle was traced and measured in Imaris so that only PNF-stained objects within that area were quantified. Each image panel represents 10^4 um^2. ***B***, Quantification of axons per 10^4 μm^2 over the recovery period measured from images show in ***A;*** (*n = 5-28 images analyzed per condition*); Student's T-test were performed against the vehicle control for each drug at each timepoint, **p < 0.05, **p < 0.01,* scale bar = 20μm.

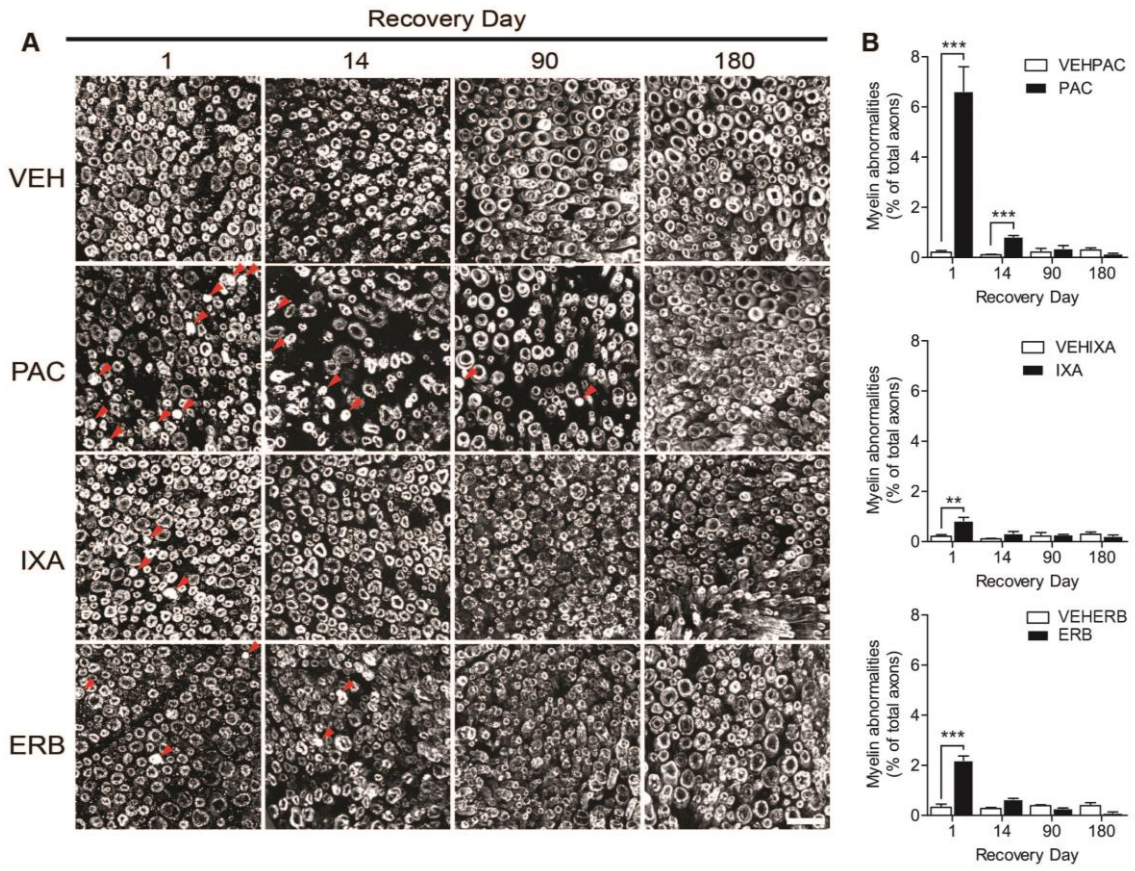

Figure 2. Myelin abnormalities persist in paclitaxel-treated animals, but are resolved after eribulin or ixabepilone by day 14. ***A,*** Representative immunofluorescent images of sciatic nerve myelin sheaths during recovery from paclitaxel, ixabepilone, eribulin or vehicle treatment. As there was no statistical difference between the respective vehicles for paclitaxel/ixabepilone and vehicle eribulin at any time point, only the vehicle for paclitaxel/ixabepilone is shown in the representative images panel. Signs of myelin abnormalities were present in all drug-treated animals, but were consistently most severe in paclitaxel-treated mice. ***B***, Quantification of nerve fiber collapses per total number of anti-myelin basic protein (MBP, white) stained objects. Collapses were defined as fragmented and/or contracted myelin sheaths coupled with a loss of PNF protein signal from the associated axons. Red arrowheads indicate myelin sheath collapses. (*n = 3-5 images analyzed per condition*); Student's T-test was performed against the vehicle control for each drug at each timepoint, **p < 0.01, ***p < 0.001, scale bar = 20μm.

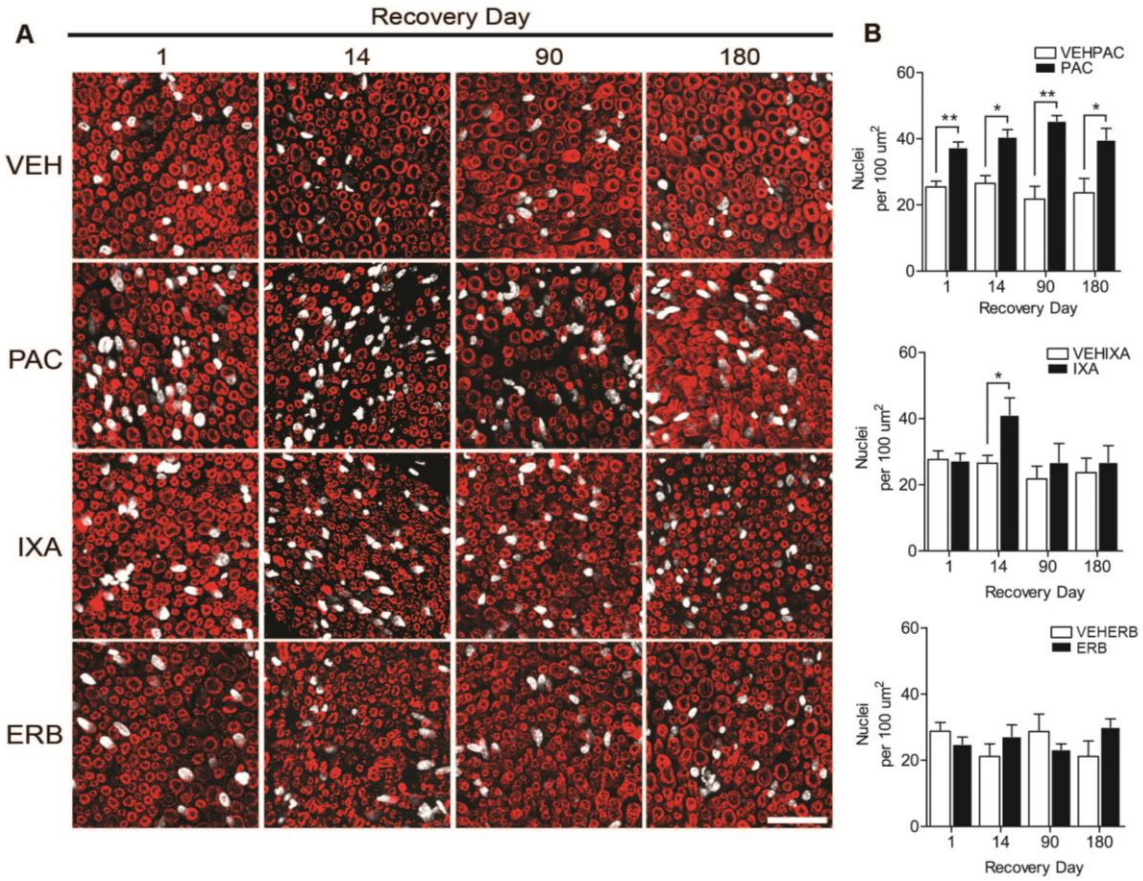

Figure 3. Paclitaxel increases Schwann cell abundance at all recovery timepoints while ixabepilone induced only at day 14 and eribulin showed no effect. ***A***, Representative immunofluorescent images of Schwann cell nuclei and myelin sheaths during recovery from paclitaxel, ixabepilone, eribulin or vehicle treatment. As there was no statistical difference between the respective vehicles for paclitaxel/ixabepilone and vehicle eribulin at any time point, only the vehicle for paclitaxel/ixabepilone is shown. Values for actual respective vehicles were used for the graphs and statistics in B. ***B***, Quantification of Schwann cell nuclei abundance during recovery as detected by DAPI (white). The myelin sheath (MBP, red) is also shown to indicate the location of axons. Scale bar = 20μm. Student's T-test was performed against the vehicle control for each drug at each timepoint, (*n = 3-5 images analyzed per condition*), *$p < 0.05$, **$p < 0.01$.

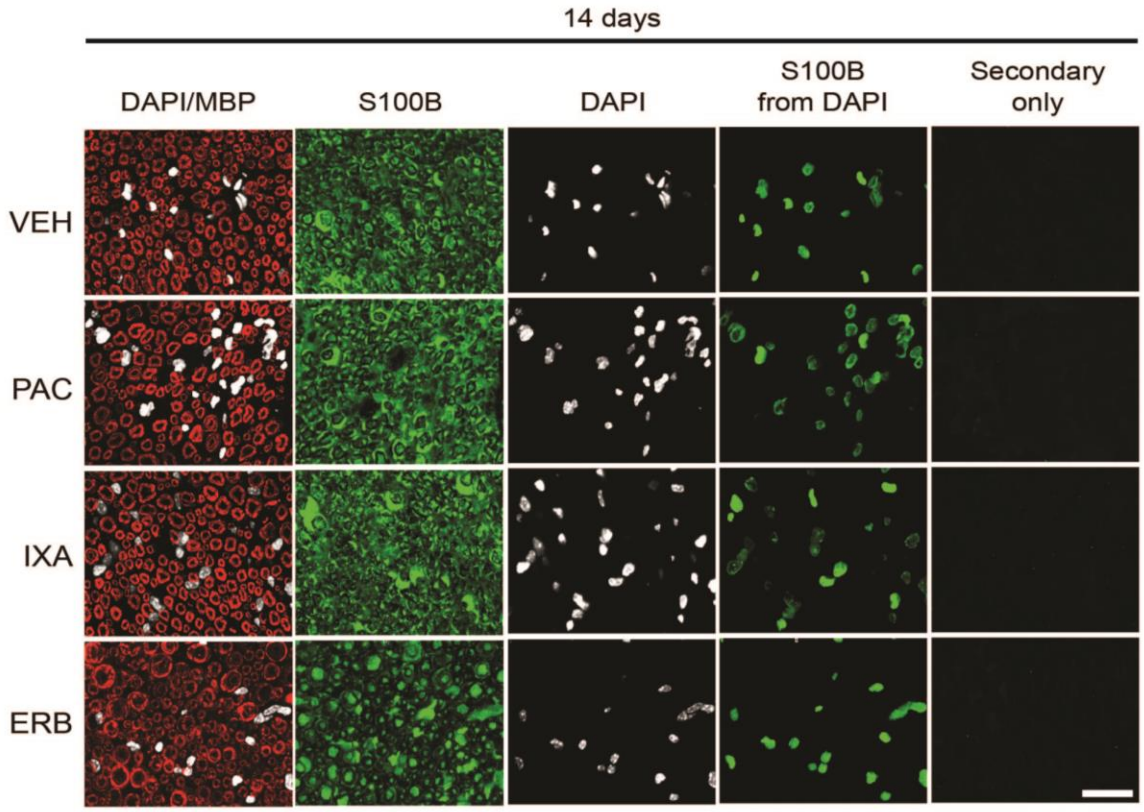

Figure 4. Additional DAPI-positive nuclei are positive for Schwann cell marker S100B at 14 days in paclitaxel-, ixabepilone-, and eribulin-treated nerves. Representative immunofluorescent images of one field of view of sciatic nerve tissue from each drug- or vehicle-treated animal . The DAPI/MBP column shows DAPI in white and myelin basic protein (MBP) in red, the S100B column shows only the S100B signal (green) from the same field of view, the DAPI column shows only the DAPI signal (white), the S100B from DAPI is only the S100B signal that colocalizes to the 3-dimensional volume of the DAPI channel, and the secondary only column shows the background signal of a section from each treatment processed using the same conditions and imaged using the same settings but omitting the primary anti-S100B antibody, indicating limited non-specific signal from the secondary antibody. As there was no difference between the respective vehicles for paclitaxel/ixabepilone and vehicle eribulin at any time point, only the vehicle for paclitaxel/ixabepilone is shown. All additional nuclei were positive for S100B in all treatments at all timepoints tested (data not shown). Scale bar = 20μm.

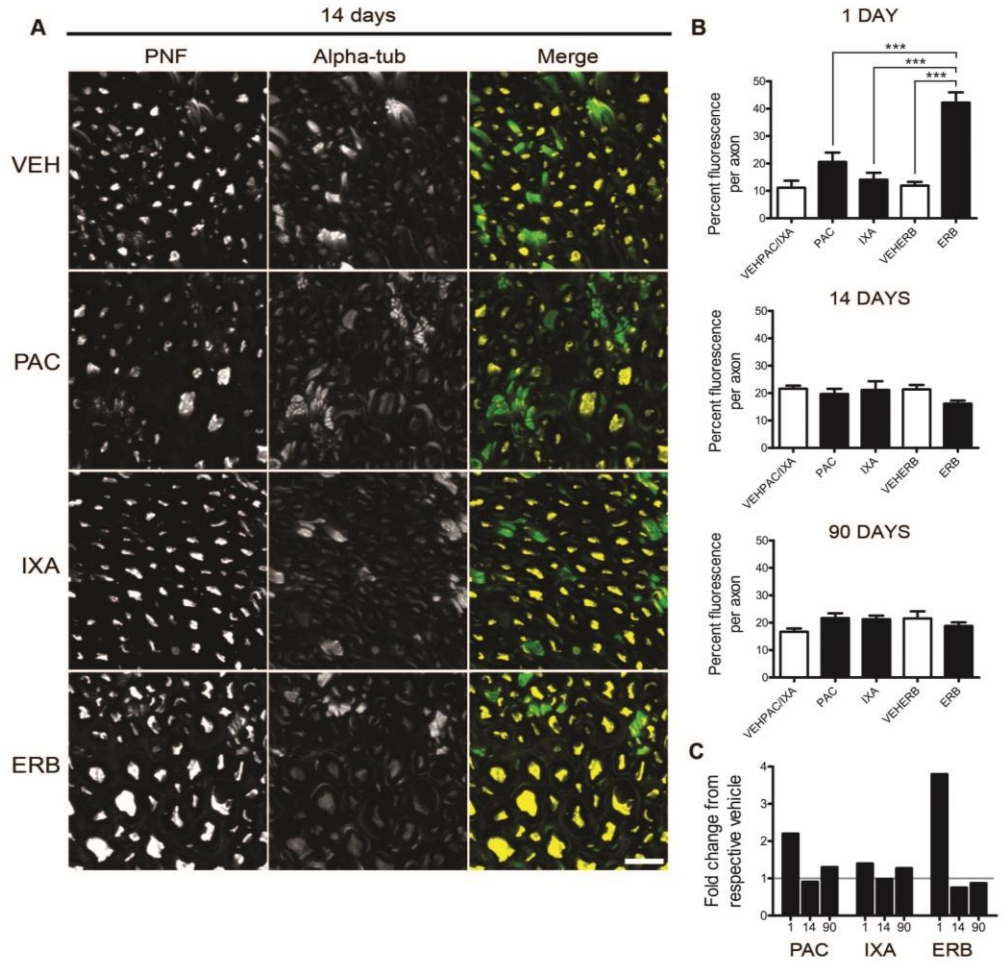

Figure 5. Axonal levels of α-tubulin rapidly return to control levels in paclitaxel- and eribulin-treated animals, with ixabepilone showing no change at any timepoint. ***A***, Representative immunofluorescent images of α-tubulin protein abundance during recovery from paclitaxel, ixabepilone, eribulin or vehicle treatment. The phosphoneurofilament column (PNF) shows only the axons. The alpha-tubulin column shows only the total alpha tubulin signal of the same field of view. The merge column shows the overlay of alpha tubulin (green) and PNF (yellow) signals. As there was no statistical difference between the respective vehicles for paclitaxel/ixabepilone and vehicle eribulin at any time point, only the vehicle for paclitaxel/ixabepilone is shown. Values for actual respective vehicles were used for the graphs and statistics in B and C. ***B***, Quantification of axonal α-tubulin levels in drug and vehicle-treated sciatic nerves following 1, 14, or 90 days of recovery. ***C***, Recovery of fold change in axonal α-tubulin abundance from respective vehicle. The horizontal gray line in C indicates a fold change of 1, or no difference from the vehicle control. Statistics: 1-way ANOVA with Tukey post-test, ****p < 0.001*, (*n = 3-5 images analyzed per condition*). Scale bar = 20μm.

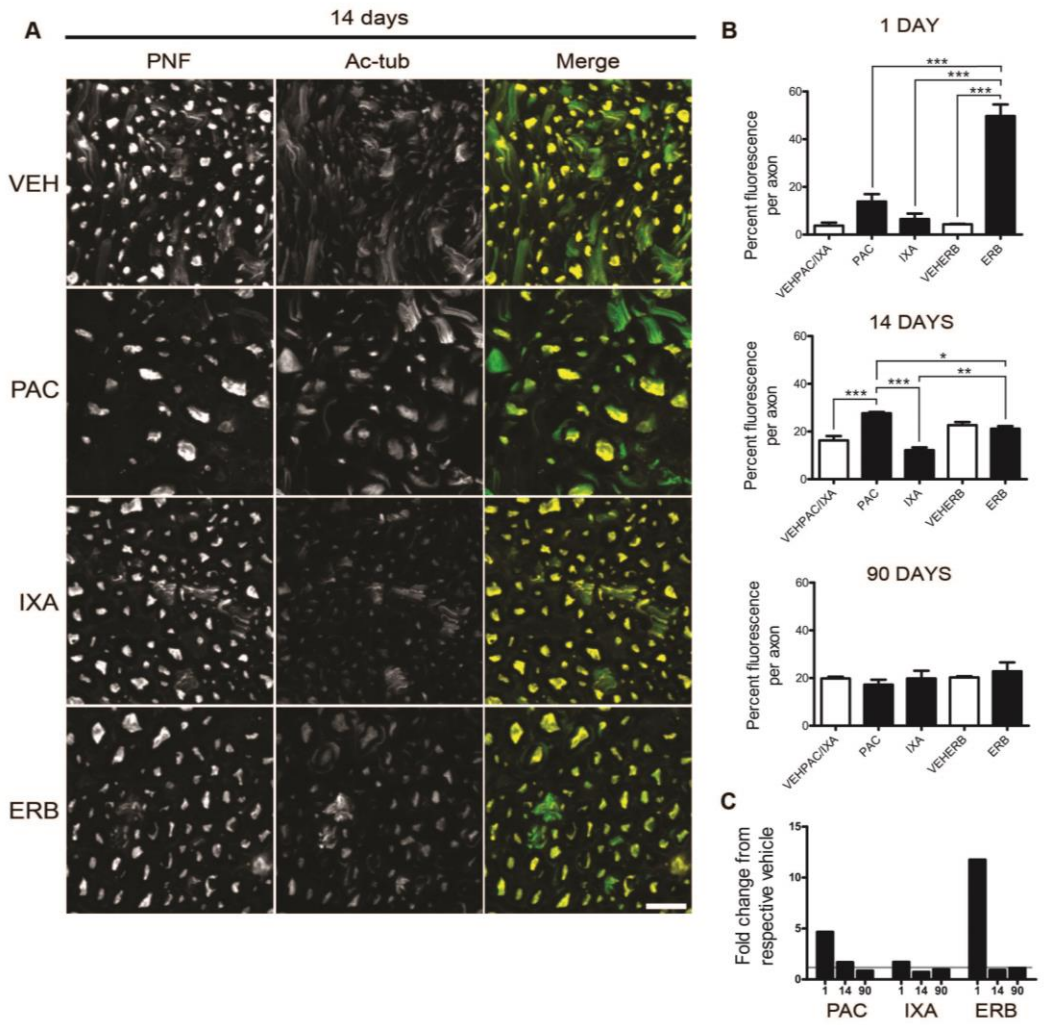

Figure 6. Increased axonal levels of acetylated α-tubulin persist in paclitaxel-treated animals while eribulin-treated animals rapidly recover to levels similar to control at day 14, and ixabepilone showing no change from its vehicle control at any timepoint. ***A***, Representative immunofluorescent images of acetylated α-tubulin protein abundance during recovery from paclitaxel, ixabepilone, eribulin or vehicle treatment. The phosphoneurofilament column (PNF) shows only the axons. The acetylated alpha-tubulin column shows only the total acetylated alpha-tubulin signal of the same field of view. The merge column shows the overlay of acetylated alpha-tubulin (green) and PNF (yellow) signals. As there was no statistical difference between the respective vehicles for paclitaxel/ixabepilone and vehicle eribulin at any time point, only the vehicle for paclitaxel/ixabepilone is shown. Values for actual respective vehicles were used for the graphs and statistics in B and C. ***B***, Quantification of axonal acetylated axonal α-tubulin levels in drug and vehicle-treated sciatic nerves following 1, 14, or 90 days of recovery ***C***, Recovery of fold change in axonal α-

tubulin abundance from respective vehicle. The horizontal gray line in C indicates a fold change of 1, or no difference from the vehicle control. Statistics: 1-way ANOVA with Tukey post-test, *$p < 0.05$, **$p < 0.01$, ***$p < 0.001$, (*n = 3-5 images analyzed per condition*). Scale bar = 20μm.

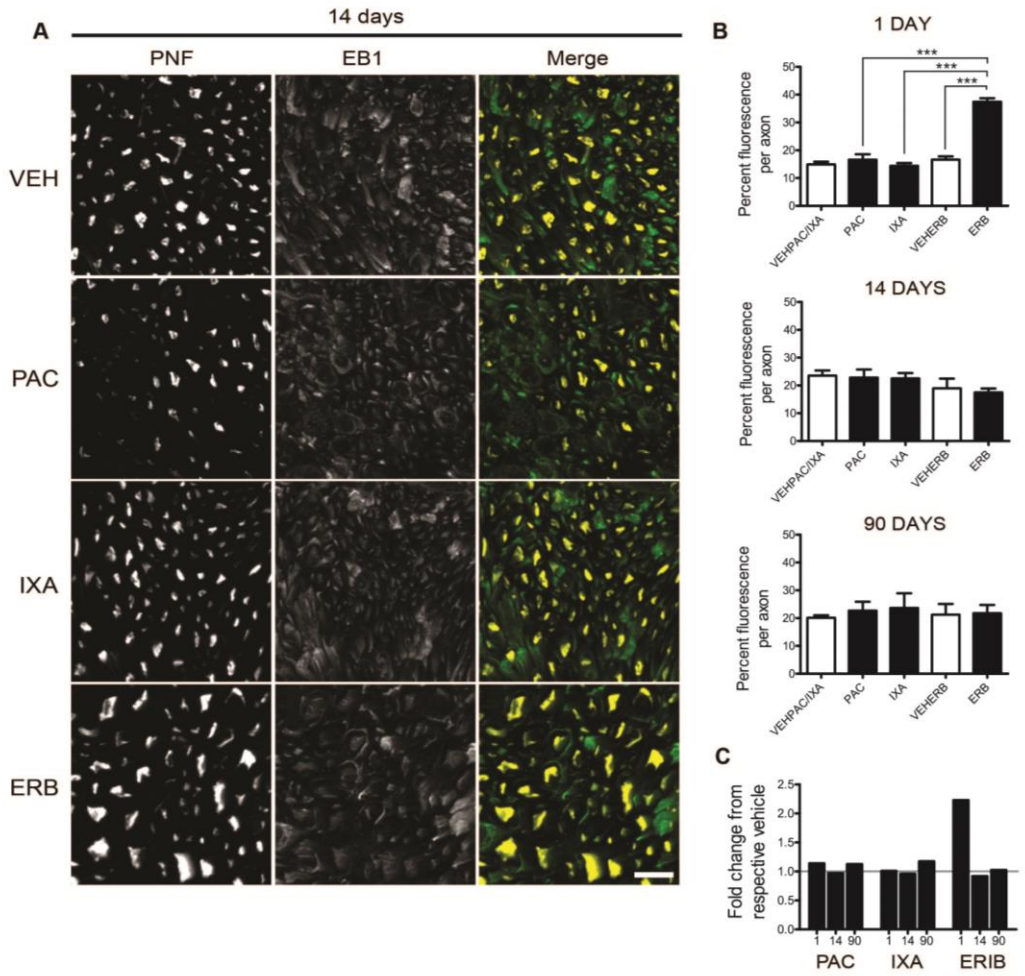

Figure 7. Axonal levels of EB1rapidly return to control levels in eribulin-treated animals, with paclitaxel and ixabepilone showing no change at any timepoint. ***A***, Representative immunofluorescent images of axonal end binding protein 1 (EB1) abundance during recovery from paclitaxel, ixabepilone, eribulin or vehicle treatment. The phosphoneurofilament column (PNF) shows only the axons. The acetylated alpha-tubulin column shows only the total EB1 signal of the same field of view. The merge column shows the overlay of EB1 (green) and PNF (yellow) signals. As there was no statistical difference between the respective vehicles for paclitaxel/ixabepilone and vehicle eribulin at any time point, only the vehicle for paclitaxel/ixabepilone is shown. Values for actual respective vehicles were used for the graphs and statistics in B and C. ***B***, Quantification of axonal EB1 levels in drug and vehicle-treated sciatic nerves following 1, 14, or 90 days of recovery. ***C***, Recovery of fold change in axonal EB1 from respective vehicle. The horizontal gray line indicates a fold change of 1, or no difference from the vehicle control. Statistics: 1-way ANOVA with Tukey post-test, ****p < 0.001*, (*n = 3-5 images analyzed per condition*). Scale bar = 20μm.

Supplemental Figure S1

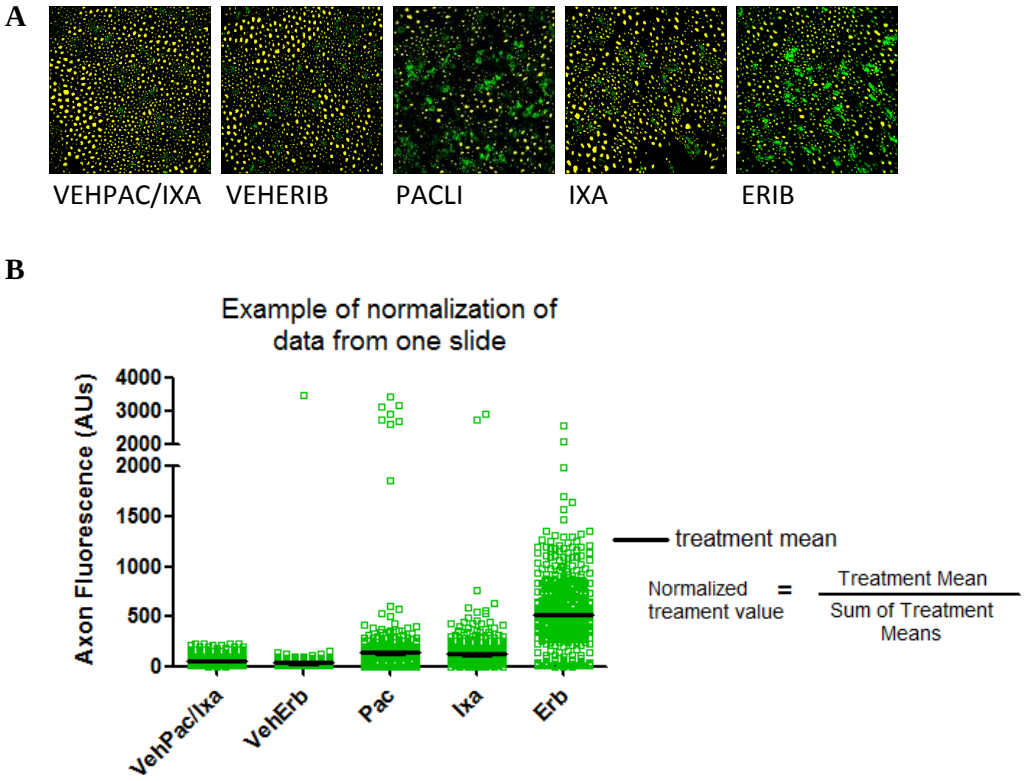

Supplementary Figure S1. Normalization of Cy2 fluorescent signal. A. Representative sections from one nerve per 5 treatment groups, stained with same antibody solution and imaged using same microscope settings. Axonal (3D) region was identified by phosphoneurofilament (PNF, yellow in fluorescent images), then Cy2 (green) inside delimited regions were quantified. **B.** The Cy2 fluorescence value identified per axon is represented by the green boxes. All axons per treatment were averaged to give the treatment mean. The treatment means were then normalized by dividing each treatment mean but the sum of treatment means observed on the slide, each normalized value was multiplied by 100, to be represented as a percent of total fluorescence observed. This was repeated twice per nerve for each of 3-5 nerves per treatment to obtain a nerve value. The mean of the 3-5 nerve values is represented in the graphs in main figures. VehPac/Ixa = Vehicle for Paclitaxel and Ixabepilone, VehErib = Vehicle for Eribulin, Pacli/Pac = Paclitaxel, Ixa = Ixabepilone, Erib = Eribulin.

Chapter IV. Digital Quantification of Neurite Outgrowth and Retraction by Phase Contrast Microscopy: a tau Perspective

Summary

The proper organization and function of the mammalian nervous system relies on neuronal processes or “neurites”, extended morphological projections that include axons and dendrites. Tau is a structural microtubule-associated protein that is widely expressed in the nervous system that mediates the establishment of cell polarity, neurite outgrowth, and axonal transport. A useful model for studying the establishment and maintenance of these neuronal structures are rat neuronal PC12 cells, which can be induced to express tau and project neurites by treating the cells with nerve growth factor (NGF). Here, we present a simple method for continuously measuring the rate of neurite outgrowth and retraction over time by neurite length and neurite area analyses. This method uses freely available ImageJ software and widely available phase contrast imaging.

Introduction

The microtubule-associated protein tau is an essential protein that promotes the highly specialized morphologies in the nervous system and has important roles in cell differentiation and polarization. Primarily an axonal protein in mature neurons (in contrast to the dendritic MAP2), tau promotes the organized stabilization of microtubules and is a key regulator of neurite formation during neuronal differentiation (Drubin et al. 1985. As an intrinsically disordered protein, tau does not adopt a compact folded structure but rather is highly flexible and mobile (Schweers et al. 1994). This flexibility allows tau to stabilize microtubules by binding to the MT surface and promoting self-assembly from tubulin

subunits (Witman et al. 1976, Gustke et al. 1994). As a result of its effects on microtubule biochemistry, tau regulates the rate of neurite elongation and stability (Esmaeli-Azad, McCarty, Feinstein 1994, Butner and Kirschner 1991, Drubin et al. 1985). Axon outgrowth is inhibited when tau is suppressed using synthetic antisense oligonucleotides, which supports tau's necessity during axon outgrowth (Caceres and Kosik, 1990). Interestingly, when non-neuronal cells are induced to express high levels of tau, they can develop cellular processes containing dense arrays of bundled microtubules that are morphologically similar to neuronal axons (Baas, Pienkowski, and Kosik, 1991, Chen et al. 1992). Taken together, these studies suggest that tau's primary function is to promote microtubule assembly and bundling during neurite outgrowth.

The rat adrenal pheochromocytoma PC12 cell line has been a useful model for studying tau action during neurite outgrowth (Greene andTischler 1976). Upon treatment with nerve growth factor (NGF), PC12 cells cease to proliferate and extend branching processes similar to those produced by primary neurons in culture (Green and Tischler 1976, Drubin et al. 1985). Treatment of PC12 cells with NGF, either alone or together with dibutyryl cAMP (dbcAMP), causes a rapid and strong induction of tau expression (Gunning et al. 1981). Tau expression is induced within 3-4 days of NGF treatment, coincident with a massive increase in microtubule assembly and neurite outgrowth. Upon NGF withdrawal, tau is quickly degraded while neurites disappear through retraction and fragmentation (Drubin et al, 1985). The ability to induce tau expression through NGF-mediated differentiation makes the PC12 line a valuable tool for investigating mechanisms of tau biology specifically and axonal homeostasis in general.

Here, we present a simple method for digitally quantifying neurite length and neurite area during differentiation of PC12 cells by phase contrast imaging. Our methods, which

should be generally adaptable to neurite outgrowth studies, take advantage of freely available ImageJ plug-ins combined with non-invasive phase contrast imaging to measure neurite morphology continuously over time. The example data presented here specifically applies to neurite outgrowth, however this method could also be used to study neurite retraction following the application of agents that perturb tau and/or microtubule stability.

Materials:

- Corning Costar 6-well or 12-well cell culture plates, flat bottom with lid, tissue culture treated, nonpyrogenic, polystyrene, sterile, 6-well Cat. 3516, 12-well Cat. 3513
- Gibco antibiotic-antimycotic 100X (contains 10,000 units/mL of penicillin, 10,000 µg/mL of streptomycin, and 25 µg/mL of Gibco Amphotericin B), Thermo Fisher Cat. 15240062, store at -20°C
- Dulbecco's modified Eagle Medium powder, high glucose, [+] L-glutamine, [+] pyridoxine hydrochloride, [+] 110 mg/L sodium pyruvate, [-] sodium bicarbonate, Gibco 12800-082, store at 4°C
- Bovine calf serum, supplemented, HyClone, Cat SH30072.03, Store at -20°C
- Heat Inactivated (HI) Horse Serum, Gibco, store at -20°C
- Poly-L-Lysine hydrobromide, Sigma P2636-100mg, in sterile water at 10 µg/mL, store at 4°C
- Sterile pipettes and Pipetteman OR glass Pasteur pipettes with rubber bulb
- N^6,2'-O-dibutyryladenosine 3',5'-cyclic monophosphate sodium salt (dbcAMP), Sigma D0260-100 mg. Make a stock solution of 250 mM in sterile DMSO, store

20uL aliquots at -20°C. The final concentration is 0.5 mM (1:500 dilution from stock)

- Nerve Growth Factor (NGF)-2.5S from murine submaxillary gland, lyophilized powder, suitable for cell culture, Sigma N6009-4X25UG, diluted to 10 µg/mL in PC12 complete media, store 20uL aliquots at -20°C
- Inverted brightfield microscope equipped with phase optics, camera, and 10X objective

Methods:

1. Cell culture and differentiation

1. Maintain PC12 cells on plastic dishes in Dulbecco's modified Eagle's medium, supplemented with 5% supplemented calf-serum, 5% horse serum, 3.7 g/L $NaHCO_3$, and 1X antibiotic/antimycotic at 37°C and 5% CO_2 until 50-75% confluent (4-7 days for a 10 cm^2 dish).
2. Coat plastic cell culture dishes to be used for neurite outgrowth assays with 10 µg/mL poly-L-lysine (PLL) in sterile water for at least 1 hour at room temperature in a cell culture hood prior to plating cells.
3. When ready to seed cells, aspirate as much of the PLL solution as possible and rinse the surface three times with enough 1X PBS to cover the bottom of the well at room temperature, leaving the last wash in the well to prevent drying of the surface. With each wash, swirl the plate to collect any un-adhered PLL (soluble PLL is toxic to cells). Set the plate aside while preparing cells.
4. Remove 80% of the media from the maintenance culture dish and discard.

5. Dislodge the cells from the surface of the maintenance culture dish by spraying the remaining media across the surface of the well using an automatic Pipetteman equipped with a 5 mL sterile pipette (alternatively, a Pasteur pipette with a rubber bulb can be used).
6. Triturate the cell suspension by drawing the cell suspension into the pipette and forcing it out against the bottom of the dish while holding the pipette opening flush against the bottom of the well. The cells are quite hardy and will not break from this treatment. Repeat 10 times until all the cell clumps are dissociated.
7. Determine the cell density using a hemocytometer. No tryphan blue is required if counting is done using a phase contrast microscope.
8. Based upon the cell density, calculate the volume of cell suspension to add to fresh media so that the final cell density will be 1-5 x 10^3 cells per cm^2 of total surface area of either 6- or 12-well cell culture plates.
9. Add an appropriate volume of the cell suspension to the total volume of media needed for seeding all dishes or wells.
10. Invert the diluted cell suspension tube 5 times to homogenize the suspension.
11. Aspirate the PBS wash from each well of the PLL coated plate and immediately add the appropriate amount of diluted cell suspension to each well.
12. Return plate to incubator at 37°C and 5% CO_2 for 1-3 hours to allow cells to adhere to the surface.
13. After 1-3 hours, apply dbcAMP in DMSO to 0.5 mM final concentration to each well from a 250 mM stock solution in DMSO. This serves to initiate rapid neurite outgrowth.
14. Return the plate to the incubator at 37°C and 5% CO_2 for 24 hours.

15. After 24 hours, add β-NGF (dissolved in complete PC12 media) to a final concentration of 10-50 ng/mL to each well.
16. Spike the media in each well every other day with NGF for the duration of the differentiation process (Figure 1A).
17. On day 5, perform a half media change and supply fresh NGF.
18. If media begins to become acidic (orange color), perform a complete media change and supply fresh NGF.
19. Cells are considered fully differentiated after 7 days of NGF treatment (8 total days of differentiation). Cells should be imaged each day of the time course for subsequent analysis (detailed below).

Notes:

- It is essential that cells are plated at a density that is low enough for neurites to be able to project without contacting other cells or neurites early in the time course. If neurites encounter other neurites, they will stop their outgrowth and this will bias neurite outgrowth measurements.
- Cell dissociation can be monitored under a microscope. If cells are still significantly clumped when plated for differentiation, increase the number of trituration cycles to get as close to single cells as possible.
- Add NGF to each well in a sufficiently large volume of complete media to minimize pipetting error. The rate of neurite outgrowth is sensitive to NGF concentration.
- If a neurite retraction experiment is performed it is essential to include an appropriate negative and/or vehicle control for any experimental condition. Ideally each multi-well plate seeded with the same cell dilution should have its own negative control on

the same plate. The negative control allows each multi-well plate to be internally controlled for variations in cell seeding density and differentiation efficiency.

- Store plates being coated with PLL at 4°C overnight if unable to seed the same day. Allow the plates to come back to room temperature in a cell culture hood for ~30 minutes before plating cells, or place in an incubator at 37°C for 10 minutes.

2. Phase contrast imaging

1. Be sure the microscope's condenser is properly aligned for Köhler illumination to achieve even illumination of the sample and to provide maximum contrast between cell bodies and neurites. To do so, bring the sample into focus under a 10X objective, then fully close the field diaphragm so that the edges of the field diaphragm are visible while looking through the eyepieces. While continuing to observe the opening through the eyepieces, adjust the height of the condenser so that the edges of the field diaphragm are sharp and well defined, then adjust the position of the field diaphragm opening using the adjustment screws so that is directly centered in the field of view. From the fully closed position, slowly open the field diaphragm until the edges of the opening are just outside the field of view.
2. Adjust the microscope's bulb intensity and camera exposure time so that the background is a medium gray and the cell bodies are not overexposed (Figure 1B). If possible, store the acquisition settings for future use.
3. Adjust the focal plane so that the neurites are in focus. The cell bodies may appear slightly out of focus but this will not affect analysis.
4. Image at least five random fields of view per well of each culture plate (Figure 1B).

Notes:

- Even illumination is critical for quantitative phase contrast microscopy. Thus, it is very important to minimize background interference and create as much contrast as possible between the background and neurites without overexposing the cell bodies. This can be achieved by ensuring the condenser is properly adjusted, the field diaphragm closed as much as possible, and the exposure properly set to adequately expose the cell's features.
- The periphery of most culture plate wells tend to have higher background and less contrast when using phase contrast. The best contrast can be achieved at or near the center of each well.
- Do not adjust the exposure settings during imaging. This will ensure that the background levels are consistent throughout the experiment and will produce higher quality neurite area measurements.

3. Neurite length measurements

1. If the NeuronJ plugin (Meijering 2017) is not already installed in ImageJ, install it by downloading the install files to ImageJ's *plugins* folder. Restart ImageJ after installing.
2. Once in Image J, open the NeuronJ plugin by selecting "NeuronJ" under the "Plugins" drop-down menu.
3. Open an image using the "Open" function under the "File" drop-down menu (Figure 2A).
4. Ensure that the scale is correctly set for the image by selecting "Set Scale" under the "Analyze" drop-down menu. Enter the known distance in pixels per micron that corresponds to the objective used. This value must be determined for each individual

microscope and camera setup using a calibrated slide. In our case the 10X objective corresponds to 1.553 pixels/μm. Change the unit of measurements to "μm." Check the "Global" setting to apply this scale to all subsequently loaded images. Select "OK" to apply the scaling.

5. Click on the "Add tracings" button on the menu bar.
6. For each neurite to be measured (criteria below), click once at the origin of the neurite at the cell body and follow along the neurite's length with the cursor. If the automatic detection does not accurately trace the neurite, click along the length of the neurite to lock the tracing at certain points along the neurite. When the end of the neurite is reached, a double click on the mouse completes the tracing.
7. When all eligible neurites have been measured within the image, click the "Measure Tracings" button on the menu bar to measure the tracings. The individual tracing lengths and a summary of all tracings within the image can be copied to a spreadsheet or graphing software for analysis.
8. Save the tracing file to the same directory as the image. When the image is opened again within NeuronJ, the tracing file will be loaded automatically (Figure 2B).
9. Before closing the image, count the number of cell bodies present. Use the "Multi-point Tool" found on the ImageJ menu bar to click on each cell body and record the final count to a spreadsheet.

Notes:

- Only neurites that originate and terminate in the same field of view should be analyzed. Any neurites that enter from outside the image or extend out of the image should be omitted from neurite length measurements.

- Neurites that cross other neurites should be excluded, as they may be stabilized as a result of their interactions. At the cell densities used here, less than 10% of neurites cross one another. If required, reduce then cell density to prevent neurites crossing one another.
- A good rule of thumb for determining what constitutes a neurite is that a "neurite" is at least as long as the diameter of the cell body.
- Holding the "Shift" key produces a straight line segment that is useful for navigating along neurites that may be close together. Inaccurate tracings can be removed by using the "Delete tracings" function on the menu bar.
- The available data in NeuronJ's measure function includes the length of each individual neurite, a sum of all lengths within an image, and mean neurite length.

4. Neurite area measurements

1. Open ImageJ and load a 10X phase-contrast image file. Ensure that the image is scaled correctly as described above.
2. Open the threshold settings under "Image," "Adjust," "Threshold."
3. Drag the upper threshold bar to the lower limit so that the number to the right displays "0." Ensure that the "Dark Background" box is selected and "Stack Histogram" is *not* selected (Figure 2C). The neurites should appear black and the background white. Drag the lower threshold bar until the background starts to be visible (as black), then make small adjustments so that the background is still white. The upper limit is typically set slightly to the left of the main peak shown on the threshold graph (Figure 2C). Small specks in the background are acceptable and will

be filtered out later. The image should be shown as thresholded as in Figure 2D. Close the threshold window (do not select "auto" or "apply" from this window).

4. Select the "Analyze Particles" option under the "Analyze" drop-down menu.
5. Enter "10-Infinity" in the "Size" box, check the box for "Pixel units," enter "0.00-0.40" in the "Circularity" box, then press OK (Figure 2F).
6. A results dialog will open after "OK" is pressed. Notice which areas were selected in the image. If the identified areas are not appropriate, close the results windows without saving and adjust the analyze particles size and circularity values until only the neurite areas are identified.
7. Once appropriate particle size and circularity settings are determined that identify only neurites, they should be applied to all images in the set without adjustment.
8. Copy the results for individual particles from the "Results" window and from the "Summary" window to a spreadsheet. Repeat steps 1-5 for at least five images per condition, making sure to copy the results to a spreadsheet after analyzing each image.

Notes:

- If necessary, remove erroneous regions of interest (ROIs) by right-clicking the entry in the results window and selecting "Cut". Each ROI is numbered for identification. The ROIs can also be overlaid onto the original image to verify neurite identification. To do so, open the original image again through ImageJ without closing the thresholded and analyzed image. Under the "Image" drop-down menu, select the "Overlay" menu and select "From ROI Manager" (Figure 2E). If desired, the ROI's

can be saved for each image by selecting “More” from the ROI Manager and selecting “Save.” Load existing ROIs by selecting “Open” from the same menu.

- The particle size and circularity settings listed here are given as starting points and should be optimized for the level of background in the image (particle size filter) and general shape of cell bodies of the neurons being analyzed (circularity filter). A larger circularity value will maintain particles that are more round (i.e. cell bodies) while a smaller value will maintain more longer and straight particles (neurites).
- Each image must be manually thresholded and the limits should be similarly set to achieve consistent analysis throughout the data set. Thus it is important during image acquisition to maintain a consistent background intensity.

5. Data Analysis

1. The average neurite length from each image (at least five per experimental condition) can be calculated in Excel and copied to a data analysis software such as GraphPad Prism for statistical analysis (Figure 2G). Using the number of cells per image, the average neurite length per cell can be calculated by dividing the sum of neurite lengths per image by the number of cells per image. The total neurite length per image can be found by taking the sum of all neurite lengths in an image, and the average per condition can be calculated by dividing this total by the number of cell bodies counted for each image.
2. The average area per image can be calculated by first adding together all the areas of all particles identified in an image and dividing by the number of cells. The sum of areas can be calculated by adding together each particle area sum from each of the 5 images analyzed.

3. To normalize area data before comparing across experiments, divide the total neurite area of each treatment well by the area of the control well. This value is the "index" value or "percent of control."

Notes:

- Each plate should be normalized to its own control before comparing values across plates so that neurite length and area measurements are internally controlled for variations in cell seeding density and growth conditions. Thus it is important to include a negative and/or vehicle control on each multi-well plate that is imaged.

Conclusions

We presented a simple method for digitally quantifying neurite length and area during differentiation of PC12 cells. This method allows continuous measurement of neurite morphology during neurite outgrowth and can also be applied to neurite degeneration in live cells. In principle, this method could be applied in studies involving rates of axon outgrowth as well as mechanisms of neurotoxicity resulting from insults to neuronal homeostasis.

Acknowledgements

We thank Dr. Mary Raven, Dr. Sarah Benbow and Dr. Julianna Erickson for technical support and protocol optimization.

Figures

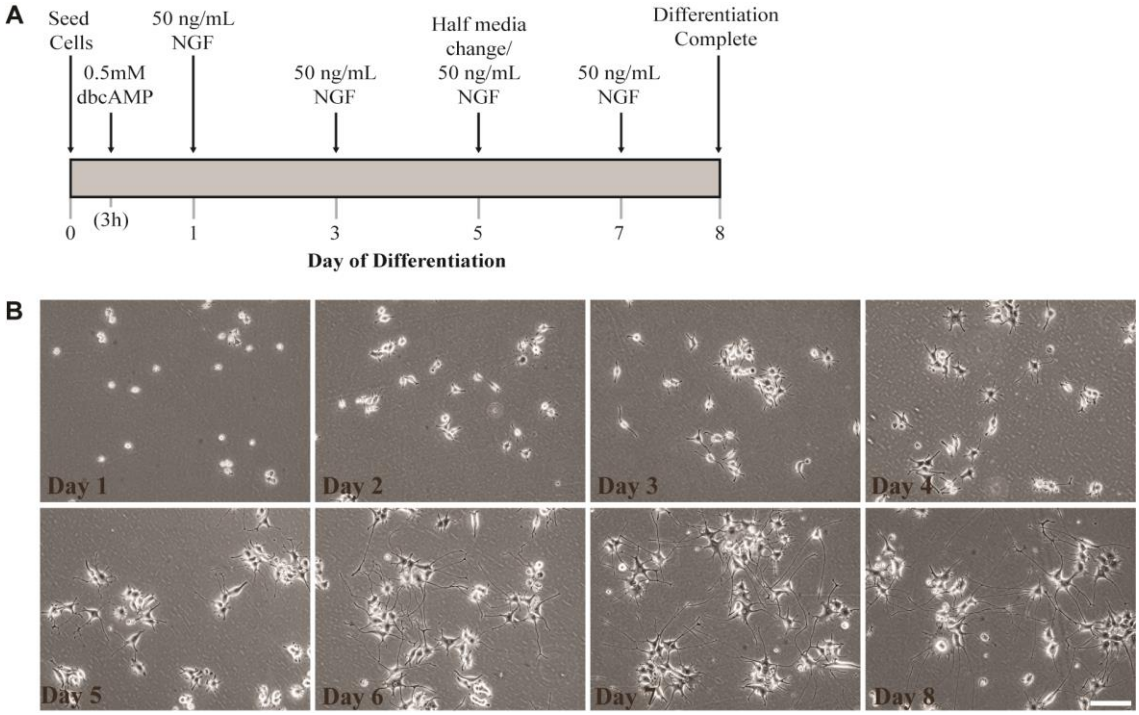

Figure 1. PC12 differentiation by nerve growth factor and dbcAMP over eight days in 5% HI-horse serum and 5% calf serum-containing media at 37C and 5% CO_2. **A**, Schedule of cell culture conditions. dbcAMP is added three hours post-seeding, then NGF is added to existing media 24 hours later and every other day following. A half media change can be performed on day 5 if necessary, but may not be required. **B**, Representative 10X phase contrast images of PC12 cells corresponding to each day of the schedule shown in A, scale bar = 100 μm.

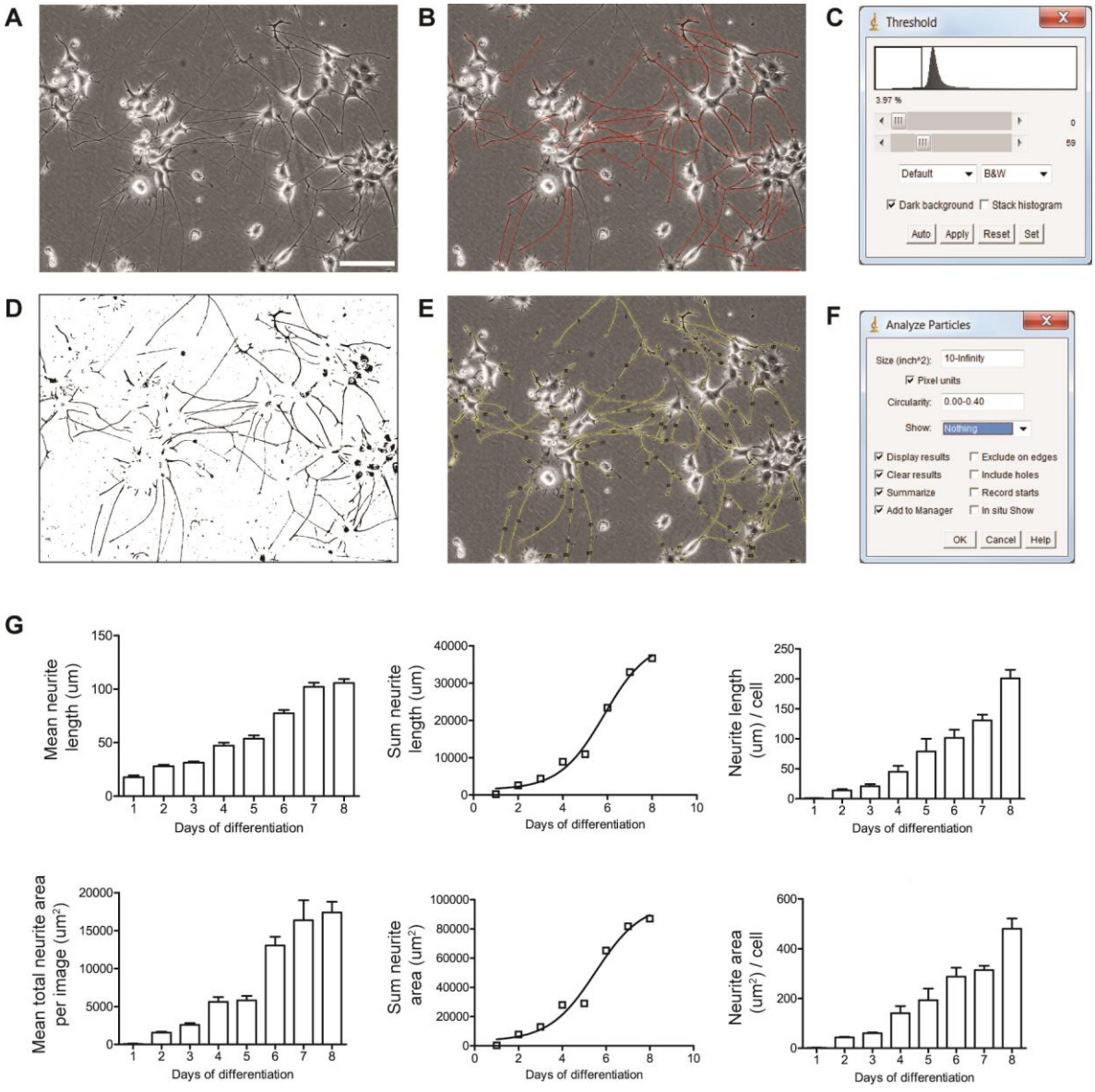
A
B
C
Threshold
3.97 %
0
59
Default
B&W
Dark background
Stack histogram
Auto
Apply
Reset
Set
D
E
F
Analyze Particles
Size (inch^2):
10-Infinity
Pixel units
Circularity:
0.00-0.40
Show:
Nothing
Display results
Exclude on edges
Clear results
Include holes
Summarize
Record starts
Add to Manager
In situ Show
OK
Cancel
Help
G
Mean neurite length (um)
Sum neurite length (um)
Neurite length (um) / cell
Mean total neurite area per image (um²)
Sum neurite area (um²)
Neurite area (um²) / cell
Days of differentiation

Figure 2. Digital quantification of neurite outgrowth in differentiated PC12 neuronal cells. **A**, Representative 10X phase contrast image of Day 8 PC12 cells, scale bar = 100 μm. **B**, Neurites traced for length measurements (red) in the NeuronJ plugin for ImageJ. **C**, Threshold settings used for neurite area measurements. Note the position of the minimum and maximum threshold values and "dark background" selection. **D**, Thresholded version of the original image shown in A. **E**, Overlay of the original image and the identified areas from the thresholded image (shown in yellow). **F**, Analyze particle settings, showing the particle size and circularity values. **G**, Representative data of neurite length and neurite area over eight days of differentiation. Measurements are from five images per timepoint. From left to right, the graphs represent the average length or area of all neurites per image for five images, the sum of the total neurite length or area for five images, and the average neurite length or area per cell (total value divided by the number of cell bodies in the corresponding image). Bar graphs are mean ± SEM, produced in GraphPad Prism.

Chapter 5: Assessment of microtubule-targeting agents' effects on neurite outgrowth, retraction, and on cytosolic α-tubulin acetylation in cultured PC12 cells

Summary

This chapter describes a progress update on investigations of the cellular and molecular mechanisms of MTA-induced neurotoxicity. Although a great many theories have been proposed to explain how inhibition of microtubule dynamics leads to degeneration of post-mitotic sensory neurons, the molecular mechanisms responsible for the induction, progression, and recovery of CIPN are still unclear. Here, we analyzed the effects of four commonly used microtubule targeting agents on cell proliferation, neurite morphology and tubulin biochemistry in neuronal PC12 cells using phase contrast microscopy and immunoblotting, respectively. Treatment with paclitaxel, ixabepilone, vincristine, or eribulin induced dose-dependent losses of neurite area, recapitulating the 'dying back' of axons observed in clinical CIPN. IC_{50}s for neurite retraction were 11.9, 11.3, 1.9, and 6.0 nM for paclitaxel, ixabepilone, vincristine, and eribulin, respectively. Compound-specific effects, such as neurite fragmentation and thinning by eribulin or neurite swelling by paclitaxel, were also observed. Finally, increasing tubulin acetylation, a marker associated with microtubule stability, was insufficient to protect cells from drug-induced loss in neurite area. Collectively, these results demonstrate that PC12 neurons are a useful model for investigating the molecular mechanisms of CIPN.

Introduction

Interference with microtubule function is a common therapeutic strategy for treating many types of cancers. The anti-mitotic activity of microtubule-targeting agents (MTAs) is

generally accepted to derive from their ability to alter normal regulatory mechanisms controlling microtubule dynamics. Disruption in the diverse functions of microtubules, such as chromosome segregation, microtubule-based transport, and cell structure, can lead to tumor cell death (Jordan et al. 1995, Jordan and Wilson 2004, Argyriou et al. 2012, Field et al. 2014, Porunchynsky et al. 2015). However, systemic administration of MTAs also exposes non-target cells of the nervous system to their action, which in turn can lead to severe and dose-limiting neuropathic side effects. Chemotherapy-induced peripheral neuropathy (CIPN) is a dose-dependent sensory neuropathic pain that ranges from numbness and tingling to hypersensitivity that originates in distal extremities (fingers and toes) and progresses proximally toward the trunk. The neurons mediating pain in CIPN are post-mitotic and thus no longer require microtubules for chromosome segregation. However, the axonal microtuble cytoskeleton is essential for structure and transport of messages and organelles back and forth from the nucleus. Therefore, the onset and progression of CIPN may result from non-mitotic effects of MTAs on axonal microtubules of peripheral nerves, such as through structural changes that alter affinity of microtubule associated proteins.

The molecular mechanisms involved in regulating MTA induced neurotoxicity during chemotherapy are poorly understood. While the in-vitro mechanisms of action of many unique agents have been well characterized in reconstitution experiments, studies focusing on the response of whole live neurons to long-term drug treatment are lacking. The rat adrenal pheochromocytoma PC12 cell line has been a useful model for studying neurite outgrowth (Greene and Tischler 1976). Upon treatment with nerve growth factor (NGF), either alone or together with dibutyryl cAMP (dbcAMP) (Figure 1A), PC12 cells cease to proliferate and extend branching processes similar to those produced by primary neurons in culture (Green and Tischler 1976, Drubin et al. 1985). Prior to NGF treatment, PC12 cells

continually divide with one cell division occurring about every 48 hours. Following NGF treatment, PC12 cells no longer divide and microtubules are primarily involved in cell structure, neurite outgrowth, and molecular transport. To compare concentrations that arrest neurite outgrowth or initiate neurite retraction with concentrations that inhibit cell division, we exposed either undifferentiated (mitotic) or differentiated (post-mitotic) PC12 cells to either paclitaxel, ixabepilone, vincristine, or eribulin and determined IC_{50}s for cell proliferation and neurite retraction, and compared these values with reported IC_{50}s for proliferation of various cancer cell lines. We found that in general, neurite retraction was initiated at lower drug concentrations than were required for inhibition of cell proliferation in PC12 cells. Vincristine was the most potent in reducing neurite area, followed by eribulin, ixabepilone, and paclitaxel. By comparing the IC50 for neurite retraction and cancer cell proliferation of each agent, we found that neurites were comparatively more tolerant of eribulin. In general, the IC50s for neurite retraction (VCR>ERB>IXA>PTX) did not correlate well with the clinical incidence of severe (grades 3/4) clinical neuropathy [VCR (31%) > PTX (27%) > IXA (20%)> ERB (7%)]. However, when compared to the IC50s for cancer cell inhibition, the ratio of inhibitory concentrations indicates that neurites were more tolerant of eribulin treatment than for paclitaxel, vincristine, and ixapilone.

Our investigations here focused on four commonly used CIPN-inducing MTAs: paclitaxel, ixabepilone, vincristine, and eribulin. Previously, our group assessed the propensity of each of these agents to induce neuropathy in a 2 week administration, maximum tolerated dose mouse model (Benbow et al. 2016). Biochemically, paclitaxel and eribulin both induced α-tubulin expression in mouse sciatic nerves (~1.9 and ~2.5 fold, respectively). Given that paclitaxel has been shown to promote microtubule stability (at least in short-term cell culture and in vitro biochemical analyses), it was not surprising that

paclitaxel treatment resulted in a ~5 fold increase in tubulin acetylation, a well-established marker for microtubule stability (Webster and Borisy 1989, Szyk et al. 2014). However, given that eribulin has been shown to be a microtubule destabilizer in short-term cell culture and in vitro biochemical experiments, it was very surprising to observe that eribulin induced tubulin acetylation by ~11 fold in the sciatic nerves. This unexpected finding led us to propose the hypothesis that the positive biochemical effects of eribulin observed in sciatic nerves of two week eribulin-treated mice compensated in part for its observed morphological deficits (Benbow et al. 2016).

An increase in acetylated tubulin levels suggests that the microtubule cytoskeleton in eribulin-treated nerves is more stable than that of paclitaxel-treated nerves, which could account for eribulin's lower incidence of severe (dose-limiting) neuropathy. Tubulin acetylation has long been used as a marker of microtubule stability (Webster and Borisy 1985; Szyk et al. 2014). Initially, acetylation was viewed more as a consequence of microtubule stability rather than as a promoter of microtubule stability. However, more recent work has suggested a more active role in promoting microtubule stabilization. For example, increasing tubulin acetylation can rescue dysfunctional axonal transport and locomotor deficits in Drosophila (Godena et al. 2014) and can promote recruitment of dynein and kinesin-1 to microtubules in vitro and in mammalian cells. Indeed, inhibition of histone deacetylase 6 (the primary tubulin deacetylase) leads to markedly increased levels of tubulin acetylation and compensates for the transport deficit in Huntington's disease (Dompierre et al., 2007). Here, to test the hypothesis that increased levels of tubulin acetylation can minimize the deleterious effects of MTAs in post-mitotic neurons, we used the small molecule tubacin to inhibit HDAC6, thereby increasing tubulin acetylation and asked whether the neurites were protected from paclitaxel and eribulin induced neurite loss.

We found that this treatment failed to protect neurites from the deleterious effects of both paclitaxel and eribulin.

Methods

Cell culture

PC12 cells were maintained in DMEM containing 5% horse serum and 5% heat-inactivated calf serum, 1X pen/strep/fungizone, and 3.7 g/mL sodium bicarbonate. Prior to differentiation, cells were seeded at 3000 cells/cm^2 (for imaging) or 10,000 cells/cm^2 (for lysates) on plastic tissue culture-treated 12-well and 6-well plates, respectively, that had previously been coated with poly-L-lysine (Sigma, 10 µg/mL in sterile water) for at least 1 hour at room temperature. Differentiation was initiated 1 hour after seeding by adding 0.5mM dbcAMP. 24hrs later NGF was added to 20ng/mL, and cells were provided fresh NGF every two days and a half media change every 4 days. Cells were differentiated for 8 days before drug-treatment in neurite retraction studies, or 5 days before neurite outgrowth studies.

Drugs

Paclitaxel, ixabepilone, vincristine, and eribulin were diluted in DMSO to stock concentrations of 1000X (1, 3, 9, 27, or 81µM). All dilutions were thawed on ice until being added to cells, and each aliquot was only used once (multiple freeze-thaws were not allowed). Tubacin (Sigma) was diluted to a stock concentration of 10mg/mL in DMSO and then diluted to 1000X concentrations in DMSO of 0.2, 0.6, 2, 6, or 10mM for 24hr dose response experiments, and used at 6uM final concentration for 24hr pre-treatment experiments. Equal volumes of DMSO were used for all treatments and one set of time-

matched vehicle controls were included on each plate. The final concentration of DMSO did not exceed 0.1%. Cells were exposed to drugs in duplicate and triplicate wells/concentration for biochemistry and microscopy, respectively.

Undifferentiated Cell Viability

Rat neuronal precursor cells (PC12) were plated at a density of 20,000 cells/cm^2 and exposed to a range of concentrations of each microtubule targeting agent for 48 hours. Cell viability was measured using the live-cell indicator calcein-AM. Live cells emit green fluorescent light which can be detected at 495nm. Using fluorescence microscopy, five different images were acquired per well (one in each corner and the center) to account for plating variability. Automated cell counting was performed using custom macros in ImageJ. Briefly, images were thresholded and binarized to allow cell identification. To determine the IC_{50} for each MTA, a dose response curve was generated in Graphpad Prism 5 and a log(inhibitor) vs. response curve with variable slope was best-fit to the number of live cells for each drug over a range of concentrations from 1nM to 243nM.

Neurite Retraction

To assess neurite morphology, triplicate wells for each condition were imaged by phase contrast microscopy. Five random fields of view from each well were captured with a 10X objective using an Olympus IX70 inverted bright field microscope equipped with phase contrast optics. Each image was processed for neurite area measurements in ImageJ using the method described in Cook et al. 2017 (see chapter 4). Briefly, each image was manually thresholded to remove the background pixels and cell bodies so that only the neurites remained. Using the analyze particles function in ImageJ with a size and circularity filter,

the neurite area was measured. Data from each plate was normalized to a vehicle control value on the same plate before comparing across plates to account for differences in cell seeding and growth conditions. For example, the neurite area of a drug-treated well was divided by the average neurite area value from the 5 control images. To maintain the variation in the control, each control value was divided by this normalizing value. The data are reported as fold change in neurite area from control.

Protein Extractions

Following drug or vehicle treatment, cells were washed once with warm PBS and 100uL extraction buffer (1% Triton-X-100/2M glycerol in 50mM Tris-HCl, 150mM NaCl, + fresh protease/phosphatase inhibitors (Thermo Halt, 1X) was added to each well of a 6-well plate. The plate was incubated at 37°C for 10 minutes before the extraction buffer was harvested from each well to a centrifuge tube and immediately placed on ice. Samples were cleared using centrifugation at 10,000 rpm for 10 minutes and placed back onto ice until gel loading.

Western Blotting

30ug of crude protein lysates were separated on 8% SDS-PAGE gels and transferred to nitrocellulose membranes using a Pierce Power Station with FastBlot semi-dry transfer plates. Briefly, the gel was incubated in water at room temperature for 5 minutes while the membrane and filter paper were incubated in Thermo 1-Step Transfer buffer for 5 minutes at room temperature before the sandwich was assembled. Excess buffer was removed by rolling a glass Pasteur pipette gently across the sandwich and blotting the excess buffer around the sandwich with a paper towel. Protein transfer was performed at 25V at 2.5A for 12 minutes. Following transfer, the membrane was washed quickly (5s) in TBST + 0.1% Tween-20, and the gel was stained with Coomassie to detect any residual protein. The

membrane was then blocked with blocking buffer (TBST + 0.1% Tween-20 + 5% non-fat milk) for 1 hour at 4°C on a plate rocker. The blocking solution was then discarded and fresh blocking solution containing primary antibodies were added and incubated at 4°C overnight on a plate rocker. The following morning, the primary solution was removed and the membranes were washed three times with TBST + 0.1% tween (without milk) for 5 minutes at room temperature. Fluorophore-conjugated secondary antibodies (Licor700 or Licor800) were added at 1:2000 in TBST + 0.1% Tween-20 + 5% milk and incubated at room temperature in the dark for 1-2 hours. The membranes were washed again three times with TBST + 0.1% tween (without milk) for 5 minutes each at room temperature and imaged on a LI-COR Odyssey Scanner (LI-COR Biosciences, Lincoln, NE).

Results

Characterization of neurite growth during PC12 differentiation

After eight days of differentiation, long neurites were present with an average neurite length of 200μm/cell (Figure 1B, C). To establish a neurite area analysis method for rapidly analyzing neurite retraction and fragmentation in phase contrast images, we first verified that the mean neurite length, sum of neurite lengths, and neurite length per cell measurements in untreated cells were equally representative in untreated cells (Figure 1C). We found these metrics were in good agreement, and proceeded with neurite area for the majority of our evaluations due to its rapid processing time and its ability to detect fragmentation events.

Paclitaxel and eribulin arrest neurite outgrowth

Due to the unexpected differences between paclitaxel and eribulin in mice (Chapter 3), we compared the effects of each agent on neurite retraction in cultured cells (neurite

elongation was not investigated for vincristine and ixabepilone). To determine concentrations at which neurite elongation is inhibited, we treated differentiating PC12 neurons with either 0.2 nM or 2.0 nM of either paclitaxel or eribulin and acquired phase contrast images 1, 3 or 23 hours after drug addition. While neurites lengthened considerably in DMSO treated controls after 23 hours, neurite extension was arrested at 2.0nM of paclitaxel and eribulin, but not at 0.2 nM of either drug (Figure 2). Paclitaxel rapidly increased neurite length after 3 hours at 2.0 nM compared to the DMSO control at 3 hours. The effect of eribulin was rapid and suppressed outgrowth within 3 hours of treatment. No significant retraction was observed at any concentration, although there was a trend for paclitaxel at 23 hours.

Quantification of drug effects on neurite area

To determine the half maximal inhibitory concentration (IC_{50}) for neurite retraction, we treated 8-day differentiated PC12 cells with a range of concentrations of paclitaxel, ixabepilone, vincristine, and eribulin for 24 hours and assessed morphology using phase contrast microscopy. Paclitaxel treatment caused a retraction and swelling of neurites, although some long neurites remained (Figure 3A). Ixabepilone was more potent than paclitaxel in reducing neurite area, with only 25% of neurite area remaining at the highest concentration tested (81 nM). Vincristine was the most potent agent tested, reducing neurite area at low nanomolar concentrations. Eribulin treatment led to thinning and fragmentation of neurites at high concentrations where very few long neurites were still present. The IC_{50} for neurite retraction for each agent was determined from the dose-response curves to be 11.9, 11.3, 1.9, and 6.0 nM for paclitaxel, ixabepilone, vincristine, and eribulin, respectively (Figure 3B Due to the stimulating effects of paclitaxel and ixabepilone, the IC_{50} for neurite

area was determined to be the concentration that decreased the maximally induced neurite area by 50%, which we refer to as the *apparent* IC_{50}. For vincristine and eribulin, both decreased neurite area at all concentrations tested and the IC_{50} was determined to be the concentration that decreased neurite by 50% from an initial value of 1. At high concentrations (100 nM), both paclitaxel and eribulin directly reduced growth cone branching and led to neurite retraction within 1 hour in a live-cell timelapse using phase imaging (Figure 4) (vincristine and ixabepilone were not investigated using timelapse imaging). Thinning and fragmentation of neurites was visible after 4 hours in eribulin-treated cells.

Inhibition of undifferentiated PC12 cell proliferation

All drugs inhibited the number of living cells at nanomolar concentrations, with potency as follows: ixabepilone > eribulin > paclitaxel > vincristine (Figure 5) (IC_{50}s 9.7, 14.6, 17, 21.6 nM, respectively). Due to the large number of cells that were still alive even at high doses of drug after 48 hours, we also calculated the percent of cells remaining for each drug as follows: 47%, 37%, 43%, and 34% for ixabepilone, eribulin, paclitaxel, and vincristine, respectively. Finally, there was no correlation between MTA mechanism of action (microtubule stabilization or destabilization) and magnitude of IC_{50}.

Comparison of IC_{50} concentrations for cell proliferation and neurite area.

Eribulin, vincristine, and paclitaxel all induced neurite retraction (at 24 hours) at lower IC_{50} values than their respective IC_{50}s for PC12 cell proliferation (at 48 hours) (Table 1). In contrast, ixabepilone was more potent in inhibiting PC12 cell proliferation than neurite area. In general, the microtubule destabilizing drugs eribulin and vincristine both required higher concentrations to inhibit PC12 cell proliferation than previously reported concentrations for inhibition of cancer cell proliferation (Smith 2016). In contrast, the microtubule stabilizing drugs paclitaxel and ixabepilone more potently inhibited PC12 cell proliferation than they did cancer cells.

Effects of paclitaxel and eribulin on cytosolic α-tubulin abundance and acetylation

Microtubule polymers are assembled from soluble subunits of α and β-tubulin, and the distribution of tubulin is roughly half polymerized in microtubule and half soluble. Sufficient levels of cytosolic tubulin are required to provide the building blocks for microtubule polymerization. In our previous work, we have shown that both paclitaxel and

eribulin treatment of mice in a maximum tolerated dose model induce total α-tubulin and tubulin acetylation at K40 in the sciatic nerve (Benbow 2016). We next asked if paclitaxel or eribulin treatment leads to a change in the abundance of cytosolic α-tubulin and acetylated tubulin. To test the effects of paclitaxel and eribulin on cytosolic tubulin abundance and acetylation, we treated differentiated PC12 cells with drug concentrations that produced neurite retraction and measured the levels of Triton-soluble cytosolic α-tubulin and cytosolic acetylated α-tubulin. A limitation to this approach is that it only provides a picture of what is occurring in the soluble pool of α-tubulin (non-cytoskeletal fraction) without providing any information on the state of tubulin or abundance of acetylation in the population or polymerized tubulin in microtubules (cytoskeletal fraction). We found that paclitaxel markedly depleted levels of cytosolic α-tubulin in a dose-dependent fashion, while levels of acetylated α-tubulin were maintained and increased slightly (Figure 6A, B). In contrast, eribulin produced mild depletive effects on α and acetylated tubulin levels at the same concentrations (Figure 6C, D).

Microtubule hyperacetylation is not protective against MTA-induced neurite retraction

Previously we found that eribulin treatment of mice in a maximum tolerated dose model led to an 11.7-fold induction of total acetylated α-tubulin levels (Benbow 2016). We hypothesized that an increase in acetylation, which was inconsistent with eribulin's known effect of destabilizing microtubules in-vitro, was a possible compensatory response that mitigated axonal loss in eribulin treated sciatic nerves (Benbow 2016). We next asked if increasing tubulin acetylation in cells was sufficient to protect neurites from drug-induced neurite retraction. First we verified that tubacin, a small molecule inhibitor of the tubulin

deactylating histone deactylase 6 (HDAC6) enzyme, did indeed increase triton-soluble (cytosolic) acetylated tubulin in differentiated PC12 cells. Tubacin increased both cytosolic α-tubulin and acetylated α-tubulin at micromolar concentrations after 24 hours of treatment (Figure 7A, B). Immunofluorescent microscopy confirmed an increase in K40 tubulin acetylation (Figure 7C). Tubulin acetylation in DMSO treated controls was primarily localized to neurites with very little signal found in cell bodies. Microscopy images did not provide sufficient resolution to discern whether the acetylated tubulin was cytoskeletal-associated or soluble due to the dense bundling of microtubules in neurites. Following treatment with tubacin, the increase in acetylation was most significant in the cell bodies with a slight increase in neurites. After confirming that tubacin treatment alone did not result in neurite retraction (Figure 7E), we pretreated differentiated PC12 cells with 6uM of tubacin for 24 hours to hyperacetylate tubulin before adding concentrations of paclitaxel and eribulin that produced reproducible effects on neurite area. Each agent was added to cultures without removing tubacin and neurite area was measured 24 hours following (Figure 7D). We found that tubacin pre-treatment failed to protect neurites from paclitaxel or eribulin induced neurite retraction (Figure 7F).

Discussion

To improve our understanding of the molecular mechanisms involved in regulating neurite loss in response to treatment with microtubule targeting agents, we characterized the effects of MTAs on differentiated PC12 neurite morphology and tubulin biochemistry. We found that treatment with both microtubule stabilizers and destabilizers led to neurite loss at generally lower concentrations of MTAs than were required for inhibition of PC12 cell proliferation. Further, there was a trend for destabilizing agents to require higher

concentrations to inhibit cell proliferation of PC12 cells than did microtubule stabilizing drugs, as compared to reported cancer cells IC_{50}s. Taken together, the post-mitotic population of microtubules in neurites of neuronal cells is more susceptible to the mechanism of action of MTAs. These findings are consistent with recent findings of the effects of paclitaxel, vincristine, and eribulin's effects on neurites per cell in an immortalized DRG cell culture model (Smith 2017, manuscript in preparation).

The drug-specific effects of shorter and swollen neurites in paclitaxel-treated cells and thinning and fragmentation in eribulin-treated cells are consistent with each of their known mechanisms of in-vitro action of stabilization and destabilization, respectively. In movies of neurite retraction with either 100pM paclitaxel or eribulin, the initial effects on growth cone branching are apparent within 1 hour (Figure 4). Given the importance of the cytoskeleton for growth cone dynamics in growing neurites, the repercussions of eribulin's microtubule destabilization are easy to understand in the context of microtubule, and thus, neurite loss. However, stabilization of the entire cytoskeleton via paclitaxel treatment also leads to neurite retraction. This contradictory result indicates that the level of microtubule stability and dynamics must be operating within a narrow window and that neurite loss occurs when the equilibrium is tipped in either direction. Consequently, low concentrations (<3 nM) of both paclitaxel and ixabepilone led to an increase in neurite area, with ixabepilone having a slightly stronger effect. However, neurite area was reduced at concentrations above 3 nM, indicating that the threshold for apparent beneficial stabilization of the microtubule cytoskeleton had been crossed. Due to the increase in neurite area in paclitaxel and ixabepilone treated cells, we calculated the half maximal inhibitory concentration by assuming that the maximally induced neurite area occurred at the lowest tested concentration of 1nM. If lower concentrations led to even greater increases in neurite area, then we would

expect the actual IC50 for inhibition of neurite area to be even lower. Therefore we assume that the apparent IC_{50}s we identify from the curve are at their maximal magnitudes. We also assume that at higher concentrations than tested (81 nM), paclitaxel reduces neurite area to zero. Based on these assumptions we report the *apparent* IC50s for neurite area for paclitaxel and ixabepilone. The IC_{50} ratio of neurite area to cancer cell proliferation for each drug was 7.5, 0.95, 1.08, and 1.51 for eribulin, vincristine, ixabepilone, and paclitaxel, respectively. This means that eribulin was 7.5 times more potent at inhibiting cancer cell proliferation than it was at reducing neurite area. Vincristine, on the other hand, required an almost equivalent concentration (ratio = 0.95). It is tempting to speculate that this differential susceptibility of neurites to MTAs is the basis for the differential induction of clinically severe neuropathy.

The lack of difference among IC_{50} values for neurite area is striking when compared to the sensitivity of cancer cells to eribulin. For example, eribulin is used clinically at 1.4 mg/m^2 per cycle, about 142 times less than the average patient dose per cycle of paclitaxel (200 mg/m^2). Yet the concentrations that reduce neurite area are only 2-fold different for these two drugs. This may mean that axonal microtubules in neurons and cancer cells respond very differently to microtubule inhibition because they are expressing different microtubule-associated proteins, post-translational modifications, or tubulin isotypes.

The result that cytosolic tubulin is depleted at paclitaxel concentrations that cause neurite retraction supports a model in which an accumulation of microtubule bundles inhibits cell function. At nanomolar paclitaxel concentrations that block mitosis in HELA cells, the mass of microtubule polymer comprises about half of the total tubulin in cells (Jamieson 2007). However, as paclitaxel concentration is increased, the mass of microtubules increases about 5-fold, leading to extensive bundling and the need for additional tubulin synthesis to

maintain cytosolic tubulin at a high enough concentration to supply the dynamic activities of non-bundled microtubules. The presence of massive bundles in paclitaxel-treated neurites may overcome the cell's ability to replenish tubulin protein or inhibit other microtubule-active proteins. Soluble tubulin is known to play a role in prevention of mitochondrial depolarization through interactions with α-tubulin's C-terminal tail and the VDAC channel of mitochondria outer membranes (Rostovtseva et al. 2008). When soluble tubulin is depleted from the cytosol, mitochondria are allowed to initiate apoptosis. Recent evidence supports a model in which cytosolic α-tubulin operates as a homeostat for microtubule health (and in turn general cell health) by regulating the mitochondria apoptotic response (Carre´ et al. 2001, Israelson et al. 2006, Barrientos et al. 2011).

The finding that increased levels of tubulin acetylation are not sufficient to protect against MTA-induced neurite loss suggests additional roles of α-tubulin acetylation in neurite stability. An important caveat of this finding is that the tubulin evaluations performed here were focused on the cysolic (Triton-soluble = noncytoskeletal associated) fraction of tubulin and not the microtubule (cytoskeletal associated) population of tubulin. Therefore we cannot conclude anything about the acetylation state of polymerized tubulin because microtubule polymers are not soluble in Triton-X-100 extracts. Further experiments should include an additional fractionation step for isolating the cytoskeletal associated population of tubulin to show changes in acetylation with respect to both microtubule associated and non-associated tubulin. A further understanding of how acetylation is involved in microtubule stability, either through local structural changes in the microtubule lattice or by the recruitment of other MAPS, will provide insight into the regulation of microtubule dynamics in populations of post-mitotic microtubules. A second caveat of this work is the method in which acetylation was increased by pharmacological inhibition of the

HDAC6 enzyme. While tubacin is a useful molecule for studying the effects of HDAC6 inhibition, evidence suggests that other proteins, such as β-tubulin and tau, are also acetylated (Chu et al., 2011). Thus is it difficult to conclude that the only effect of HDAC6 inhibition via tubacin is α-tubulin hyperacetylation. Further experiments should focus on specific overexpression of the tubulin acetylating enzyme αTAT1 to increase acetylation of microtubules specifically without off-target effects of inhibiting deacetylating enzymes.

Figures

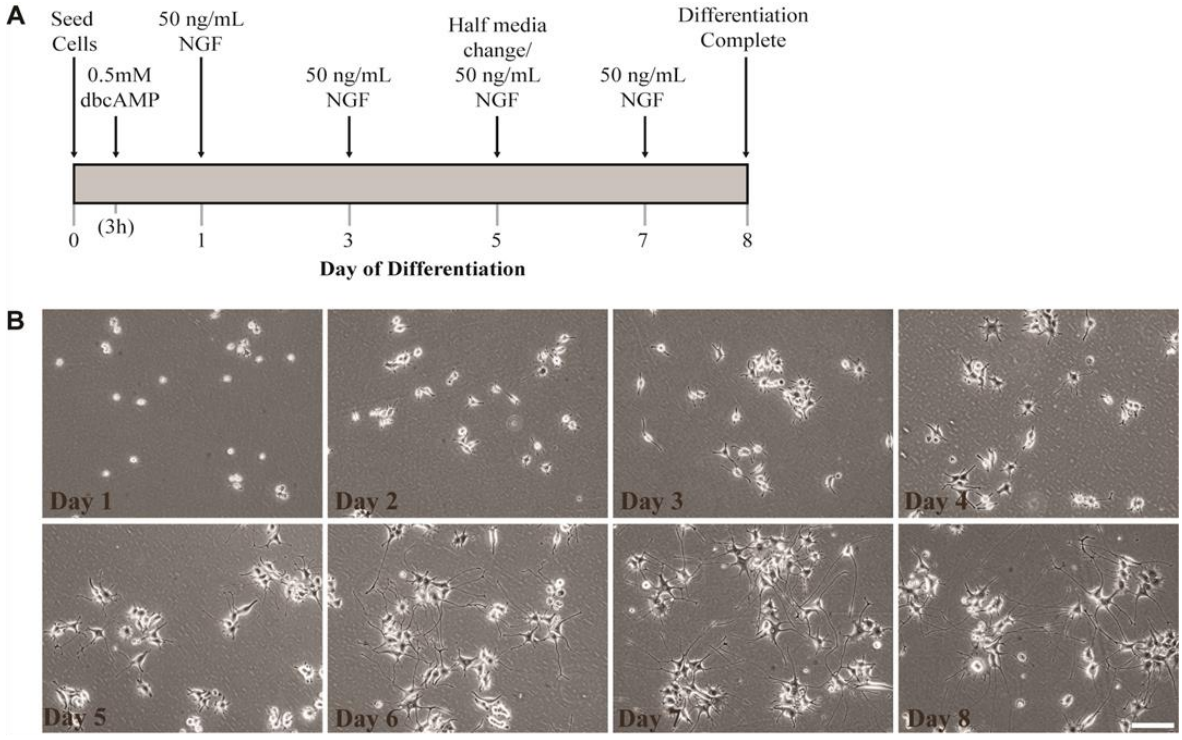
A
Seed Cells
0.5mM dbcAMP
50 ng/mL NGF
50 ng/mL NGF
Half media change/ 50 ng/mL NGF
50 ng/mL NGF
Differentiation Complete
0
(3h)
1
3
5
7
8
Day of Differentiation
B
Day 1
Day 2
Day 3
Day 4
Day 5
Day 6
Day 7
Day 8
C
Mean neurite length (um)
Sum neurite length (um)
Neurite length (um) / cell
Mean total neurite area per image (um²)
Sum neurite area (um²)
Neurite area (um²) / cell
Days of differentiation

Figure 1. PC12 differentiation by nerve growth factor and dbcAMP over eight days in 5% HI-horse serum and 5% calf serum-containing media at 37C and 5% CO_2. **A**, Schedule of cell culture conditions. dbcAMP is added three hours post-seeding, then NGF is added to existing media 24 hours later and every other day following. A half media change can be performed on day 5 if necessary, but may not be required. **B**, Representative 10X phase contrast images of PC12 cells corresponding to each day of the schedule shown in A, scale bar = 100 μm. **C**, Neurite length and area measurements over eight days of differentiation. Measurements are from five images per timepoint. From left to right, the graphs represent the average length or area of all neurites per image for five images, the sum of the total neurite length or area for five images, and the average neurite length or area per cell (total value divided by the number of cell bodies in the corresponding image). Bar graphs are mean ± SEM, produced in GraphPad Prism.

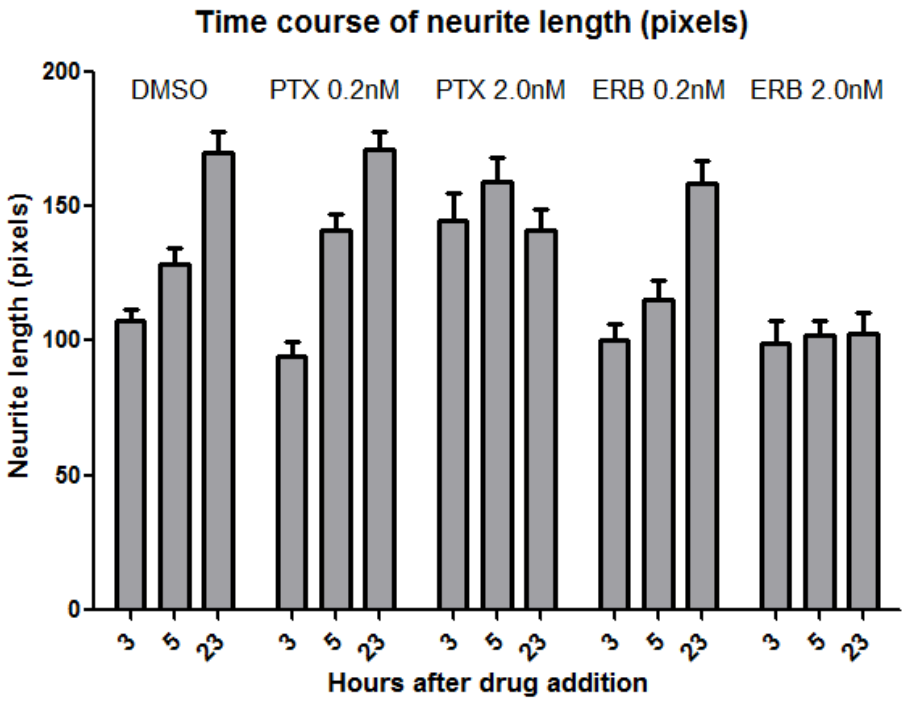

Figure 2. Low nanomolar concentrations of paclitaxel and eribulin arrest neurite outgrowth. 8-day differentiated PC12 cells were treated with either 0.2nM or 2.0nM of paclitaxel (16% IC_{50} for neurite area at 24 hours) or eribulin (30% IC_{50} for neurite area at 24 hours) for 3, 5, and 23 hours. At each timepoint, phase contrast images were taken and neurite lengths were analyzed from at least 5 images for each condition and averaged. For each drug, 2.0nM was sufficient to arrest neurite outgrowth.

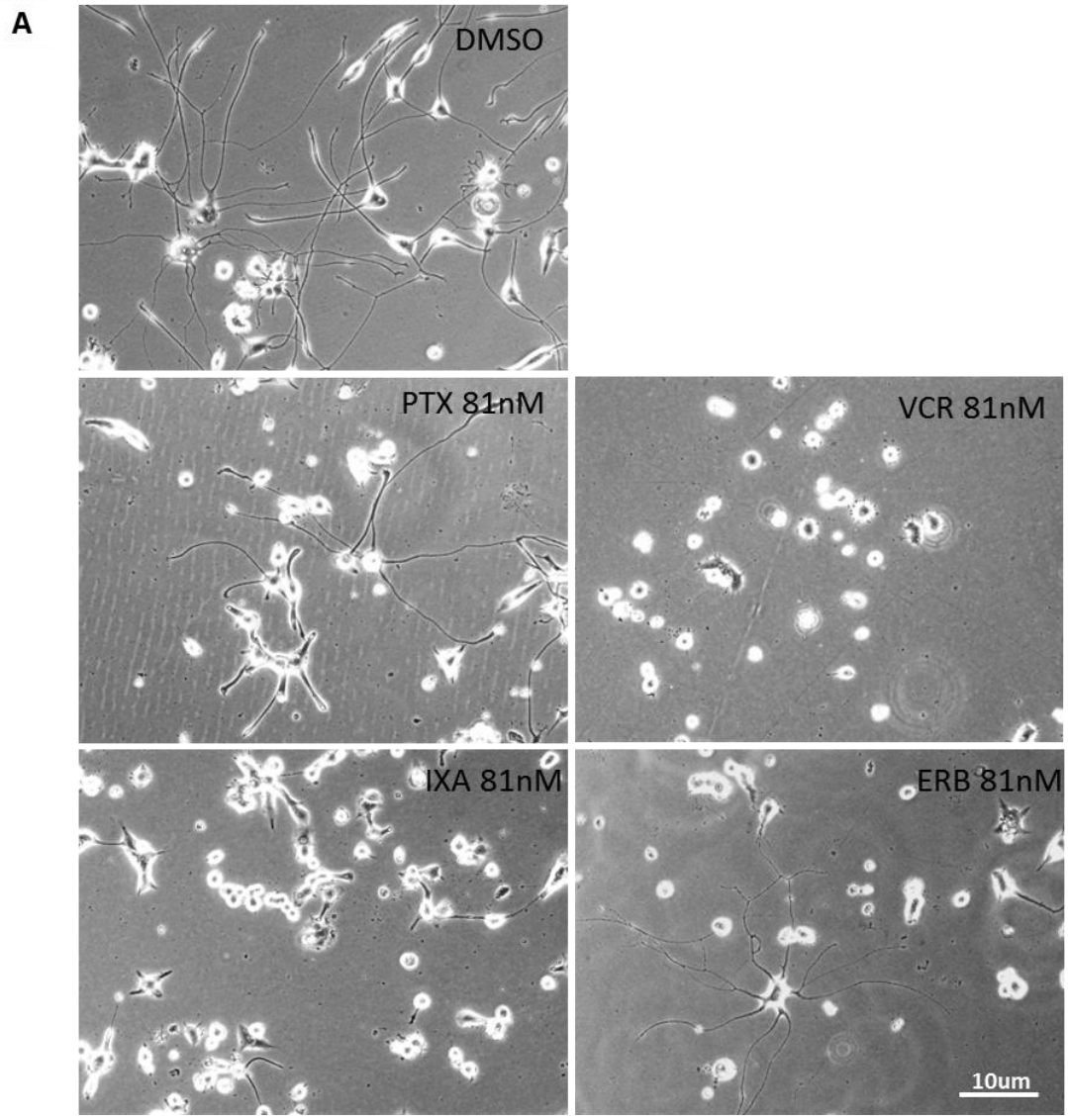
A
DMSO
PTX 81nM
VCR 81nM
IXA 81nM
ERB 81nM
10um

B

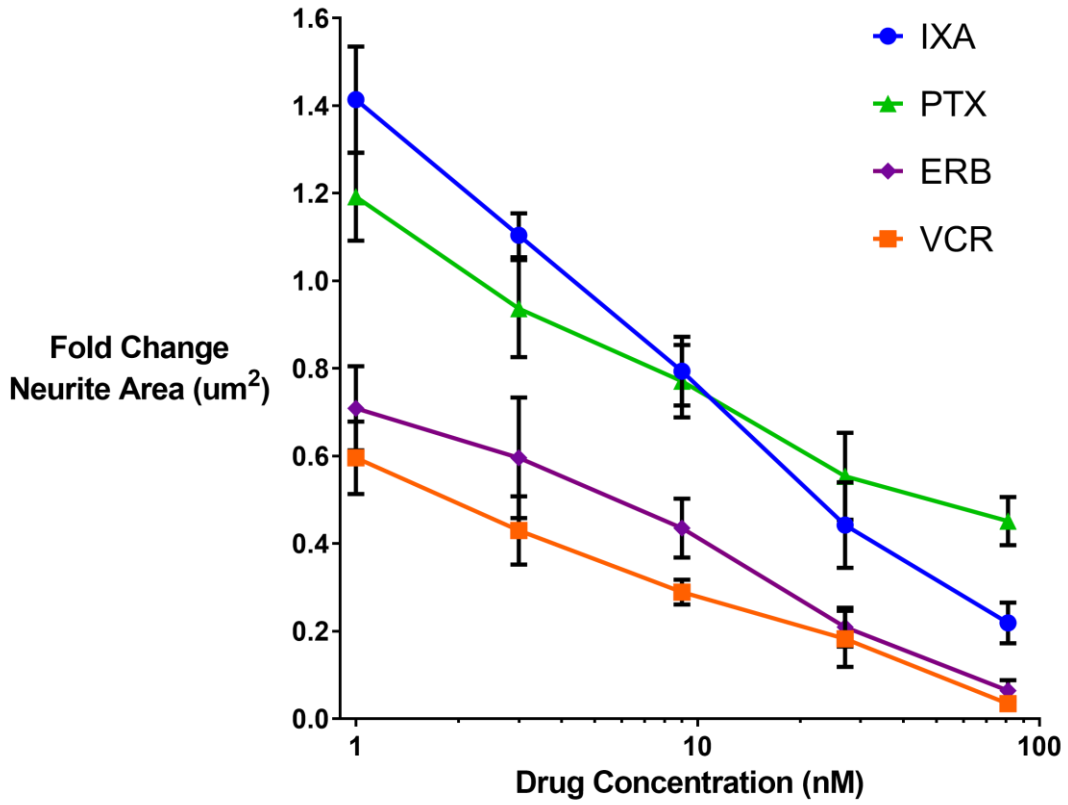

Figure 3. Quantification of drug effects on neurite area of cultured PC12 neurons. Differentiated PC12 cells were treated with each agent for 24 hours before taking phase contrast images and neurite area measurements. A, representative images of each agent's effects on neurite morphology. B, Quantification of neurite area after treatment with either paclitaxel, ixabepilone, vincristine, or eribulin. Student's T-tests from DMSO control * = $P<0.05$, ** = $P<0.01$, *** $P<0.001$.

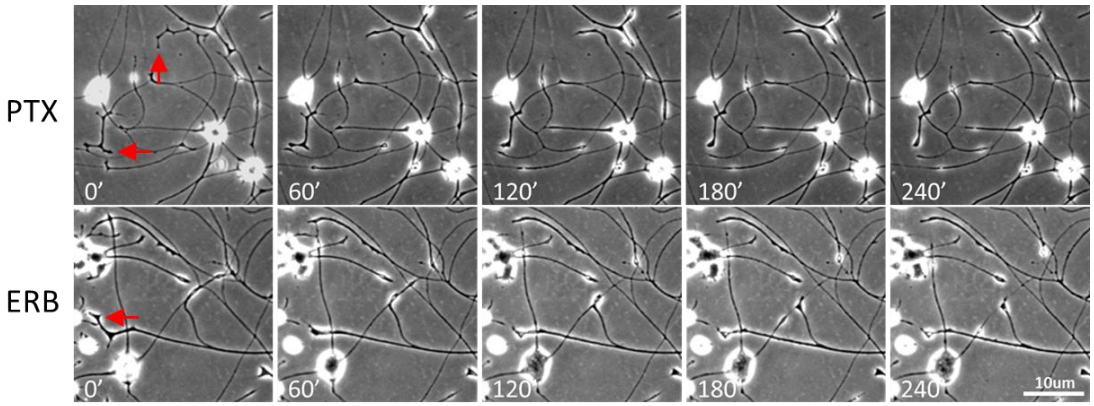

Figure 4. Paclitaxel or eribulin treatment rapidly reduces growth cone branching and leads to neurite retraction. 8 day differentiated PC12 cells were treated with 100pM of either eribulin or paclitaxel and imaged live at 37°C/5% CO_2 over the course of 4 hours using phase contrast microscopy. The red arrows indicate growth cones that display retraction over the time course.

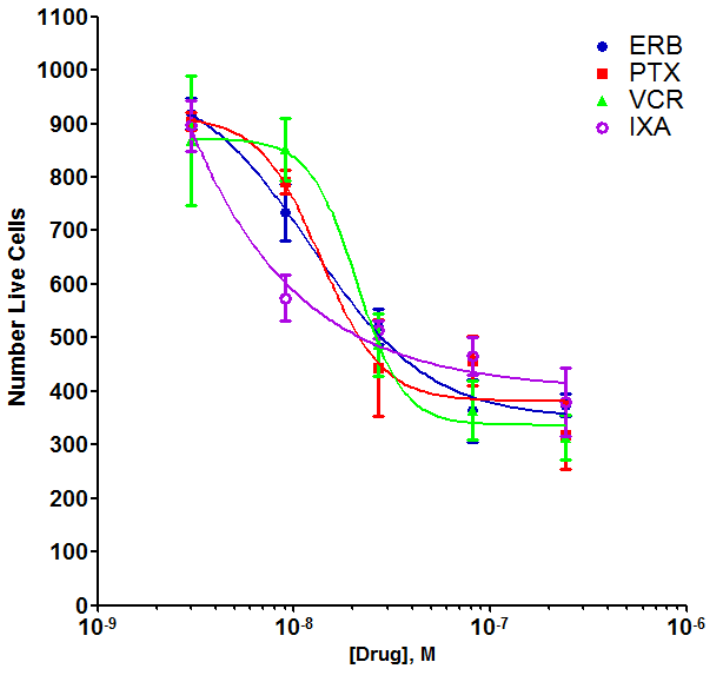

Figure 5. Dose-response for number of live undifferentiated PC12 cells 48 hours after drug addition. PC12 cells will continue to divide until differentiation is initiated by addition of dbcAMP/NGF (the time of cell division is about 48 hours). All drugs decreased the number of living cells, with potency as follows: Ixabepilone > Eribulin > Paclitaxel > Vincristine.

Table 1. Summary of IC50 values for cell proliferation and neurite area

Drug	Effect on Microtubules	IC_{50} Values (nM)			Neurite Area/Proliferation IC_{50} Ratios	
		Cancer Cells	Neuronal PC12 Cells			
		Proliferation	Proliferation	Neurite area	Neuronal PC12 cells	Cancer Cells
Eribulin	Destabilizes	0.8	14.6	6	0.41	7.50
Vincristine	Destabilizes	2	21.6	1.9	0.09	0.95
Paclitaxel	Stabilizes	11	17	11.9*	0.70	1.08
Ixabepilone	Stabilizes	7.5	9.7	11.3*	1.16	1.51

*Apparent IC_{50} for neurite area.

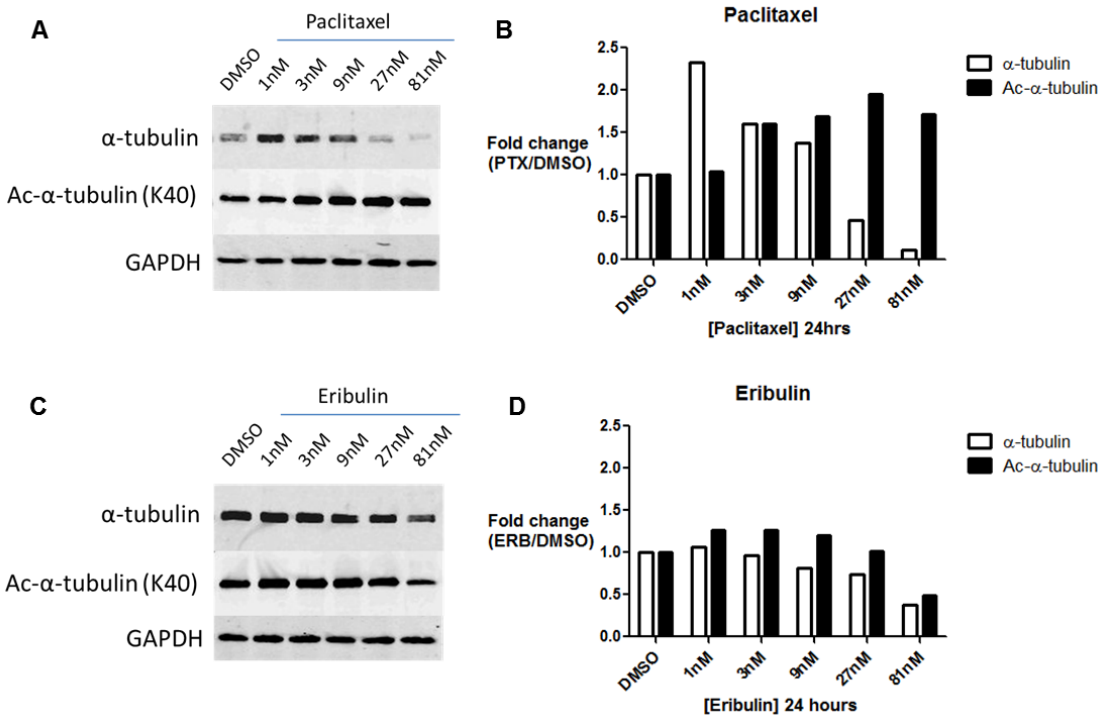

Figure 6. Paclitaxel was more potent in altering the abundance and acetylation of cytosolic (non-cytoskeletal associated) tubulin. Differentiated PC12 cells were treated with either paclitaxel or eribulin for 24 hours. Extraction buffer containing TritonX-100 detergent was used to collect the cytosolic fraction of tubulin from the cells. A, paclitaxel depletes α-tubulin from the non-cytoskeletal fraction and increases the acetylated of soluble tubulin in western blots for α-tubulin, acetylated α-tubulin, and GAPDH. B, Quantification of protein abundance normalized to the GAPDH loading control. C, Eribulin, in contrast, had mild effects on the abundance of α- and acetylated α-tubulin in the Triton-soluble protein fraction.

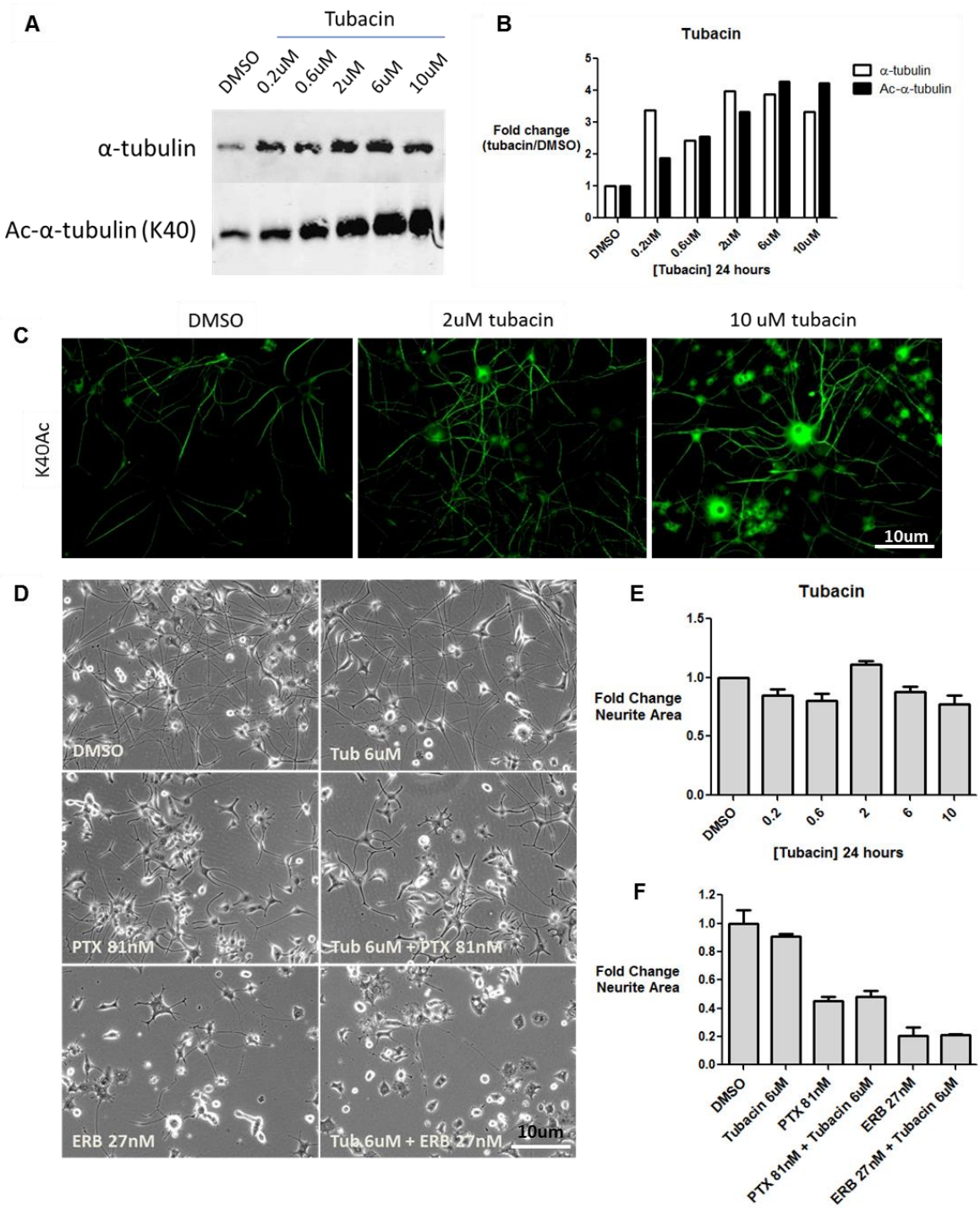
A
Tubacin
DMSO
0.2uM
0.6uM
2uM
6uM
10uM
α-tubulin
Ac-α-tubulin (K40)
B
Tubacin
α-tubulin
Ac-α-tubulin
Fold change (tubacin/DMSO)
[Tubacin] 24 hours
C
DMSO
2uM tubacin
10 uM tubacin
K40Ac
10um
D
DMSO
Tub 6uM
PTX 81nM
Tub 6uM + PTX 81nM
ERB 27nM
Tub 6uM + ERB 27nM
10um
E
Tubacin
Fold Change Neurite Area
[Tubacin] 24 hours
F
Fold Change Neurite Area
DMSO
Tubacin 6uM
PTX 81nM
PTX 81nM + Tubacin 6uM
ERB 27nM
ERB 27nM + Tubacin 6uM

Figure 7. Pretreated with tubacin does not protect from paclitaxel or eribulin-induced neurite retraction of PC12 cells. A, Treatment of differentiated PC12 cells with tubacin, a small molecule inhibitor of HDAC6, increases acetylation of soluble tubulin. B, Quantification of the fold change of α and acetylated tubulin from the DMSO-treated control. C, The intensity and distribution of acetylated tubulin in fluorescence microscopy images with anti-K40Ac antibody. D, Representative phase contrast images after treatment with the indicated agents. E, Dose response of neurite area to tubacin alone. F, Quantification of neurite area after treatment with conditions in D.

VI. General Conclusions and Future Directions

At the outset of the work presented here, it was unknown in the field how peripheral axons responded morphologically and biochemically to treatment with agents that perturb microtubules, and if their effects correlated with the severity of neuropathy. We found that for the commonly used chemotherapies paclitaxel and eribulin the morphological effects reflect their respective rates of severe neuropathy and that eribulin induced interesting biochemical changes that may reflect compensatory responses of neurons to microtubule inhibition. This was a novel idea and illustrates our lack of understand of the mechanisms involved in axonal microtubule maintenance. Our initial work was the first to describe the changes in axonal α-tubulin abundance and acetylation in peripheral axons upon treatment with these agents. We inferred the state of microtubule stability using these measurements and speculated that eribulin is unique in that it does induce morphological deficits but that the positive biochemical changes create a more stable and functional microtubule cytoskeleton. This work was important because it allowed us to compare multiple agents with known in-vitro effects on microtubules with their effects on dynamics in a living animal.

Understanding the mechanisms of axonal microtubule maintenance has implications in many neurodegenerative diseases where microtubule dynamics or mass is affected. Our group has contributed the first systematic study on the recovery from these agents in a mouse model and found that paclitaxel induces long-lasting changes through yet unknown mechanisms. The field may now recognize the importance of compensatory mechanisms that regulate the onset, progression, and recovery from neuropathy. The microtubule-based approach our group has taken illustrates the importance in recognizing that microtubule targeting agents may affect microtubules in a complex system such as a neuron differently

than they would in purified in-vitro systems over short durations. If I were to remain in the field my primary research focus would the identification of molecular players that monitor and respond to alterations in axonal microtubule dynamics. For example, upon treatment with paclitaxel, how does the cell detect and respond to microtubule stabilization? Which pathways are activated? Does it involve active processes of axon degeneration or passive neurotrophic atrophy? The establishment of an in-vitro cell culture model in this work is a first step in this direction as cells better recapitulate the complex environment of the peripheral nervous system than purified systems.

References

Aguilar, A., Becker, L., Tedeschi, T., Heller, S., Iomini, C., & Holzbaur, E. (2014). α –Tubulin K40 acetylation is required for contact inhibition of proliferation and cell – substrate adhesion. Mol Bio Cell 2:257-66. https://doi.org/10.1091/mbc.E13-10-0609

Akerley W, Herndon JE, Egorin MJ, et al. Weekly, high-dose paclitaxel in advanced lung carcinoma: a phase II study with pharmacokinetics by the Cancer and Leukemia Group B. *Cancer* 2003; 97:2480-6.

Akhmanova A, Steinmetz MO (2008) Tracking the ends: a dynamic protein network controls the fate of microtubule tips. Nat Rev Mol Cell Biol 9:309–322. doi:10.1038/nrm2369

Akhmanova A, Steinmetz MO (2015) Control of microtubule organization and dynamics: two ends in the limelight. Nat Rev Mol Cell Biol 16:711-726 doi:10.1038/nrm4084

Alba E, Martin M, Ramos M, et al. Multicenter randomized trial comparing sequential with concomitant administration of doxorubicin and docetaxel as first-line treatment of metastatic breast cancer: a Spanish Breast Cancer Research Group (GEICAM-9903) phase III study. *J Clin Oncol* 2004; 22:2587-93.

Alberti P, Cavaletti G. Management of side effects in the personalized medicine era: chemotherapy-induced peripheral neuropathy. Methods Mol Biol. 2014;1175:301-322.

Alessandri-Haber, N., Dina, O. a, Yeh, J. J., Parada, C. a, Reichling, D. B., & Levine, J. D. (2004). Transient receptor potential vanilloid 4 is essential in chemotherapy-induced neuropathic pain in the rat. *The Journal of neuroscience : the official journal of the Society for Neuroscience*, *24*(18), 4444–52. doi:10.1523/JNEUROSCI.0242-04.2004

Almeida-Souza L, Timmerman V, Janssens S (2011) Microtubule dynamics in the peripheral nervous system: A matter of balance. Bioarchitecture 1:267–270. doi:10.4161/bioa.1.6.19198

Alushin GM, et al. (2014) High-resolution microtubule structures reveal the structural transitions in αβ-tubulin upon GTP hydrolysis. Cell 157(5):1117–1129.

Argyriou AA, Bruna J, Marmiroli P, Cavaletti G (2012) Chemotherapy-induced peripheral neurotoxicity (CIPN): an update. Crit Rev Oncol Hematol 82:51-77 doi:10.1016/j.critrevonc.2011.04.012

Argyriou AA, Koltzenburg M, Polychronopoulos P, et al. Peripheral nerve damage associated with administration of taxanes in patients with cancer. Crit Rev Oncol Hematol 2008; 66:218-28.

Argyriou AA, Kyritsis AP, Makatsoris T, Kalofonos HP (2014) Chemotherapy-induced peripheral neuropathy in adults: a comprehensive update of the literature. Cancer Manag Res 6:135-147 doi:10.2147/cmar.s44261

Argyriou AA, Marmiroli P, Cavaletti G, Kalofonos HP (2011) Epothilone-induced peripheral neuropathy: a review of current knowledge *Journal of Pain and Symptom Management* 42:931-940.

Argyriou AA, Polychronopoulos P, Iconomou G, et al. Paclitaxel plus carboplatininduced peripheral neuropathy. A prospective clinical and electrophysiological study in patients suffering from solid malignancies. *J Neurol* 2005; 252:1459-64.

Argyriou AA, Polychronopoulos P, Koutras A, et al. Clinical and electrophysiological features of peripheral neuropathy induced by administration of cisplatin plus paclitaxel-based chemotherapy. *Eur J Cancer Care* (Engl) 2007; 16:231-7.

Argyriou AA, Polychronopoulos P, Koutras A, et al. Is advanced age associated with increased incidence and severity of chemotherapy-induced peripheral neuropathy? *Support Care Cancer* 2006; 14:223-9.

Argyriou AA, Polychronopoulos P, Koutras A, Iconomou G, Iconomou A, Kalofonos HP, Chroni E. Peripheral neuropathy induced by administration of cisplatin- and paclitaxel-based chemotherapy: could it be predicted? Support Care Cancer 2005b;13:647–51.

Argyriou, A. a, Bruna, J., Marmiroli, P., & Cavaletti, G. (2012). Chemotherapy-induced peripheral neurotoxicity (CIPN): an update. Critical Reviews in Oncology/hematology, 82(1), 51–77.

Argyriou, A. a, Marmiroli, P., Cavaletti, G., & Kalofonos, H. P. (2011). Epothilone-induced peripheral neuropathy: a review of current knowledge. *Journal of pain and symptom management*, *42*(6), 931–40. doi:10.1016/j.jpainsymman.2011.02.022

Avila J, Dominguez J, Diaz-Nido J (1994) Regulation of microtubule dynamics by microtubule-associated protein expression and phosphorylation during neuronal development. Int J Dev Biol 38:13–25

Baas PW, Pienkowski TP, Kosik KS. (1991) Processes induced by tau expression in Sf9 cells have an axon-like microtubule organization. Journal of Cell Biology, Volume 15, number 5, 1333-1344.

Babetto, E., Beirowski, B., Russler, E. V, Milbrandt, J., & DiAntonio, A. (2013). The Phr1 ubiquitin ligase promotes injury-induced axon self-destruction. *Cell reports*, *3*(5), 1422–9. doi:10.1016/j.celrep.2013.04.013

Badros A, Goloubeva O, Dalal JS, et al. Neurotoxicity of bortezomib therapy in multiple myeloma: a single-center experience and review of the literature. Cancer. 2007;110(5):1042-1049.

Bai, R. L., Nguyen, T. L., Burnett, J. C., Atasoylu, O., Munro, M. H. G., Pettit, G. R., Smith, A. B., Gussio, R., and Hamel, E. (2011) Interactions of Halichondrin B and Eribulin with Tubulin *J. Chem. Inf. Model.* 51, 1393– 1404.

Banerjee A (2002) Increased levels of tyrosinated a-, bIII-, and bIVtubulin isotypes in paclitaxel-resistant MCF-7 breast cancer cells. Biochem Biophys Res Commun 293:598–601. doi:10.1016/S0006-291X(02)00269-3

Barrientos, S. a, Martinez, N. W., Yoo, S., Jara, J. S., Zamorano, S., Hetz, C., … Court, F. a. (2011). Axonal degeneration is mediated by the mitochondrial permeability transition pore. The Journal of Neuroscience : The Official Journal of the Society for Neuroscience, 31(3), 966–78. https://doi.org/10.1523/JNEUROSCI.4065-10.2011

Baselga J, Gianni L, Llombart A, et al. Predicting response to ixabepilone: genomics study in patients receiving single agent ixabepilone as neoadjuvant treatment for breast cancer. *Breast Cancer Res Treat* 2005; 94(suppl 1):31-2 .(Abstract 305).

Benbow, S.J., Cook, B.M., Reifert, J., Wozkiak, K.M., Slusher, B.S., Littlefield, B.A., Wilson, L., Jordan, M.A. and Feinstein, S.C. (2015) Distinct Morphological and Molecular Responses to Paclitaxel and Eribulin Administration in Mouse Sciatic Nerve: a Microtubule Based Rationale for Differential Induction of Chemotherapy-Induced Peripheral Neuropathy. *Neurotoxicology Research* 29(2):299-313.

Bhatnagar B, Gilmore S, Goloubeva O, et al. Chemotherapy dose reduction due to chemotherapy induced peripheral neuropathy in breast cancer patients receiving chemotherapy in the neoadjuvant or adjuvant settings: a single-center experience. SpringerPlus. 2014;3:366.

Bhattacharya R, Yang H, Cabral F (2011) Class V beta-tubulin alters dynamic instability and stimulates microtubule detachment from centrosomes. Mol Biol Cell 22:1025-1034 doi:10.1091/mbc.E10-10-0822

Bhattacharya, M. R. C., Gerdts, J., Naylor, S. a, Royse, E. X., Ebstein, S. Y., Sasaki, Y., … DiAntonio, A. (2012). A model of toxic neuropathy in Drosophila reveals a role for MORN4 in promoting axonal degeneration. *The Journal of neuroscience : the official journal of the Society for Neuroscience*, *32*(15), 5054–61. doi:10.1523/JNEUROSCI.4951-11.2012

Black MM, Keyser P (1987) Acetylation of alpha-tubulin in cultured neurons and the induction of alpha-tubulin acetylation in PC12 cells by treatment with nerve growth factor. J Neurosci 7:1833-1842

Bloom, a J., Miller, B. R., Sanes, J. R., & DiAntonio, A. (2007). The requirement for Phr1 in CNS axon tract formation reveals the corticostriatal boundary as a choice point for cortical axons. *Genes & development*, *21*(20), 2593–606. doi:10.1101/gad.1592107

Blum JL, Dees EC, Chacko A, et al. Phase II trial of capecitabine and weekly paclitaxel as first-line therapy for metastatic breast cancer. *J Clin Oncol* 2006; 24: 4384-90.

Boehmerle W, Huehnchen P, Peruzzaro S, Balkaya M, Endres M (2014) Electrophysiological, behavioral and histological characterization of paclitaxel, cisplatin, vincristine and bortezomib-induced neuropathy in C57Bl/6 mice. *Scientific Reports* 4:6370.

Boehmerle W, Huehnchen P, Peruzzaro S, Balkaya M, Endres M (2014) Electrophysiological, behavioral and histological characterization of paclitaxel, cisplatin, vincristine and bortezomibinduced neuropathy in C57Bl/6 mice. Sci Rep 4:6370.

Bonneterre J, Roche H, Monnier A, et al. Docetaxel vs 5-fluorouracil plus vinorelbine in metastatic breast cancer after anthracycline therapy failure. *Br J Cancer* 2002; 87:1210-5.

Boyette-Davis J, Xin W, Zhang H, Dougherty PM (2011) Intraepidermal nerve fiber loss corresponds to the development of taxolinduced hyperalgesia and can be prevented by treatment with minocycline. Pain 152:308–313. doi:10.1016/j.pain.2010.10.030

Boyette-Davis, J. a, Cata, J. P., Driver, L. C., Novy, D. M., Bruel, B. M., Mooring, D. L., … Dougherty, P. M. (2013). Persistent chemoneuropathy in patients receiving the plant alkaloids paclitaxel and vincristine. *Cancer chemotherapy and pharmacology*, *71*(3), 619–26. doi:10.1007/s00280-012-2047-z

Bunker JM, Wilson L, Jordan MA, Feinstein SC (2004) Modulation of microtubule dynamics by tau in living cells: implications for development and neurodegeneration. Mol Biol Cell 15:2720-2728 doi:10.1091/mbc.E04-01-0062

Butner KA, Kirschner MW. (1991) Tau protein binds to microtubules through a flexible array of distributed weak sites. J Cell Biol 115(3):717-30.

Caceres A, Kosik KS. (1990) Inhibition of neurite polarity by tau antisense oligonucleotides on neurite formation of cultured cerebellar macroneurons. Nature 343, 461-463.

Calhoun EA, Welshman EE, Chang CH, et al. Psychometric evaluation of the Functional Assessment of Cancer Therapy/Gynecologic Oncology Group-Neurotoxicity (Fact/GOG-Ntx) questionnaire for patients receiving systemic chemotherapy. Int J Gynecol Cancer. 2003;13(6):741-748.

Campone M, Cortes-Funes H, Vorobiof D, et al. Vinflunine: a new active drug for second-line treatment of advanced breast cancer. Results of a phase II and pharmacokinetic study in patients progressing after first-line anthracycline/taxane-based chemotherapy. *Br J Cancer* 2006; 95:1161-6.

Carlson, K., & Ocean, A. J. (2011). Peripheral neuropathy with microtubule-targeting agents: occurrence and management approach. *Clinical breast cancer*, *11*(2), 73–81. doi:10.1016/j.clbc.2011.03.006

Carozzi VA, Canta A, Chiorazzi A (2015) Chemotherapy-induced peripheral neuropathy: What do we know about mechanisms? Neurosci Lett 596:90-107 doi:10.1016/j.neulet.2014.10.014

Carozzi VA, Renn CL, Bardini M, Fazio G, Chiorazzi A, Meregalli C, Oggioni N, Shanks K, Quartu M, Serra MP, Sala B, Cavaletti G, Dorsey SG (2013) Bortezomib-induced painful peripheral neuropathy: an electrophysiological, behavioral, morphological and mechanistic study in the mouse. PLoS One 8:e72995 doi:10.1371/journal.pone.0072995

Carre´ M, Andre´ N, Carles G, Borghi H, Brichese L, Briand C, et al. Tubulin is an inherent component of mitochondrial membranes that interacts with the voltage-dependent anion channel. J Biol Chem 2002;277(37):33664–9.

Cascinu S, Catalano V, Cordella L, et al. Neuroprotective effect of reduced glutathione on oxaliplatin-based chemotherapy in advanced colorectal cancer: a randomized, double-blind, placebo-controlled trial. *J Clin Oncol* 2002; 20:3478-83.

Cavaletti G, Bogliun G, Marzorati L, et al. Grading of chemotherapy-induced peripheral neurotoxicity using the Total Neuropathy Scale. Neurology. 2003;61(9):1297-1300.

Cavaletti G, Cavalletti E, Oggioni N, et al. Distribution of paclitaxel within the nervous system of the rat after repeated intravenous administration. *Neurotoxicology* 2000; 21:389-93.

Cavaletti G, Frigeni B, Lanzani F, et al. Chemotherapy-induced peripheral neurotoxicity assessment: a critical revision of the currently available tools. Eur J Cancer. 2010;46(3):479-494.

Cavaletti G, Frigeni B, Lanzani F, et al. The Total Neuropathy Score as an assessment tool for grading the course of chemotherapy-induced peripheral neurotoxicity: comparison with the National Cancer Institute-Common Toxicity Scale. *J Peripher Nerv Syst* 2007; 12:210-5.

Cavaletti G, Jann S, Pace A, et al. Multi-center assessment of the Total Neuropathy Score for chemotherapy-induced peripheral neurotoxicity. *J Peripher Nerv Syst* 2006; 11:135-41.

Cavaletti G, Marmiroli P. Chemotherapy-induced peripheral neurotoxicity. Nat Rev Neurol. 2010;6(12):657-666.

Cavaletti G, Tredici G, Braga M, et al. Experimental peripheral neuropathy induced in adult rats by repeated intraperitoneal administration of taxol. *Exp Neurol* 1995; 133:64-72.

Cavaletti G. Chemotherapy-induced peripheral neurotoxicity (CIPN): what we need and what we know. J Periph Nerv Syst. 2014;19(2):66-76.

Chambers, S.M., Qi, Y., Mica, Y., Lee, G., Zhang, X.J., Niu, L., Bilsland, J., Cao, L., Stevens, E., Whiting, P., Shi, S.H. and Studer, L. (2012) Combined small-molecule inhibition accelerates developmental timing and converts human pluripotent stem cells into nociceptors. *Nat Biotechnol*. 30:715-720.

Chaudhry V, Chaudhry M, Crawford TO, et al. Toxic neuropathy in patients with pre-existing neuropathy. *Neurology* 2003; 60:337-40.

Chaudhry V, Rowinsky EK, Sartorius SE, et al. Peripheral neuropathy from taxol and cisplatin combination chemotherapy: clinical and electrophysiological studies. *Ann Neurol* 1994; 35:304-11.

Chen J, Kanai Y, Cowan NJ, Hirokawa N. (1992) Projection domains of MAP2 and tau determine spacings between microtubules in dendrites and axons. Nature 17;360 (6405):674-7.

Chen, L., Wang, Z., Ghosh-Roy, A., Hubert, T., Yan, D., O'Rourke, S., … Chisholm, A. D. (2011). Axon regeneration pathways identified by systematic genetic screening in C. elegans. *Neuron*, *71*(6), 1043–57. doi:10.1016/j.neuron.2011.07.009

Chiorazzi A, Nicolini G, Canta A, et al. Experimental epothilone B neurotoxicity: results of in vitro and in vivo studies. *Neurobiol Dis* 2009; 35:270-7.

Choi YJ, Di Nardo A, Kramvis I, Meikle L, Kwiatkowski DJ, Sahin M, He X (2008) Tuberous sclerosis complex proteins control axon formation. Genes Dev 22:2485–2495

Chu, C. W., F. Hou, ., H. Zou. 2011. A novel acetylation of b-tubulin by San modulates microtubule polymerization via down-regulating tubulin incorporation. Mol. Biol. Cell. 22:448–456.

Chung, K., Wallace, J., Kim, S.-Y., Kalyanasundaram, S., Andalman, A. S., Davidson, T. J., … Deisseroth, K.

(2013). Structural and molecular interrogation of intact biological systems. *Nature*. doi:10.1038/nature12107

Cortes J, Baselga J. Targeting the microtubules in breast cancer beyond taxanes: the epothilones. *Oncologist* 2007; 12:271-80.

Cortes J, Montero AJ, Gluck S (2012) Eribulin mesylate, a novel microtubule inhibitor in the treatment of breast cancer. Cancer Treat Rev 38:143-151 doi:10.1016/j.ctrv.2011.03.006

Cortes J, O'Shaughnessy J, Loesch D, et al. Eribulin monotherapy versus treatment of physician's choice in patients with metastatic breast cancer (EMBRACE): a phase 3 open-label randomised study. Lancet. 2011;377(9769):914–923.

Cortes J, O'Shaughnessy J, Loesch D, Blum JL, Vahdat LT, Petrakova K, Chollet P, Manikas A, Diéras V, Delozier T, Vladimirov V, Cardoso F, Koh H, Bougnoux P, Dutcus CE, Seegobin S, Mir D, Meneses N, Wanders J, Twelves C; EMBRACE (Eisai Metastatic Breast Cancer Study Assessing Physician's Choice Versus E7389) investigators. Eribulin monotherapy versus treatment of physician's choice in patients with metastatic breast cancer (EMBRACE): a phase 3 open-label randomised study. Lancet. 2011 Mar 12;377(9769):914-23.

Coyne PJ, Wan W, Dodson P, et al. A trial of Scrambler therapy in the treatment of cancer pain syndromes and chronic chemotherapy-induced peripheral neuropathy. J Pain Palliat Care Pharmacother. 2013;27(4):359-364.

Creppe C, Malinouskaya L, Volvert ML, Gillard M, Close P, Malaise O, Laguesse S, Cornez I, Rahmouni S, Ormenese S, Belachew S, Malgrange B, Chapelle JP, Siebenlist U, Moonen G, Chariot A, Nguyen L (2009) Elongator controls the migration and differentiation of cortical neurons through acetylation of alpha-tubulin. Cell 136:551-564 doi:10.1016/j.cell.2008.11.043

Crispino, M., Chun, J. T., Cefaliello, C., & Capano, C. P. (2013). Local gene expression in nerve endings, 1–19. https://doi.org/10.1002/dneu.

Cueva JG, Hsin J, Huang KC, Goodman MB. Posttranslational acetylation of alpha-tubulin constrains protofilament number in native microtubules. Curr Biol. 2012; 22:1066–1074. [PubMed: 22658592]

Cueva, J. G., J. Hsin, M. B. Goodman. 2012. Posttranslational acetylation of a-tubulin constrains protofilament number in native microtubules. Curr. Biol. 22:1066–1074.

de la Morena Barrio P, Conesa MÁ, González-Billalabeitia E, Urrego E, García-Garre E, García-Martínez E, Poves MZ, Vicente V, de la Peña FA. Delayed recovery and increased severity of Paclitaxel-induced peripheral neuropathy in patients with diabetes. J Natl Compr Canc Netw. 2015 Apr;13(4):417-23.

de Pennart H, Houliston E, Maro B (1988) Post-translational modifications of tubulin and the dynamics of microtubules in mouse oocytes and zygotes. Biol Cell 64:375–378

Denduluri N, Low JA, Lee JJ, et al. Phase II trial of ixabepilone, an epothilone B analog, in patients with metastatic breast cancer previously untreated with taxanes. *J Clin Oncol* 2007; 25:3421-7.

Derry, W. B., Wilson, L and Jordan, M.A. (1993) Substoichiometric binding of Taxol suppresses microtubule dynamics. *Biochemistry* 34: 2203-2211.

Dimopoulos MA, Mateos MV, Richardson PG, et al. Risk factors for, and reversibility of, peripheral neuropathy associated with bortezomib-melphalan-prednisone in newly diagnosed patients with multiple myeloma: subanalysis of the phase 3 VISTA study. Eur J Haematol. 2011;86(1):23-31.

Dompierre JP, Godin JD, Charrin BC, Cordelieres FP, King SJ, Humbert S, Saudou F (2007) Histone deacetylase 6 inhibition compensates for the transport deficit in Huntington's disease by increasing tubulin acetylation. J Neurosci 27:3571-3583 doi:10.1523/jneurosci.0037-07.2007

Dougherty, P. M., Cata, J. P., Cordella, J. V, Burton, A., & Weng, H.-R. (2004). Taxol-induced sensory disturbance is characterized by preferential impairment of myelinated fiber function in cancer patients. *Pain*, *109*(1-2), 132–42. doi:10.1016/j.pain.2004.01.021

Dreicer R, Li S, Manola J, Haas NB, Roth BJ, Wilding G; Eastern Cooperative Oncology Group. Phase 2 trial of epothilone B analog BMS-247550 (ixabepilone) in advanced carcinoma of the urothelium (E3800): a trial of the Eastern Cooperative Oncology Group. Cancer. 2007 Aug 15;110(4):759-63.

Drubin DG, Feinstein SC, Shooter EM, Kirschner MW. (1985) Nerve growth factor-induced neurite outgrowth in PC12 cells involves the coordinate induction of microtubule assembly and assembly-promoting factors. Journal of Cell Biology. Nov; 101(5 Pt 1):1799-807.

du Bois A, Luck HJ, Meier W, et al Arbeitsgemeinschaft Gynakologische Onkologie Ovarian Cancer Study Group. A randomized clinical trial of cisplatin/paclitaxel versus carboplatin/paclitaxel as first-line treatment of ovarian cancer. *J Natl Cancer Inst* 2003; 95:1320-9.

England JD, Gronseth GS, Franklin G, et al. Practice parameter: the evaluation of distal symmetric polyneuropathy: the role of autonomic testing, nerve biopsy, and skin biopsy (an evidence-based review). Report of the American Academy of Neurology, the American Association of Neuromuscular and Electrodiagnostic Medicine,

Eniu A, Palmieri FM, Perez EA. Weekly administration of docetaxel and paclitaxel in metastatic or advanced breast cancer. *Oncologist* 2005; 10:665-85.

Esmaeli-Azad, B., McCarty, J. and Feinstein, S.C. (1994) Sense and Antisense Transfection Analysis of Tau Function: Tau Is a Limiting Factor for Neurite Outgrowth and Provides Structural Stability to Neuronal Processes. *Journal of Cell Science* 107:869-879.

European Federation of Neurological Societies/Peripheral Nerve Society Guideline on the use of skin biopsy in the diagnosis of small fiber neuropathy. Report of a joint task force of the European Federation of Neurological Societies and the Peripheral Nerve Society. *J Peripher Nerv Syst* 2010; 15:79-92.

Fang, Y., & Bonini, N. M. (2012). Axon degeneration and regeneration: insights from Drosophila models of nerve injury. *Annual review of cell and developmental biology*, *28*, 575–97. doi:10.1146/annurev-cellbio-101011-155836

Fehrenbacher JC (2015) Chemotherapy-induced peripheral neuropathy. Prog Mol Biol Transl Sci 131:471-508 doi:10.1016/bs.pmbts.2014.12.002

Feldhaus, M. J., Siegel, R. W., Opresko, L. K., Coleman, J. R., Feldhaus, J. M. W., Yeung, Y. A., … Wittrup, K. D. (2003). Flow-cytometric isolation of human antibodies from a nonimmune Saccharomyces cerevisiae surface display library, *21*(February), 163–170. doi:10.1038/nbt785

Field JJ, Kanakkanthara A, Miller JH (2014) Microtubule-targeting agents are clinically successful due to both mitotic and interphase impairment of microtubule function. Bioorg Med Chem 22:5050-5059 doi:10.1016/j.bmc.2014.02.035

Flatters, S. J. L., & Bennett, G. J. (2006). Studies of peripheral sensory nerves in paclitaxel-induced painful peripheral neuropathy: evidence for mitochondrial dysfunction. *Pain*, *122*(3), 245–57. doi:10.1016/j.pain.2006.01.037

Fu S, Gordon T. The cellular and molecular basis of peripheral nerve regeneration. Mol Neurobiol.14(1-2):67–116. [PubMed: 9170101]

Fukuyama, K., Yoshida, M., Yamashita, a, Deyama, T., Baba, M., Suzuki, a, … Ohno, S. (2000). MAPK upstream kinase (MUK)-binding inhibitory protein, a negative regulator of MUK/dual leucine zipper-bearing kinase/leucine zipper protein kinase. *The Journal of biological chemistry*, *275*(28), 21247–54. doi:10.1074/jbc.M001488200

Fumoleau P, Delgado FM, Delozier T, et al. Phase II trial of weekly intravenous vinorelbine in first-line advanced breast cancer chemotherapy. *J Clin Oncol* 1993; 11:1245-52.

Gallo, K. a, & Johnson, G. L. (2002). Mixed-lineage kinase control of JNK and p38 MAPK pathways. *Nature reviews. Molecular cell biology*, *3*(9), 663–72. doi:10.1038/nrm906

Gay DA, Yen TJ, Lau JT, Cleveland DW (1987) Sequences that confer β-tubulin autoregulation through modulated mRNA stability reside within exon 1 of a β-tubulin mRNA Cell 50:671- 679

Geraldo S, Khanzada UK, Parsons M, Chilton JK, Gordon-Weeks PR (2008) Targeting of the F-actin-binding protein drebrin by the microtubule plus-tip protein EB3 is required for neuritogenesis. Nat Cell Biol 10:1181-1189 doi:10.1038/ncb1778

Gerdts, J., Summers, D. W., Sasaki, Y., DiAntonio, a., & Milbrandt, J. (2013). Sarm1-Mediated Axon Degeneration Requires Both SAM and TIR Interactions. *Journal of Neuroscience*, *33*(33), 13569–13580. doi:10.1523/JNEUROSCI.1197-13.2013

Giannakakou P, Nakano M, Nicolaou KC, O'Brate A, Yu J, Blagosklonny MV, Greber UF, Fojo T (2002) Enhanced microtubule-dependent trafficking and p53 nuclear accumulation by suppression of microtubule dynamics. Proc Natl Acad Sci U S A 99:10855-10860 doi:10.1073/pnas.132275599

Godena VK, Brookes-Hocking N, Moller A, Shaw G, Oswald M, Sancho RM, Miller CC, Whitworth AJ, De Vos KJ (2014) Increasing microtubule acetylation rescues axonal transport and locomotor deficits caused by LRRK2 Roc-COR domain mutations. Nat Commun 5:5245 doi:10.1038/ncomms6245

Goode BL, Feinstein SC. (1994) Identification of a novel microtubule binding and assembly domain in the developmentally regulated inter-repeat region of tau. Journal of Cell Biology. Mar; 124(5):769-82.

Gradishar WJ (2011) The place for eribulin in the treatment of metastatic breast cancer. Curr Oncol Rep 13:11-16 doi:10.1007/s11912-010-0145-9

Gradishar WJ, Tjulandin S, Davidson N, et al. Phase III trial of nanoparticle albu- min-bound paclitaxel compared with polyethylated castor oil-based paclitaxel in women with breast cancer. J Clin Oncol 2005; 23:7794-803.

Gradishar WJ. Albumin-bound paclitaxel: a next-generation taxane. *Expert Opin Pharmacother* 2006; 7:1041-53.

Greene LA, Tischler AS. (1976) Establishment of a noradrenergic clonal line of rat adrenal pheochromocytoma cells which respond to nerve growth factor. Proc Natl Acad Sci. 73(7):2424-8.

Griffin JW, McArthur JC, Polydefkis M. Assessment of cutaneous innervation by skin biopsies. *Curr Opin Neurol* 2001; 14:655-9.

Grisold W, Cavaletti G, Windebank AJ. Peripheral neuropathies from chemotherapeutics and targeted agents: diagnosis, treatment, and prevention. Neuro Oncol. 2012 Sep;14 Suppl 4:iv45-54.

Grueber, W. B., Ye, B., Moore, A. W., Jan, L. Y., Jan, Y. N., & Francisco, S. (2003). Dendrites of Distinct Classes of Drosophila Sensory Neurons Show Different Capacities for Homotypic Repulsion, *13*, 618–626. doi:10.1016/S

Gu C, Zhou W, Puthenveedu MA, Xu M, Jan YN, Jan LY (2006) The microtubule plus-end tracking protein EB1 is required for Kv1 voltage-gated K+ channel axonal targeting. Neuron 52:803-816 doi:10.1016/j.neuron.2006.10.022

Gundersen GG, Khawaja S, Bulinski JC (1987) Postpolymerization detyrosination of alphatubulin: a mechanism for subcellular differentiation of microtubules. J Cell Biol 105:251-264

Gunning PW, Landreth GE, Bothwell MA, Shooter EM. (1981) Differential and synergistic actions of nerve growth factor and cyclic AMP in PC12 cells. Journal of Cell Biology. May;89(2):240-5.

Gunning PW, Letourneau PC, Landreth GE, Shooter EM. (1981) The action of nerve growth factor and dibutyryl adenosine cyclic 3':5'-monophosphate on rat pheochromocytoma reveals distinct stages in the mechanisms underlying neurite outgrowth. J Neurosci 1(10):1085-95.

Guo, L., Hamre, J., Eldridge, S., Behrsing, H. P., Cutuli, F. M., Mussio, J., & Davis, M. (2017). Multiparametric Image Analysis of Rat Dorsal Root Ganglion Cultures to Evaluate Peripheral Neuropathy-Inducing Chemotherapeutics. Toxicological Sciences, 156(1), kfw254.

Gustke N, Trinczek B, Biernat J, Mandelkow EM, Mandelkow E. (1994) Domains of tau protein and interactions with microtubules. Biochemistry 16;33(32):9511-22.

Haggarty, S. J., Koeller, K. M., Wong, J. C., Grozinger, C. M. and Schreiber, S. L. (2003). Domain-selective small-molecule inhibitor of histone deacetylase 6 (HDAC6)-mediated tubulin deacetylation. Proc. Natl. Acad. Sci. USA 100, 4389-4394.

Hammond, J., Cai, D., & Verhey, K. (2008). Tubulin modifications and their cellular functions. *Current opinion in cell biology*, *20*(1), 71–76. Retrieved from http://www.sciencedirect.com/science/article/pii/S0955067407001780

Han, Y., Smith, M. T., & Bergdahl, A. (2013). Pathobiology of cancer chemotherapy-induced peripheral neuropathy (CIPN), *4*(December), 1–16. https://doi.org/10.3389/fphar.2013.00156

Heller BA, Ghidinelli M, Voelkl J, Einheber S, Smith R, Grund E, Morahan G, Chandler D, Kalaydjieva L, Giancotti F, King RH, Fejes-Toth AN, Fejes-Toth G, Feltri ML, Lang F, Salzer JL (2014) Functionally distinct PI 3-kinase pathways regulate myelination in the peripheral nervous system. J Cell Biol 204:1219–1236. doi:10.1083/jcb.201307057

Hensley ML, Hagerty KL, Kewalramani T, et al. American Society of Clinical Oncology 2008 clinical practice guideline update: use of chemotherapy and radiation therapy protectants. *J Clin Oncol* 2009; 27:127-45.

Hershman DL, Lacchetti C, Dworkin RH, et al. Prevention and management of chemotherapy-induced peripheral neuropathy in survivors of adult cancers: American Society of Clinical Oncology clinical practice guideline. J Clin Oncol. 2014;32(18):1941-1967.

Hershman DL, Weimer LH, Wang A, Kranwinkel G, Brafman L, Fuentes D, Awad D, Crew KD. Association between patient reported outcomes and quantitative sensory tests for measuring long-term neurotoxicity in breast cancer survivors treated with adjuvant paclitaxel chemotherapy. Breast Cancer Res Treat. 2011 Feb;125(3):767-74.

Hilkens PH, Verweij J, Vecht CJ, et al. Clinical characteristics of severe peripheral neuropathy induced by docetaxel (Taxotere). *Ann Oncol* 1997; 8:187-90.

Hirokawa N, Shiomura Y, Okabe S. (1988) Tau proteins: the molecular structure and mode of binding on microtubles. Journal of Cell Biology, Volume 107:1449-1459.

Howes, S. C., G. M. Alushin, ., E. Nogales. 2014. Effects of tubulin acetylation and tubulin acetyltransferase binding on microtubule structure. Mol. Biol. Cell. 25:257–266.

Israelson, A., Brdiczka, D., & Sheu, S. S. (2006). The Voltage-Dependent Anion Channel (VDAC): Function in Intracellular Signalling , Cell Life and Cell Death, 2249–2270.

Jaggi, A. S., & Singh, N. (2012). Mechanisms in cancer-chemotherapeutic drugs-induced peripheral neuropathy. *Toxicology*, *291*(1-3), 1–9. doi:10.1016/j.tox.2011.10.019

Jamieson SM, Liu J, Hsu T, et al. Paclitaxel induces nucleolar enlargement in dorsal root ganglion neurons in vivo reducing oxaliplatin toxicity. *Br J Cancer* 2003; 88:1942-7.

Jamieson, S. M. F., Liu, J. J., Connor, B., Dragunow, M., & McKeage, M. J. (2007). Nucleolar enlargement, nuclear eccentricity and altered cell body immunostaining characteristics of large-sized sensory neurons following treatment of rats with paclitaxel. NeuroToxicology, 28(6), 1092–1098.

Janes K, Little JW, Li C, Bryant L, Chen C, Chen Z, Kamocki K, Doyle T, Snider A, Esposito E, Cuzzocrea S, Bieberich E, Obeid L, Petrache I, Nicol G, Neumann WL, Salvemini D (2014) The development and maintenance of paclitaxel-induced neuropathic pain require activation of the sphingosine 1-phosphate receptor subtype 1. J Biol Chem 289:21082-21097 doi:10.1074/jbc.M114.569574

Jang, J., Wang, Y., Lalli, M.A., Guzman, E., Godshalk, S.E., Zhou, H. and Kosik, K.S. (2016) Primary Cilium-Autophagy-Nrf2 (PAN) Axis Activation Commits Human Embryonic Stem Cells to a Neuroectoderm Fate. *Cell*. (in press; available online March 24, 2016)

Janke C (2014) The tubulin code: molecular components, readout mechanisms, and functions. J Cell Biol 206:461-472 doi:10.1083/jcb.201406055

Janke, C., & Chloë Bulinski, J. (2011). Post-translational regulation of the microtubule cytoskeleton: mechanisms and functions. Nature Reviews. Molecular Cell Biology, 12(12), 773–786. https://doi.org/10.1038/nrm3227

Jaworski J, Kapitein LC, Gouveia SM, Dortland BR, Wulf PS, Grigoriev I, Camera P, Spangler SA, Di Stefano P, Demmers J, Krugers H, Defilippi P, Akhmanova A, Hoogenraad CC (2009) Dynamic microtubules regulate dendritic spine morphology and synaptic plasticity. Neuron 61:85-100 doi:10.1016/j.neuron.2008.11.013

Jiang K, Akhmanova A (2011) Microtubule tip-interacting proteins: a view from both ends. Curr Opin Cell Biol 23:94–101. doi:10.1016/j.ceb.2010.08.008

Jimenez-Mateos EM, Paglini G, Gonzalez-Billault C, Caceres A, Avila J (2005) End binding protein-1 (EB1) complements microtubule-associated protein-1B during axonogenesis. J Neurosci Res 80:350–359. doi:10.1002/jnr.20453

Jones SE, Erban J, Overmoyer B, et al. Randomized phase III study of docetaxel compared with paclitaxel in metastatic breast cancer. J Clin Oncol 2005; 23:5542- 51.

Jordan MA, Kamath K, Manna T, Okouneva T, Miller HP, Davis C, Littlefield BA, Wilson L (2005) The primary antimitotic mechanism of action of the synthetic halichondrin E7389 is suppression of microtubule growth. Mol Cancer Ther 4:1086-1095 doi:10.1158/1535-7163.mct-04-0345

Jordan, M.A. and Wilson, L. (2004) Microtubules as a target for anticancer drugs. *Nat Rev Cancer* 4:253- 265.

Jordan, M.A., Thrower, D. and Wilson L. (1992) Effects of vinblastine, podophyllotoxin and nocodazole on mitotic spindles. Implications for the role of microtubule dynamics in mitosis. *J Cell Sci.* 102:401- 416.

Jordan, M.A., Toso, R.J., Thrower, D and Wilson, L. (1993) Mechanism of mitotic block and inhibition of cell proliferation by Taxol at low concentrations *Proceedings of the National Academy of Sciences USA* 90:9552-9556.

Julius, D., & Basbaum, a I. (2001). Molecular mechanisms of nociception. *Nature*, *413*(6852), 203–10. https://doi.org/10.1038/35093019

Kamath K, Wilson L, Cabral F, Jordan MA (2005) BetaIII-tubulin induces paclitaxel resistance in association with reduced effects on microtubule dynamic instability. J Biol Chem 280:12902-12907 doi:10.1074/jbc.M414477200

Kaul, N., Soppina, V., & Verhey, K. J. (2014). Effects of alpha-tubulin K40 acetylation and detyrosination on kinesin-1 motility in a purified system. Biophysical Journal, 106(12), 2636–2643.

Kawakami K, Tunoda T, Takiguchi T, et al. Factors exacerbating peripheral neuropathy induced by paclitaxel plus carboplatin in non-small cell lung cancer. Oncol Res. 2012;20(4):179-185.

Kidwell KM, Yothers G, Ganz PA, et al. Long-term neurotoxicity effects of oxaliplatin added to fluorouracil and leucovorin as adjuvant therapy for colon cancer: results from National Surgical Adjuvant Breast and Bowel Project trials C-07 and LTS-01. Cancer. 2012;118(22):5614-5622.

Konishi, Y., & Setou, M. (2009). Tubulin tyrosination navigates the kinesin-1 motor domain to axons, 12(5), 559–567. https://doi.org/10.1038/nn.2314

Kumar P, WittmannT (2012)+TIPs:ping-pong along microtubule ends. Trends Cell Biol 22:418–428. doi:10.1016/j.tcb.2012.05.005

Kuruvilla G, Perry S, Wilson B, et al. The natural history of vincristine-induced laryngeal paralysis in children. *Arch Otolaryngol Head Neck Surg* 2009; 135:101-5.

Lapointe NE, Morfini G, Brady ST, Feinstein SC, Wilson L, Jordan M (2013) Effects of eribulin, vincristine, paclitaxel and ixabepilone on fast axonal transport and kinesin-1 driven microtubule gliding: Implications for chemotherapy-induced peripheral neuropathy. Neurotoxicology doi:10.1016/j.neuro.2013.05.008

Latiff ZA, Kamal NA, Jahendran J, et al. Vincristine-induced vocal cord palsy: case report and review of the literature. *J Pediatr Hematol Oncol* 2010; 32:407-10.

Lauria G, Lombardi R, Borgna M, et al. Intraepidermal nerve fiber density in rat foot pad: neuropathologic-neurophysiologic correlation. *J Peripher Nerv Syst* 2005; 10:202-8.

Lavoie Smith EM, Barton DL, Qin R, et al. Assessing patient-reported peripheral neuropathy: the reliability and validity of the European Organization for Research and Treatment of Cancer QLQ-CIPN20 Questionnaire. Qual Life Res. 2013;22(10):2787-2799.

Lee FY, Borzilleri R, Fairchild CR, et al. Preclinical discovery of ixabepilone, a highly active antineoplastic agent. *Cancer Chemother Pharmacol* 2008; 63:157-66.

Lee FY, Borzilleri R, Fairchild CR, Kim SH, Long BH, Reven- tos-Suarez C et al (2001) BMS-247550: a novel epothilone analog with a mode of action similar to paclitaxel but possessing superior anti-tumor efficacy. *Clin Cancer Res* 7:1429–1437 .

Lee FY, Smykla R, Johnston K, et al. Preclinical efficacy spectrum and pharmacokinetics of ixabepilone. *Cancer Chemother Pharmacol* 2009; 63:201-12.

Lee JJ, Swain SM. Peripheral neuropathy induced by microtubule-stabilizing agents. J Clin Oncol 2006; 24:1633-42.

Levy DB, Smith KJ, Beazer-Barclay Y, Hamilton SR, Vogelstein B, Kinzler KW (1994) Inactivation of both APC alleles in human and mouse tumors. Cancer Res 54:5953–5958

Lewcock, J. W., Genoud, N., Lettieri, K., & Pfaff, S. L. (2007). The ubiquitin ligase Phr1 regulates axon outgrowth through modulation of microtubule dynamics. *Neuron*, *56*(4), 604–20. doi:10.1016/j.neuron.2007.09.009

Lipton RB, Apfel SC, Dutcher JP, Rosenberg R, Kaplan J, Berger A, et al. Taxol produces a predominantly sensory neuropathy. Neurology 1989;39:368–73.

Low JA, Wedam SB, Lee JJ, et al. Phase II clinical trial of ixabepilone (BMS- 247550), an epothilone B analog, in metastatic and locally advanced breast cancer. *J Clin Oncol* 2005; 23:2726-34.

Lu Q, Luduena RF (1993) Removal of beta III isotype enhances taxol induced microtubule assembly. Cell Struct Funct 18:173-182

Lutz, A. B., & Barres, B. A. (2014). Review Contrasting the Glial Response to Axon Injury in the Central and Peripheral Nervous Systems. *DEVCEL*, *28*(1), 7–17. https://doi.org/10.1016/j.devcel.2013.12.002

Mandelkow, E.M., Mandelkow, E., and Milligan, R.A. (1991). Microtu- bule dynamics and microtubule caps: a time-resolved cryo-electron parmicroscopy study. J. Cell Biol. *114*, 977–991

Margolis RL, Wilson L. Opposite end assembly and disassembly of microtubules at steady state in vitro. Cell 13: 1-8 1978

Markman M. Chemotherapy-associated neurotoxicity: an important side effect--impacting on quality, rather than quantity, of life. J Cancer Res Clin Oncol. 1996;122(9):511-512.

Matsuyama SS, Jarvik LF (1989) Hypothesis: microtubules, a key to Alzheimer disease. Proc Natl Acad Sci USA 86:8152–8156 Maurer SP, Fourniol FJ, Bohner G, Moores CA, Surrey T (2012) Ebs recognize a nucleotide-dependent structural cap at growing microtubule ends. Cell 149:371–382. doi:10.1016/j.cell.2012.02.049

Matsuyama, A., Shimazu, T., Sumida, Y., Saito, A., Yoshimatsu, Y., Seigneurin-Berny, D., … Yoshida, M. (2002). In vivo destabilization of dynamic microtubules by HDAC6-mediated deacetylation. *The EMBO Journal*, *21*(24), 6820–31.

Maurer SP, Fourniol FJ, Bohner G, Moores CA, Surrey T (2012) EBs recognize a nucleotidedependent structural cap at growing microtubule ends. Cell 149:371-382 doi:10.1016/j.cell.2012.02.049

Mehler, M. F., & Mattick, J. S. (2007). Noncoding RNAs and RNA Editing in Brain Development , Functional Diversification , and Neurological Disease, 799–823. doi:10.1152/physrev.00036.2006.

Meijering E. (2017) NeuronJ 1.4.2, https://imagescience.org/meijering/software/neuronj/

Melki, R., Carlier, M.F., Pantaloni, D., and Timasheff, S.N. (1989). Cold depolymerization of microtubules to double rings: geometric stabilization of assemblies. Biochemistry *28*, 9143–9152.

Merianda, T. T., Gomes, C., Yoo, S., Vuppalanchi, D., & Twiss, J. L. (2013). Axonal Localization of Neuritin/CPG15 mRNA in Neuronal Populations through Distinct 5’ and 3' UTR Elements. *Journal of Neuroscience*, *33*(34), 13735–13742. doi:10.1523/JNEUROSCI.0962-13.2013

Microtubule-targeting agents augment the toxicity of DNA-damaging agents by disrupting intracellular trafficking of DNA repair proteins. Proc Natl Acad Sci U S A 112:1571-1576 doi:10.1073/pnas.1416418112

Mielke S, Sparreboom A, Steinberg SM, et al. Association of paclitaxel pharmacokinetics with the development of peripheral neuropathy in patients with advanced cancer. *Clin Cancer Res* 2005; 11:4843-50.

Millecamps S, Julien JP. Axonal transport deficits and neurodegenerative diseases. Nat Rev Neurosci 2013;14:161–76.

Miller AB, Hoogstraten B, Staquet M, et al. Reporting results of cancer treatment. *Cancer* 1981; 47:207-14.

Miller KD, Wang M, Gralow J, et al. A randomized phase III trial of paclitaxel versus paclitaxel plus bevacizumab as first-line therapy for locally recurrent or metastatic breast cancer: a trial coordinated by the Eastern Cooperative Oncology Group (E2100). *Breast Cancer Res Treat* 2005; 94(suppl 1):S6 (Abstract 3).

Miller, B. R., Press, C., Daniels, R. W., Sasaki, Y., Milbrandt, J., & DiAntonio, A. (2009). A dual leucine kinase-dependent axon self-destruction program promotes Wallerian degeneration. *Nature neuroscience*, *12*(4), 387–9. doi:10.1038/nn.2290

Miltenburg NC, Boogerd W. Chemotherapy-induced neuropathy: a comprehensive survey. Cancer Treat Rev. 2014;40(7):872-882.

Morfini GA, Burns M, Binder LI, Kanaan NM, LaPointe N, Bosco DA, Brown RH, Jr., Brown H, Tiwari A, Hayward L, Edgar J, Nave KA, Garberrn J, Atagi Y, Song Y, Pigino G, Brady ST (2009) Axonal transport defects in neurodegenerative diseases. J Neurosci 29:12776-12786 doi:10.1523/jneurosci.3463-09.2009

Morfini GA, Burns MR, Stenoien DL, Brady ST. Axonal transport. In: Brady ST, Siegel G, Albers RW, Price D, editors. Basic neurochemistry 8th ed. New York, NY: Academic Press; 2011, pp. 146–64.

Morris PG, Fornier MN. Microtubule active agents: beyond the taxane frontier.*Clin Cancer Res* 2008; 14:7167-72.

Moughamian AJ, Osborn GE, Lazarus JE, Maday S, Holzbaur EL (2013) Ordered recruitment of dynactin to the microtubule plusend is required for efficient initiation of retrograde axonal transport. J Neurosci 33:13190–13203. doi:10.1523/jneurosci.0935-13.2013

Muguruma T, Sakura S, Kirihara Y, Saito Y (2006) Comparativesomatic and visceral antinociception and neurotoxicity of intrathecal bupivacaine, levobupivacaine, and dextrobupivacaine in rats. Anesthesiology 104:1249–1256

Nabholtz JM, Gelmon K, Bontenbal M, et al. Multicenter, randomized comparative study of two doses of paclitaxel in patients with metastatic breast cancer. *J Clin Oncol* 1996; 14:1858-67.

Nogales, E., Wolf, S.G., Khan, I.A., Ludueña, R.F. and Downing, K.H. (1995) Structure of tubulin at 6.5 A and location of the taxol-binding site. *Nature*. 375:424-427.

O'Shaughnessy JA, Blum JL, Sandbach JF, et al. Weekly nanoparticle albumin paclitaxel (Abraxane) results in long-term disease control in patients with taxane-refractory metastatic breast cancer. *Breast Cancer Res Treat* 2004; 88:S65 (Abstract 1070).

Ocean AJ, Vahdat LT. Chemotherapy-induced peripheral neuropathy: pathogenesis and emerging therapies. *Support Care Cancer* 2004; 12:619-25.

Oken MM, Creech RH, Tormey DC, et al. Toxicity and response criteria of the Eastern Cooperative Oncology Group. *Am J Clin Oncol* 1982; 5:649-55. 25. National Cancer Institute Common Terminology Criteria for Adverse Events Criteria (NCI CTCAE) for Peripheral Neuropathy Version 4.0. Available at: http://www.evs.nci.nih.gov/ftp1/CTCAE/About.html. Accessed: August 06, 2010. *Oncol* 1995; 13:2575-81.

Osmani K, Vignes S, Aissi M, Wade F, Milani P, Lévy BI, Kubis N. Taxane-induced peripheral neuropathy has good long-term prognosis: a 1- to 13-year evaluation. J Neurol. 2012 Sep;259(9):1936-43.

Østerlind K, Sanchez JM, Zatloukal P, et al. Phase I/II dose escalation trial of patupilone every 3 weeks in patients with non-small cell lung cancer. *J Clin Oncol* 2005; 23:647s (Abstract 7110).

Pace A, Nisticò C, Cuppone F, Bria E, Galiè E, Graziano G, Natoli G, Sperduti I, Jandolo B, Calabretta F, Tomao S, Terzoli E. Peripheral neurotoxicity of weekly paclitaxel chemotherapy: a schedule or a dose issue? Clin Breast Cancer. 2007 Apr;7(7):550-4.

Pachter JS, Yen TJ, Cleveland DW (1987) Autoregulation of tubulin expression is achieved through specific degradation of polysomal tubulin mRNAs Cell 51:283-292

Palazzo, A. et al. (2003) Cell biology: tubulin acetylation and cell motility. Nature 421, 230

Panda, D., Miller, H. P. & Wilson, L. Rapid treadmilling of MAP-free brain microtubules in vitro and its suppression by tau. Proc. Natl Acad. Sci. USA 96, 12459–12464 (1999).

Pareyson, D., Saveri, P., Sagnelli, A., & Piscosquito, G. (2015). Neuroscience Letters Mitochondrial dynamics and inherited peripheral nerve diseases. Neuroscience Letters, 596, 66–77. https://doi.org/10.1016/j.neulet.2015.04.001

Park SB, Goldstein D, Krishnan AV, Lin CS, Friedlander ML, Cassidy J, Koltzenburg M, Kiernan MC. Chemotherapy-induced peripheral neurotoxicity: a critical analysis. CA Cancer J Clin. 2013 Nov-Dec;63(6):419-37.

Parness, J. and Horwitz, S.B. (1981) Taxol binds to polymerized tubulin in vitro. *J. Cell Biology* 91:479-487.

Perez EA, Lerzo G, Pivot X, et al. Efficacy and safety of ixabepilone (BMS-247550), a novel epothilone analog, in a phase II study of patients with advanced breast cancer resistant to an anthracycline, a taxane, and capecitabine. *J Clin Oncol* 2007; 25: 3407-14.

Perez EA, Pivot X, Vrdoljak E, et al. A prospective characterization of the resolution of ixabepilone induced peripheral neuropathy: data from a large registrational program in patients with metastatic breast cancer. *Cancer Res* 2009; 69(suppl 2):401-2 (Abstract 6140).

Perez EA, Vogel CL, Irwin DH, et al. Multicenter phase II trial of weekly paclitaxel in women with metastatic breast cancer. *J Clin Oncol* 2001; 19:4216-23.

Perez EA, Lerzo G, Pivot X, Thomas E, Vahdat L, Bosserman L, Viens P, Cai C, Mullaney B, Peck R, Hortobagyi GN. Efficacy and safety of ixabepilone (BMS-247550) in a phase II study of patients with advanced breast cancer resistant to an anthracycline, a taxane, and capecitabine. J Clin Oncol. 2007 Aug 10;25(23):3407-14.

Persohn E, Canta A, Schoepfer S, et al. Morphological and morphometric analysis of paclitaxel and docetaxel-induced peripheral neuropathy in rats. *Eur J Cancer* 2005; 41:1460-6.

Peters CM, Jimenez-Andrade JM, Jonas BM, Sevcik MA, Koewler NJ, Ghilardi JR, Wong GY, Mantyh PW (2007a) Intravenous paclitaxel administration in the rat induces a peripheral sensory neuropathy characterized by macrophage infiltration and injury to sensory neurons and their supporting cells. Exp Neurol 203:42-54 doi:10.1016/j.expneurol.2006.07.022

Peters CM, Jimenez-Andrade JM, Kuskowski MA, Ghilardi JR, Mantyh PW (2007b) An evolving cellular pathology occurs in dorsal root ganglia, peripheral nerve and spinal cord following intravenous administration of paclitaxel in the rat. Brain Res 1168:46-59 doi:10.1016/j.brainres.2007.06.066

Piperno G, LeDizet M, Chang XJ (1987) Microtubules containing acetylated alpha-tubulin in mammalian cells in culture. J Cell Biol 104:289–302

Polomano RC, Mannes AJ, Clark US, et al. A painful peripheral neuropathy in the rat produced by the chemotherapeutic drug, paclitaxel. *Pain* 2001; 94:293-304.

Poruchynsky, M. S., Komlodi-pasztor, E., Trostel, S., Wilkerson, J., Regairaz, M., Pommier, Y., … Guha, U. (2014). Microtubule-targeting agents augment the toxicity of DNA-damaging agents by disrupting intracellular trafficking of DNA repair proteins. https://doi.org/10.1073/pnas.1416418112

Postma TJ, Aaronson NK, Heimans JJ, et al. The development of an EORTC quality of life questionnaire to assess chemotherapy-induced peripheral neuropathy: the QLQ-CIPN20. Eur J Cancer. 2005;41(8):1135-1139.

Postma TJ, Heimans JJ, Muller MJ, et al. Pitfalls in grading severity of chemotherapy- induced peripheral neuropathy. *Ann Oncol* 1998; 9:739-44.

Postma TJ, Heimans JJ. Grading of chemotherapy-induced peripheral neuropathy. *Ann Oncol* 2000; 11:509-13.

Postma TJ, Benard BA, Huijgens PC, Ossenkoppele GJ, Heimans JJ. Long-term effects of vincristine on the peripheral nervous system. J Neurooncol. 1993;15:23-27.

Press, C., & Milbrandt, J. (2008). Nmnat delays axonal degeneration caused by mitochondrial and oxidative stress. *The Journal of neuroscience : the official journal of the Society for Neuroscience*, *28*(19), 4861–71. doi:10.1523/JNEUROSCI.0525-08.2008

Puhalla S, Brufsky A. Ixabepilone: a new chemotherapeutic option for refractory metastatic breast cancer. Biologics. 2008 Sep;2(3):505-15.

Quincy DA, Davis A, Yoshimatsu K, Kishi Y, Yu MJ, Littlefield BA (2001) In vitro and in vivo anticancer activities of synthetic macrocyclic ketone analogues of halichondrin B. Cancer Res 61:1013-1021

Ranganathan S, Benetatos CA, Colarusso PJ, Dexter DW, Hudes GR (1998) Altered beta-tubulin isotype expression in paclitaxel resistant human prostate carcinoma cells. Br J Cancer 77:562–566

Ranganathan S, Dexter DW, Benetatos CA, Chapman AE, Tew KD, Hudes GR (1996) Increase of beta(III)- and beta(IVa)-tubulin isotopes in human prostate carcinoma cells as a result of estramustine resistance. Cancer Res 56:2584-2589

Rao RD, Michalak JC, Sloan JA, et al. Efficacy of gabapentin in the management of chemotherapy-induced peripheral neuropathy: a phase 3 randomized, double-blind, placebo-controlled, crossover trial (N00C3). Cancer. 2007;110(9):2110-2118.

Reed, N. a, Cai, D., Blasius, T. L., Jih, G. T., Meyhofer, E., Gaertig, J., & Verhey, K. J. (2006). Microtubule acetylation promotes kinesin-1 binding and transport. Current Biology : CB, 16(21), 2166–72. https://doi.org/10.1016/j.cub.2006.09.014

Rinkevich Y, Montoro DT, Muhonen E, Walmsley GG, Lo D, Hasegawa M, Januszyk M, Connolly AJ, Weissman IL, Longaker MT (2014) Clonal analysis reveals nervedependent and independent roles on mammalian hind limb tissue maintenance and regeneration. Proc Natl Acad Sci U S A 111:9846-9851 doi:10.1073/pnas.1410097111

Rivera E, Cianfrocca M. Overview of neuropathy associated with taxanes for the treatment of metastatic breast cancer. Cancer Chemother Pharmacol. 2015 Apr;75(4):659-70.

Robey R, Burotto M, Sackett D, Guha U, Fojo AT. (2015) Microtubule-targeting agents augment the toxicity of DNA-damaging agents by disrupting intracellular trafficking of DNA repair proteins. *Proceedings of the National Academy of Sciences USA* 112:1571-1576.

Roché H, Yelle L, Cognetti F, Mauriac L, Bunnell C, Sparano J, Kerbrat P, Delord JP, Vahdat L, Peck R, Lebwohl D, Ezzeddine R, Curé H. Phase II clinical trial of ixabepilone (BMS-247550), an epothilone B analog, as first-line therapy in patients with metastatic breast cancer previously treated with anthracycline chemotherapy. J Clin Oncol. 2007 Aug 10;25(23):3415-20.

Rodionov, V. I. & Borisy, G. G. Microtubule treadmilling in vivo. Science 275, 215–218 (1997).

Rosenberg, A. F., Wolman, M. a, Franzini-Armstrong, C., & Granato, M. (2012). In vivo nerve-macrophage interactions following peripheral nerve injury. *The Journal of neuroscience : the official journal of the Society for Neuroscience*, *32*(11), 3898–909. doi:10.1523/JNEUROSCI.5225-11.2012

Rostovtseva TK, Sheldon KL, Hassanzadeh E,Monge C, Saks V, Bezrukov SM, et al. Tubulin binding blocks mitochondrial voltage-dependent anion channel and regulates respiration. Proc Natl Acad Sci 2008;105(48): 18746–51.

Rotshenker S (2011) Wallerian degeneration: the innate-immune response to traumatic nerve injury. J Neuroinflammation 8:109 doi:10.1186/1742-2094-8-109

Rowinsky EK, Eisenhauer EA, Chaudhry V, et al. Clinical toxicities encountered by paclitaxel (Taxol). *Semin Oncol* 1993; 20(suppl3):1-15.

Rubin EH, Rothermel J, Tesfaye F, et al. Phase I dose-finding study of weekly single-agent patupilone in patients with advanced solid tumours. *J Clin Oncol* 2005; 23:9120-9.

Rugo HS, Campone M, Amadori D, et al. Randomized study of weekly vs every 3 week ixabepilone plus bevacizumab (ixa/bev) vs paclitaxel plus bev (pac/bev) as first-line therapy for metastatic breast cancer (MBC): final results. *J Clin Oncol* 2010; 28(15S):123S (Abstract 1040).

Sahenk Z, Barohn R, New P, et al. Taxol neuropathy. Electrodiagnostic and sural nerve biopsy findings. *Arch Neurol* 1994; 51:726-9.

Sarris AH, Hagemeister F, Romaguera J, et al. Liposomal vincristine in relapsed non-Hodgkin's lymphomas: early results of an ongoing phase II trial. Ann Oncol 2000; 11:69-72.

Savage C, Hamelin M, Culotti JG, Coulson A, Albertson DG, Chalfie M (1989) mec-7 is a beta-tubulin gene required for the production of 15-protofilament microtubules in Caenorhabditis elegans. Genes Dev 3:870-881

Saxton, W. M., & Hollenbeck, P. J. (2012). The axonal transport of mitochondria. https://doi.org/10.1242/jcs.053850

Schmalbruch H. (1986) Fiber composition of the sciatic nerve. Anat. Rec. May;215(1):71-81.

Schmid P, Kiewe P, Possinger K, et al. Phase I study of the novel fully synthetic epothilone sagopilone (ZK-EPO) in patients with solid tumors. *Ann Oncol* 2010; 21:633-9.

Schnaar RL, Gerardy-Schahn R, Hildebrandt H (2014) Sialic acids in the brain: gangliosides and polysialic acid in nervous system development, stability, disease, and regeneration. Physiol Rev 94:461–518. doi:10.1152/physrev.00033.2013

Schweers O, Schönbrunn-Hanebeck E, Marx A, Mandelkow E. (1994) Structural studies of tau protein and Alzheimer paired helical filaments show no evidence for β-structure. J Biol Chem. Sep 30; 269(39):24290-7

Seidman AD, Berry D, Cirrincione C, et al. CALGB 9840: phase III study of weekly paclitaxel via 1-hour infusion versus standard 3h infusion every third week in the treatment of metastatic breast cancer (MBC), with trastuzumab (T) for HER2 positive MBC and randomized for T in HER2 normal MBC. *J Clin Oncol* 2004; 22(14S): (Abstract 512).

Seidman AD, Tiersten A, Hudis C, et al. Phase II trial of paclitaxel by 3-hour infusion as initial and salvage chemotherapy for metastatic breast cancer. J Clin Oncol 1995; 13:2575-81.

Seretny M, Currie GL, Sena ES, et al. Incidence, prevalence, and predictors of chemotherapy-induced peripheral neuropathy: a systematic review and meta-analysis. Pain. 2014;155(12):2461-2470.

Shimozuma K, Ohashi Y, Takeuchi A, et al. Feasibility and validity of the Patient Neurotoxicity Questionnaire during taxane chemotherapy in a phase III randomized trial in patients with breast cancer: N-SAS BC 02. Support Care Cancer. 2009;17(12):1483-1491.

Shin, J. E., Cho, Y., Beirowski, B., Milbrandt, J., Cavalli, V., & DiAntonio, A. (2012). Dual leucine zipper kinase is required for retrograde injury signaling and axonal regeneration. *Neuron*, *74*(6), 1015–22. doi:10.1016/j.neuron.2012.04.028

Siau C, Xiao W, Bennett GJ. Paclitaxel- and vincristine-evoked painful peripheral neuropathies: loss of epidermal innervation and activation of Langerhans cells. *Exp Neurol* 2006; 201:507-14.

Smith JA, Slusher BS, Wozniak KM, Farah MH, Smiyun G, Wilson L, Feinstein S, Jordan MA (2016) Structural basis for induction of peripheral neuropathy by microtubule-targeting cancer drugs. Cancer Res doi:10.1158/0008-5472.can-15-3116

Smith JA, Wilson L, Azarenko O, Zhu X, Lewis BM, Littlefield BA, Jordan MA (2010) Eribulin binds at microtubule ends to a single site on tubulin to suppress dynamic instability. Biochemistry 49:1331-1337 doi:10.1021/bi901810u

Smith JW II, Vukelja SJ, Rabe AC, et al. Preliminary toxicity results of a phase II randomized trial of weekly or every 3-week ixabepilone in metastatic breast cancer (MBC). *Cancer Res* 2009; 69(24 suppl 3):856s (Abstract 6099).

Smith RE, Brown AM, Mamounas EP, et al. Randomized trial of 3-hour versus 24-hour infusion of high-dose paclitaxel in patients with metastatic or locally advanced breast cancer: National Surgical Adjuvant Breast and Bowel Project Protocol B-26. *J Clin Oncol* 1999; 17:3403-11.

Smith, J. A., Wilson, L., Azarenko, O., Zhu, X. J., Lewis, B. M., Littlefield, B. A., and Jordan, M. A. (2010) Eribulin Binds at Microtubule Ends to a Single Site on Tubulin To Suppress Dynamic Instability *Biochemistry* 49, 1331-1337.

Song Y, Brady ST (2015) Post-translational modifications of tubulin: pathways to functional diversity of microtubules. Trends Cell Biol 25:125-136 doi:10.1016/j.tcb.2014.10.004

Soppina, V., Herbstman, J. F., Skiniotis, G., & Verhey, K. J. (2012). Luminal Localization of a -tubulin K40 Acetylation by Cryo-EM Analysis of Fab-Labeled Microtubules, 7(10), 1–9. https://doi.org/10.1371/journal.pone.0048204

Sparano JA, Vrdoljak E, Rixe O, et al. Randomized phase III trial of ixabepilone plus capecitabine versus capecitabine in patients with metastatic breast cancer previously treated with an anthracycline and a taxane. *J Clin Oncol* 2010; 28:3256-63. 63.

Sparano JA, Wang M, Martino S, et al. Weekly paclitaxel in the adjuvant treatment of breast cancer. *N Engl J Med* 2008; 358:1663-71.

Steinberg M. Ixabepilone: a novel microtubule inhibitor for the treatment of locally advanced or metastatic breast cancer. Clin Ther 2008;30:1590-617

Storey DJ, Colvin L, Scott AC, et al. Treatment of chemotherapy-induced peripheral neuropathy (CIPN) with topical menthol: a phase 1 study. J Clin Oncol. 2010;28(15)(suppl):9129.

Stubblefield MD, Burstein HJ, Burton AW, et al. NCCN task force report: management of neuropathy in cancer. J Natl Compr Canc Netw 2009; 7(suppl 5):1-26.

Stubblefield MD, Vahdat LT, Balmaceda CM, et al. Glutamine as a neuroprotective agent in high-dose paclitaxel-induced peripheral neuropathy: a clinical and electrophysiologic study. *Clin Oncol* (R Coll Radiol) 2005; 17:271-6.

Swain SM, Arezzo JC. Neuropathy associated with microtubule inhibitors: diagnosis, incidence, and management. *Clin Adv Hematol Oncol* 2008; 6:455-67.

Szyk, A., Deaconescu, A. M., Spector, J., Goodman, B., Valenstein, M. L., Ziolkowska, N. E., … Roll-mecak, A. (2016). HHS Public Access, 157(6), 1405–1415. https://doi.org/10.1016/j.cell.2014.03.061.Molecular

Tabernero J, Climent MA, Lluch A, et al. A multicentre, randomised phase II study of weekly or 3-weekly docetaxel in patients with metastatic breast cancer. *Ann Oncol* 2004; 15:1358-65.

Tanner, K. D., Levine, J. D., & Topp, K. S. (1998). Microtubule disorientation and axonal swelling in unmyelinated sensory axons during vincristine-induced painful neuropathy in rat. *The Journal of comparative neurology*, *395*(4), 481–92. Retrieved from http://www.ncbi.nlm.nih.gov/pubmed/9619501

Tasnim A, Rammelkamp Z, Slusher AB, Wozniak K, Slusher BS, Farah MH. Paclitaxel causes degeneration of both central and peripheral axon branches of dorsal root ganglia in mice. BMC Neuroscience. 2016;17:47.

Tedeschi, A., & Bradke, F. (2013). The DLK signalling pathway-a double-edged sword in neural development and regeneration. EMBO Reports, 1–10. https://doi.org/10.1038/embor.2013.64

Thibault, K., Van Steenwinckel, J., Brisorgueil, M.-J., Fischer, J., Hamon, M., Calvino, B., & Conrath, M. (2008). Serotonin 5-HT2A receptor involvement and Fos expression at the spinal level in vincristine-induced neuropathy in the rat. *Pain*, *140*(2), 305–22. doi:10.1016/j.pain.2008.09.006

Thomas E, Tabernero J, Fornier M, et al. Phase II clinical trial of ixabepilone (BMS-247550), an epothilone B analog, in patients with taxane-resistant metastatic breast cancer. *J Clin Oncol* 2007; 25:3399-406.

Thomas ES, Gomez HL, Li RK, et al. Ixabepilone plus capecitabine for metastatic breast cancer progressing after anthracycline and taxane treatment. *J Clin Oncol* 2007; 25:5210-7.

Thomas E, Tabernero J, Fornier M, Conté P, Fumoleau P, Lluch A, Vahdat LT, Bunnell CA, Burris HA, Viens P, Baselga J, Rivera E, Guarneri V, Poulart V, Klimovsky J, Lebwohl D, Martin M. Phase II clinical trial of ixabepilone (BMS-247550), an epothilone B analog, in patients with taxane-resistant metastatic breast cancer. J Clin Oncol. 2007 Aug 10;25(23):3399-406.

Towle MJ, Salvato KA, Budrow J, Wels BF, Kuznetsov G, Aalfs KK, Welsh S, Zheng W, Seletsky BM, Palme MH, Habgood GJ, Singer LA, Dipietro LV, Wang Y, Chen JJ, Quincy DA, Davis A, Yoshimatsu K, Kishi Y, Yu MJ, Littlefield BA (2001) In vitro and in vivo anticancer activities of synthetic macrocyclic ketone analogues of halichondrin B. Cancer Res 61:1013–1021

Tsujino H, Kondo E, Fukuoka T, Dai Y, Tokunaga A, Miki K, Yonenobu K, Ochi T, Noguchi K (2000) Activating transcription factor 3 (ATF3) induction by axotomy in sensory and motoneurons: A novel neuronal marker of nerve injury. Mol Cell Neurosci 15:170-182 doi:10.1006/mcne.1999.0814

Tuxen MK, Hansen SW. Neurotoxicity secondary to antineoplastic drugs. *Cancer Treat Rev* 1994; 20:191-214.

Twelves C, Cortes J, Vahdat L, Olivo M, He Y, Kaufman PA, Awada A. Efficacy of eribulin in women with metastatic breast cancer: a pooled analysis of two phase 3 studies. Breast Cancer Res Treat. 2014 Dec;148(3):553-61.

Twelves C, Cortes J, Vahdat L, Olivo M, He Y, Kaufman PA, Awada A. Efficacy of eribulin in women with metastatic breast cancer: a pooled analysis of two phase 3 studies. Breast Cancer Res Treat. 2014 Dec;148(3):553-61.

US Department of Health and Human Services. Common Terminology Criteria for Adverse Events (CTCAE). Version 4.0. Published May 28, 2009.

Vahdat L, Papadopoulos K, Lange D, et al. Reduction of paclitaxel-induced peripheral neuropathy with glutamine. *Clin Cancer Res* 2001; 7:1192-7.

Vahdat L. Ixabepilone: a novel antineoplastic agent with low susceptibility to multiple tumor resistance mechanisms. *Oncologist* 2008; 13:214-21.

Vahdat LT, Garcia AA, Vogel C, Pellegrino C, Lindquist DL, Iannotti N, Gopalakrishna P, Sparano JA. Eribulin mesylate versus ixabepilone in patients with metastatic breast cancer: a randomized Phase II study comparing the incidence of peripheral neuropathy. Breast Cancer Res Treat. 2013 Jul;140(2):341-51.

Vahdat LT, Thomas E, Roche H, et al. Ixabepilone (Ixa)-associated peripheral neuropathy (PN): retrospective review of data from phase II and III clinical trials. *Ann Oncol* 2010; 21(suppl 8):viii109 (Abstract 320P).

Verhey K. J. and Gaertig J. (2007) The tubulin code. Cell Cycle 6, 2152– 2160.

Verstappen CC, Koeppen S, Heimans JJ, et al. Dose-related vincristine-induced peripheral neuropathy with unexpected off-therapy worsening. *Neurology* 2005;

Viens P, Petit T, Yovine A, et al. A phase II study of a paclitaxel and oxaliplatin combination in platinum-sensitive recurrent advanced ovarian cancer patients. *Ann Oncol* 2006; 17:429-36.

Vitre B, Coquelle FM, Heichette C, Garnier C, Chretien D, Arnal I (2008) EB1 regulates microtubule dynamics and tubulin sheet closure in vitro. Nat Cell Biol 10:415-421 doi:10.1038/ncb1703

Vogel C, O'Rourke M, Winer E, et al. Vinorelbine as first-line chemotherapy for advanced breast cancer in women 60 years of age or older. Ann Oncol 1999; 10:397- 402.

Walter WJ, Beranek V, Fischermeier E, Diez S (2012) Tubulin acetylation alone does not affect kinesin-1 velocity and run length in vitro. PLoS One 7:e42218. doi:10.1371/journal.pone.0042218

Wang WS, Lin JK, Lin TC, et al. Oral glutamine is effective for preventing oxaliplatin-induced neuropathy in colorectal cancer patients. *Oncologist* 2007; 12:312-9.

Wang, M. S., Davis, A. a, Culver, D. G., & Glass, J. D. (2002). WldS mice are resistant to paclitaxel (taxol) neuropathy. *Annals of neurology*, *52*(4), 442–7. doi:10.1002/ana.10300

Watanabe, M., Tsukiyama, T., & Hatakeyama, S. (2007). Protection of vincristine-induced neuropathy by WldS expression and the independence of the activity of Nmnat1. *Neuroscience letters*, *411*(3), 228–32. doi:10.1016/j.neulet.2006.09.068

Watkins, T. a, Wang, B., Huntwork-Rodriguez, S., Yang, J., Jiang, Z., Eastham-Anderson, J., … Lewcock, J. W. (2013). DLK initiates a transcriptional program that couples apoptotic and regenerative responses to axonal injury. *Proceedings of the National Academy of Sciences of the United States of America*, *110*(10), 4039–4044. doi:10.1073/pnas.1211074110

Webster DR, Borisy GG (1989) Microtubules are acetylated in domains that turn over slowly. J Cell Sci 92 (Pt 1):57-65

Welsbie, D. S., Yang, Z., Ge, Y., Mitchell, K. L., Zhou, X., Martin, S. E., … Zack, D. J. (2013). Functional genomic screening identifies dual leucine zipper kinase as a key mediator of retinal ganglion cell death. *Proceedings of the National Academy of Sciences of the United States of America*, *110*(10), 4045–50. doi:10.1073/pnas.1211284110

Willis, D. E., Xu, M., Donnelly, C. J., Tep, C., Kendall, M., Erenstheyn, M., … Twiss, J. L. (2011). Axonal Localization of transgene mRNA in mature PNS and CNS neurons. *The Journal of neuroscience : the official journal of the Society for Neuroscience*, *31*(41), 14481–7. doi:10.1523/JNEUROSCI.2950-11.2011

Windebank AJ, Grisold W (2008) Chemotherapy-induced neuropathy Journal of the peripheral nervous system : *Journal of the Peripheral Nervous System* 13:27-46.

Winer EP, Berry DA, Woolf S, et al. Failure of higher dose paclitaxel to improve outcome in patients with metastatic breast cancer: Cancer and Leukemia Group B trial. *J Clin Oncol* 2004; 22:2061-8.

Witman GB, Cleveland DW, Weingarten MD, Kirschner MW. (1976) Tubulin requires tau for growth onto microtubule initiating sites. Proc Natl Acad Sci. 73(11):4070-4.

Woolf, C. J., & Ma, Q. (2007). Nociceptors--noxious stimulus detectors. *Neuron*, *55*(3), 353–64. https://doi.org/10.1016/j.neuron.2007.07.016

Wozniak KM, Nomoto K, Lapidus RG, Wu Y, Carozzi V, Cavaletti G, Hayakawa K, Hosokawa S, Towle MJ, Littlefield BA, Slusher BS (2011) Comparison of neuropathy-inducing effects of eribulin mesylate, paclitaxel, and ixabepilone in mice. Cancer Res 71:3952- 3962 doi:10.1158/0008-5472.can-10-4184

Wozniak KM, Vornov JJ, Wu Y, Nomoto K, Littlefield BA, DesJardins C, Yu Y, Lai G, Reyderman L, Wong N, Slusher BS (2016) Sustained Accumulation of Microtubule-Binding Chemotherapy Drugs in the

Peripheral Nervous System: Correlations with Time Course and Neurotoxic Severity. Cancer Res 76:3332-3339 doi:10.1158/0008- 5472.can-15-2525

Wozniak, K. M., Nomoto, K., Lapidus, R. G., Wu, Y., Carozzi, V., Cavaletti, G., … Slusher, B. S. (2011). Comparison of neuropathy-inducing effects of eribulin mesylate, paclitaxel, and ixabepilone in mice. *Cancer research*, *71*(11), 3952–62. doi:10.1158/0008-5472.CAN-10-4184

Xiao, W. H., & Bennett, G. J. (2008). Chemotherapy-evoked neuropathic pain: Abnormal spontaneous discharge in A-fiber and C-fiber primary afferent neurons and its suppression by acetyl-L-carnitine. *Pain*, *135*(3), 262–70. doi:10.1016/j.pain.2007.06.001

Yan, D., Wu, Z., Chisholm, A. D., & Jin, Y. (2009). The DLK-1 kinase promotes mRNA stability and local translation in C. elegans synapses and axon regeneration. *Cell*, *138*(5), 1005–18. doi:10.1016/j.cell.2009.06.023

Yoo, S., Kim, H. H., Kim, P., Donnelly, C. J., Kalinski, A. L., Vuppalanchi, D., … Twiss, J. L. (2013). A HuD-ZBP1 ribonucleoprotein complex localizes GAP-43 mRNA into axons through its 3' untranslated region AU-rich regulatory element. Journal of Neurochemistry, 126(6), 792–804. https://doi.org/10.1111/jnc.12266

Yoshida M (2002) In vivo destabilization of dynamic microtubules by HDAC6-mediated deacetylation. EMBO J. 2002 Dec 16;21(24):6820-31.

Zelek L, Barthier S, Riofrio M, et al. Weekly vinorelbine is an effective palliative regimen after failure with anthracyclines and taxanes in metastatic breast carcinoma. *Cancer* 2001; 92:2267-72.

Zhang H, Li Y, de Carvalho-Barbosa M, Kavelaars A, Heijnen CJ, Albrecht PJ, Dougherty PM (2016) Dorsal root ganglion infiltration by macrophages contributes to paclitaxel chemotherapy induced peripheral neuropathy. J Pain doi:10.1016/j.jpain.2016.02.011

Zhang T, Yao S, Wang P, Yin C, Xiao C, Qian M, Liu D, Zheng L, Meng W, Zhu H, Liu J, Xu H, Mo X (2011) ApoA-II directs morphogenetic movements of zebrafish embryo by preventing chromosome fusion during nuclear division in yolk syncytial layer. J Biol Chem 286:9514-9525 doi:10.1074/jbc.M110.134908